To the Graduate Council:

I am submitting herewith a dissertation written by James Andrew Ridnour entitled "METHODOLOGY FOR EVALUATING VEHICLE FATIGUE LIFE AND DURABILITY." I have examined the final paper copy of this dissertation for form and content and recommend that it be accepted in partial fulfillment of the requirements for the degree of Doctor of Philosophy, with a major in Mechanical Engineering.

Jeff Freeman, Major Professor

We have read this dissertation
and recommend its acceptance:

J.A.M. Boulet

David Icove

John D. Landes

John Landes

Accepted for the Council:

Vice Provost and Dean of Graduate Studies

METHODOLOGY FOR EVALUATING VEHICLE FATIGUE LIFE AND DURABILITY

A Dissertation
Presented for the
Doctor of Philosophy
Degree
The University of Tennessee, Knoxville

James Andrew Ridnour
December 2003

This thesis is dedicated to my mother Annie Jo Ridnour who has always encouraged, helped, and believed in me.

ACKNOWLEDGEMENTS

I would like to thank God for giving me the ability to achieve my goals. I am grateful to all the people who have helped me throughout my academic career. I would like to thank my major professor Dr. Jeff Freeman. I would also like to thank the other members of my graduate committee: Dr. J.A.M. Boulet, Dr. David Icove, and Dr. John Landes. Finally, I would like to thank everyone who has supported and believed in me.

ABSTRACT

Vehicle durability, which defines the useful life of a vehicle, is a high priority for some consumers. Life consumption monitoring can be used to determine fatigue damage by directly or indirectly monitoring the loads placed on critical vehicle components that are susceptible to failure from fatigue damage. By monitoring vehicle life consumption, the Army can predict mechanical failures before they occur and determine the useful life of vehicles. The example vehicle used for this study is the M1101 High Mobility Trailer (HMT) that is normally towed behind a High Mobility Multi-purpose Wheeled Vehicle (HMMWV). As originally designed, the HMT experiences a fatigue failure of the drawbar.

For this analysis, experimental data was taken from a HMT traveling over known test courses. The data was used to validate a computer simulation, and to determine the feasibility of life consumption monitoring. Multivariate regressions and principal component analysis (PCA) were used to determine which sensors most accurately reflect the loads on the drawbar at the failure point. Regression and dynamic models were made after the proper decimation and filtering of the data was determined. The models were then used to predict the fatigue life of the trailer.

The results of this study show that simulations can be modified to be representative of the vehicle being tested. The results also show that the fatigue life and durability of the vehicle can be predicted with a model and data from sensors placed on the vehicle.

TABLE OF CONTENTS

CHAPTER **PAGE**

1 Introduction..1

1.1 Project Background...1

1.1.1 Terrain Sensing...8

1.3 Project Objectives...11

1.4 Project Scope..11

2 Literature Review...13

2.1 Terrain Monitoring...13

2.2 Durability Analysis...13

2.3 Parameter Identification...16

3 Method..19

3.1 Regression Analysis...20

3.2 Principal Component Analysis (PCA)..22

3.3 Fatigue Life Calculation...24

3.4 Decimation and Filtering..26

4 Data Collection and DADS Validation..27

4.1 Test Setup...27

4.2 Test Data...33

4.3 Data Reduction Results..35

4.3.2 Strain Data..36

4.3.3 Accelerometer Data..40

4.3.4 Rate-gyro Data 49

4.3.5 Linear Displacement Transducer Data 52

4.3.6 Pressure Transducer Data 54

4.4 DADS Validation...56

5 PSD Conversion..61

5.1 Introduction..61

5.2 PSD 61

5.3 PSD Conversion Method 62

5.4 PSD Conversion Results..65

6 Surge Brake Analysis 71

6.1 Hydraulic Surge Brake Operation 71

6.2 Test Data 72

6.2.1 Belgian Block..75

6.2.2 Perryman #3 79

6.3 Analysis Method..83

6.3.1 Regression Analysis for Belgian Block (Brakes enabled) 84

6.3.2 Regression Analysis for Belgian Block (Brakes disabled) 91

6.3.4 Regression with Concatenated Data for Belgian Block 94

6.3.5 Principal Component Analysis for Belgian Block (Brakes Enabled) 101

6.3.6 Regression Analysis for Perryman #3 (Brakes Enabled) 107

6.3.7 Regression Analysis for Perryman #3 (Brakes Disabled) 109

6.3.8 Regression with Concatenated Data for Perryman #3 111

6.3.9 Principal Component Analysis for Perryman #3 (Brakes Enabled)...............112

6.3.10 Principal Component Analysis for Perryman #3 (Brakes Disabled) 123
7 Regression Analysis..129
7.1 Data Filtering 139
8 Fatigue Life...149
9 Dynamic Model 163
10 Results and Conclusions 173
11 Future Work..177
List of References 179
Vita 183

LIST OF TABLES

TABLE **PAGE**

4.1: Data acquisition system channel assignments. 28

4.2: Test matrix data file names 34

4.3: Analog low-pass anti-aliasing cutoff frequencies. 34

4.4: Experimental data file format 35

4.5: Strain amplitude distribution data 37

4.6: Principal strain amplitude distribution data. 37

4.7: Acceleration amplitude distribution data (brakes disabled) 41

4.8: Acceleration amplitude distribution data (brakes enabled) 41

4.9: Rate-gyro distribution data (brakes disabled) 50

4.10: Rate-gyro distribution data (brakes enabled) 50

4.11: Linear displacement distribution data (brakes disabled) 52

4.12: Linear displacement distribution data (brakes enabled) 52

4.13: Brake pressure distribution data (brakes disabled). 54

4.14: Other amplitude distribution data (brakes enabled). 54

4.15: DADS validation statistics 57

5.1: Univariate statistics for terrain data. 66

6.1: Listing of Data Acquisition Channels and Grouping 73

6.2: Statistics for brake pressures for Belgian Block at 15 mph with brakes enabled. 76

6.3: Correlation coefficient between brake pressures for Belgian Block at 15 mph with brakes enabled. 76

6.4: Statistics for brake pressures for Belgian Block at 15 mph with brakes disabled......77

6.5: Statistics for brake pressures for Perryman #3 test course at 15 mph with brakes enabled.......80

6.6: Correlation coefficient between brake pressures for Perryman #3 test course at 15 mph with brakes enabled. 80

6.7: Statistics for brake pressures for Perryman #3 at 15 mph with brakes disabled. 81

6.8: Correlation coefficient between brake pressures for Perryman #3 at 15 mph with brakes disabled.......82

6.9: Column and variable numbers for data channels of reduced data sets.......85

6.10: R^2 values for all models for Belgian Block at 15 mph with brakes enabled. 90

6.11: R^2 values for all Belgian Block at 15 mph with brakes disabled regression models. 92

6.12: R^2 values for all Belgian Block at 15 mph with brakes disabled and enabled regression model, with brake pressure variables included. 100

6.13: R^2 values for all Belgian Block at 15 mph with brakes disabled and enabled regression models, with brake pressure variables removed.......101

6.14: PC scores for Belgian Block at 15 mph brake pressure variables. 103

6.15: Input measurement components to PCs 2, 31, and 33, for Belgain Block at 15 mph with brakes enabled. 104

6.16: R^2 values for all models for Perryman #3 test course at 15 mph with brakes enabled. 109

6.17: R^2 values for all Perryman #3 at 15 mph with brakes disabled regression models. 110

6.18: R^2 values for Perryman #3 at 15 mph with brakes disabled and enabled regression model, with brake pressure variables included.......111

6.19: R^2 values for Perryman #3 at 15 mph with brakes disabled and enabled regression model, with brake pressure variables removed.......112

6.20: PC scores for Perryman #3 at 15 mph with brakes enabled pressure variables. 114

6.21: Input measurement components to PCs 5, 32, and 33, for Perryman #3 at 15 mph with brakes enabled. 115

6.22: PC scores for Perryman #3 at 15 mph with brakes enabled pressure variables, half of data. 119

6.23: Input measurement components to PCs 32 and 33 for Perryman #3 at 15 mph with brakes enabled, half of data. 120

6.24: PC scores for Perryman #3 at 15 mph with brakes disabled pressure variables. ...124

6.25: Input measurement components to PCs 11, 12, 13, and 14 for Perryman #3 at 15 mph with brakes disabled. 125

7.1: Input variables. 130

7.2: Lowest average prediction errors for Belgian Block and Perryman #3 test runs. 140

7.3: Forward selection R^2 values for Belgian Block and Perryman #3 145

7.4: Average regression error for selected variables using test data from Belgian Block and Perryman #3 at 15 mph with brakes enabled. 147

8.1: Fatigue life estimates in hours. 153

8.2: Fatigue life estimates in miles. 153

8.3: Minimum error and from original life prediction and corresponding cutoff frequencies. 156

8.4: Minimum error and corresponding cutoff frequencies 158

8.5: Fatigue life estimates and prediction errors at a cutoff frequency of 17.172 Hz. 159

8.6: Minimum error and corresponding cutoff frequencies for model using unfiltered strain data for model training 160

8.7: Fatigue life estimates and prediction errors from model trained with unfiltered strain data, at a cutoff frequency of 16.667 Hz. 160

8.8: Fatigue life estimates and prediction errors from model trained with unfiltered strain data, at a cutoff frequency of 17.172 Hz. 162

9.1: Best fit for each model type and data set. 166

9.2: Best fit for SS model for each training (model) and test data set. 169

9.3: Error and life prediction for SS model of concatenated data for various test data sets. 170

LIST OF FIGURES

FIGURE **PAGE**

1.1: HMT towed by a HMMWV. 2

1.2: High-mobility trailer. 2

1.3: Broken drawbar. 3

1.4: Trailers in desert. 4

1.5: Vibration mode 1. 5

1.6: DADS model and simulation. 5

1.7: Drawbar life prediction using DRAW software. 7

1.8: PSD from Perryman #3 test course. 8

1.9: TSS/VSS accelerometer mounting location. 10

1.10: TSS/VSS controller located in cab of vehicle. 10

4.1: Strain gage rosette at failure location. 30

4.2: Accelerometers and strain gages on drawbar of HMT. 31

4.3: HMT testing instrumentation 32

4.4: Tri-axial accelerometer and rate gyro at trailer CG location. 32

4.5: Longitudinal strain averages for each rosette direction 37

4.6: Longitudinal strain peaks for each rosette direction. 38

4.7: Longitudinal strain RMS for each rosette direction. 38

4.8: Long. strain percentiles for each rosette direction (brakes disabled). 39

4.9: Long. strain percentiles for each rosette direction (brakes enabled). 39

4.10: Comparing strain and principal strain. 40

4.11: Average vertical accelerations for several trailer locations....................................42

4.12 Average transverse accelerations for several trailer locations.................................42

4.13: Average longitudinal accelerations for several trailer locations. 43

4.14: Vertical RMS accelerations for several trailer locations..43

4.15: Transverse RMS accelerations for several trailer locations. 44

4.16: Longitudinal RMS accelerations for several trailer locations. 44

4.17: Peak vertical accelerations for several trailer locations..45

4.18: Peak transverse accelerations for several trailer locations. 45

4.19: Peak longitudinal accelerations for several trailer locations. 46

4.20: Vertical accel. statistics for several trailer locations (brakes disabled)..................46

4.21: Vertical accel. statistics for several trailer locations (brakes enabled)...................47

4.22: Transverse accel. statistics for several trailer locations (brake disabled)................47

4.23: Transverse accel. statistics for several trailer locations (brake enabled)................48

4.24: Long. accel. statistics for several trailer locations (brake disabled)........................48

4.25: Long. accel. statistics for several trailer locations (brake enabled).........................49

4.26: Trailer CG pitch rate statistics...50

4.27: Trailer CG roll rate statistics. 51

4.28: Trailer CG yaw rate statistics. 51

4.29: Trailer CS shock displacement statistics. 53

4.30: Trailer RS shock displacement statistics. 53

4.31: Trailer master cylinder pressure statistics. 55

4.32: Trailer CS wheel cylinder pressure statistics...55

4.33: Trailer RS wheel cylinder pressure statistics............56

4.34: Principal strain 1 for experimental and simulated data. 57

4.35: Principal strain 2 for experimental and simulated data. 58

4.36: PSD of principal strain 1 for experimental and simulated data. 59

4.37: PSD for principal strain 2 for experimental and simulated data............59

5.1: PSD conversion Fortran subroutine............64

5.2: Belgian Block terrain data. 66

5.3: Perryman #3 terrain data............67

5.4: Belgian Block FFT. 68

5.5: Perryman #3 FFT. 68

5.6: Belgian Block PSD. 69

5.7: Perryman #3 PSD. 69

6.1: Typical hydraulic surge brake hitch assembly 72

6.2: Surge brake response for Belgian Block at 15 mph with brakes enabled. 77

6.3: Surge brake response for Belgian Block at 15 mph with brakes disabled. 78

6.4: Surge brake response for Perryman #3 test course at 15 mph. 81

6.5: Surge brake response for Perryman #3 at 15 mph with brakes disabled. 82

6.6: Residual plot for Belgian Block at 15 mph with brakes enabled longitudinal strain regression model, with interaction terms and brake pressure data included. 87

6.7: Residual plot for Belgian Block at 15 mph with brakes enabled longitudinal strain regression model, with interaction terms and brake pressure data removed. 87

6.8: Residual plot for Belgian Block at 15 mph with brakes enabled longitudinal strain regression model, without interaction terms and brake pressure data included. 89

6.9: Residual plot for Belgian Block at 15 mph with brakes enabled longitudinal strain regression model, without interaction terms and brake pressure data removed. 89

6.10: Residual plot for Belgian Block at 15 mph with brakes disabled longitudinal strain regression model, with interaction terms included and brake pressure data removed. 93

6.11: Residual plot for Belgian Block at 15 mph with brakes disabled longitudinal strain regression model, without interaction terms and brake pressure data removed. 94

6.12: Residual plot for Belgian Block at 15 mph with brakes disabled and enabled longitudinal strain regression model with interaction terms, brake pressure data and class included. 98

6.13: Residual plot for Belgian Block at 15 mph with brakes disabled and enabled longitudinal strain regression model with interaction terms, brake pressure data removed and class included. 98

6.14: Residual plot for Belgian Block at 15 mph with brakes disabled and enabled longitudinal strain regression model with interaction terms, brake pressure data included and class removed. 99

6.15: Residual plot for Belgian Block at 15 mph with brakes disabled and enabled longitudinal strain regression model with interaction terms, brake pressure data and class removed. 99

6.16: Percent of information explained by each PC for Belgian Block at 15 mph..........103

6.17: PC 1 vs. PC2 for Belgian Block at 15 mph with brakes enabled. 105

6.18: Average strain prediction error for Belgian Block at 15 mph with brakes enabled. 106

6.19: Correlation coefficient between Z scores and training data for Belgian Block at 15 mph with brakes enabled. 106

6.20: Percent of information explained by each PC for Perryman #3 at 15 mph with brakes enabled. 113

6.21: PC 1 vs. PC2 for Perryman #3 at 15 mph with brakes enabled.............................115

6.22: Average strain prediction error for Perryman #3 at 15 mph with brakes enabled..117

6.23: Correlation coefficient between Z scores and training data for Perryman #3 at 15 mph with brakes enabled. 117

6.24: Percent of information explained by each PC for Perryman #3 at 15 mph with brakes enabled, half of data. 119

6.25: PC 1 vs. PC2 for Perryman #3 at 15 mph, brakes enabled, half of data....120

6.26: Average strain prediction error for Perryman #3 at 15 mph with brakes enabled, half of data. 122

6.27: Correlation coefficient between Z scores and training data for Perryman #3 at 15 mph with brakes enabled, half of data. 122

6.28: Percent of information explained by each PC for Perryman #3 at 15 mph with brakes disabled....124

6.29: PC 1 vs. PC2 for Perryman #3 at 15 mph with brakes disabled....126

6.30: Average strain prediction error for Perryman #3 at 15 mph with brakes disabled.127

6.31: Correlation coefficient between Z scores and training data for Perryman #3 at 15 mph with brakes enabled, half of data. 127

7.1: Regression output for Belgian Block at 15 mph with brakes disabled, decimated by 6 using all variables. 130

7.2: Regression output for Belgian Block at 15 mph with brakes enabled, decimated by 6 using all variables. 131

7.3: Error in single variable prediction for Belgian Block decimated by 6....131

7.4: PSD for longitudinal strain for Belgian Block at 15 mph. 133

7.5: Regression output for Belgian Block at 15 mph with the brakes disabled and decimated by 25, using all variables....134

7.6: Regression output for Belgian Block at 15 mph with the brakes enabled and decimated by 25, using all variables....134

7.7: Error in single variable prediction for Belgian Block at 15 mph data decimated by 25. 135

7.8: Regression output for Perryman #3 at 15mph with brakes disabled and decimated by 25, using all variables. 137

7.9: Regression output for Perryman #3 at 15mph with brakes enabled and decimated by 25, using all variables. 137

7.10: Error in single variable prediction for Perryman #3 at 15mph, decimated by 25..138

7.11: Effects of filter cutoff frequency on average error from Belgian Block at 15 mph with brakes disabled and decimated by 25. 140

7.12: Effects of filter cutoff frequency on average error from Belgian Block at 15 mph with brakes enabled and decimated by 25. 141

7.13: Effects of filter cutoff frequency on average error from Perryman #3 at 15 mph with brakes disabled and decimated by 25. 141

7.14: Effects of filter cutoff frequency on average error from Perryman #3 at 15 mph with brakes enabled and decimated by 25. 142

7.15: Effects of filter cutoff frequency on strain data from Perryman #3 at 15 mph with brakes disabled and decimated by 25. 144

7.16: Effects of filter cutoff frequency on strain data from Perryman #3 at 15 mph with brakes enabled and decimated by 25. 144

8.1: S-N curve fitted for WAFO. 150

8.2: Rainflow cycle count. 151

8.3: Rainflow amplitude distribution. 151

8.4: Effects of cutoff frequency on fatigue life prediction. 154

8.5: Effects of cutoff frequency on fatigue life prediction, given and predicted strains. 154

8.6: Fatigue life of the data set after filtering compared to the predicted fatigue life after filtering. 156

8.7: Effects of cutoff frequency on fatigue fife prediction error from original estimate using filtered training data. 157

8.8: Effects of cutoff frequency on fatigue life prediction error from original estimate using filtered accelerations and unfiltered strain training data. 160

9.1: Model output for Perryman #3 at 15 mph without brakes 166

9.2: Model output for Perryman #3 at 15 mph with brakes. 167

9.3: Model output for Belgian Block at 15 mph without brakes. 167

9.4: Model output for Belgian Block at 15 mph with brakes. 168

9.5: Model output for concatenated data set...168

9.6: Simulated output for concatenated data set for various SS models.........................169

9.7: Simulated and measured SS model output for concatenated data set.................171

Nomenclature

Units

deg/sec	degrees per. second
ft	feet
g's	gravity
Hz	hertz
in	inches
ksi	thousand pounds per. square inch
mph	miles per. hour
psi	pounds per. square inch
sec	seconds
µinch	microinch
µinch/inch	microinch per. inch

Abbreviations

Accel.	Acceleration
ALT	Accelerated Life Testing
ARMAX	Auto-Regression Moving Average with eXogenous inputs
ARX	Auto-Regression with eXogenous inputs
ATC	Aberdeen Test Center
BJ	Box Jenkins
BS	British Standard Institution
Btm.	Bottom
CAD	Computer Aided Drafting
CG	Center of Gravity

CMS	Component Mode Synthesis
Cos	Cosine
CS	Curbside
Cyl.	Cylinder
DADS	Dynamic Analysis Design System
Disp.	Displacement
DRAW	Durability and Reliability Analysis Workspace
Drwbr.	Drawbar
E	Elastic Modulus
FEA	Finite Element Analysis
FFT	Fast Fourier Transform
For.	Forward
Fs	Sampling Frequency
GE	Generalized Erying
HMMWV	High Mobility Multi-purpose Wheeled Vehicle
HMT	High Mobility Trailer
IPL	Inverse Power Law
ISO	International Organization for Standardization
L	Longitudinal
Long.	Longitudinal
N/A	Not Applicable
NASA	National Aeronautics and Space Administration
OE	Output Error
PC	Principal Component
PCA	Principal Component Analysis
PoF	Physics of Failure
Press.	Pressure

PSD	Power Spectral Density
R^2	Coefficient of Determination
RMS	Root Mean Square
RS	Roadside
Sin	Sine
S-N	Stress-Life
SS	State-Space
SVD	Singular Value Decomposition
T	Transverse
Trans.	Transverse
Triang.	Triangle
TSS/VSS	Terrain Sensor System / Vibration Severity Sensor
V	Vertical
Var.	Variable
Vert.	Vertical
WAFO	Wave Analysis for Fatigue and Oceanography
YPG	Yuma Proving Grounds

Chapter 1 Introduction

Vehicle durability, which defines the useful life of a vehicle, is a high priority for some consumers. Recently, the U.S. Army has begun to assess vehicle durability in terms of life consumption, and is currently supporting research into a "physics of failure" approach to monitoring vehicle life consumption based on fatigue. Life consumption monitoring can be used to determine fatigue damage by directly or indirectly monitoring the loads placed on critical vehicle components that are susceptible to failure from fatigue damage. By monitoring vehicle life consumption, the Army can predict mechanical failures before they occur and prevent mission critical breakdowns. Life consumption monitoring also decreases maintenance costs by improving maintenance and parts handling, and by determining the useful life of vehicles so that well used vehicles can be retired instead of unnecessarily repaired.

1.1 Project Background

The example vehicle for this study is the M1101 High Mobility Trailer (HMT), which is normally towed behind a High Mobility Multi-purpose Wheeled Vehicle (HMMWV), as shown in Figure 1.1. The HMT, shown in Figure 1.2, is a small trailer that is used to carry a payload both on and off road. The trailer has hydraulic surge brakes that slow the trailer as the HMMWV decelerates.

As originally designed, the HMT experiences a fatigue failure of the drawbar, as shown in Figure 1.3. Note that the surge brake assembly and the safety chains are located on the broken portion of the drawbar. This failure allows the trailer to break

Figure 1.1: HMT towed by a HMMWV.

Figure 1.2: High-mobility trailer.

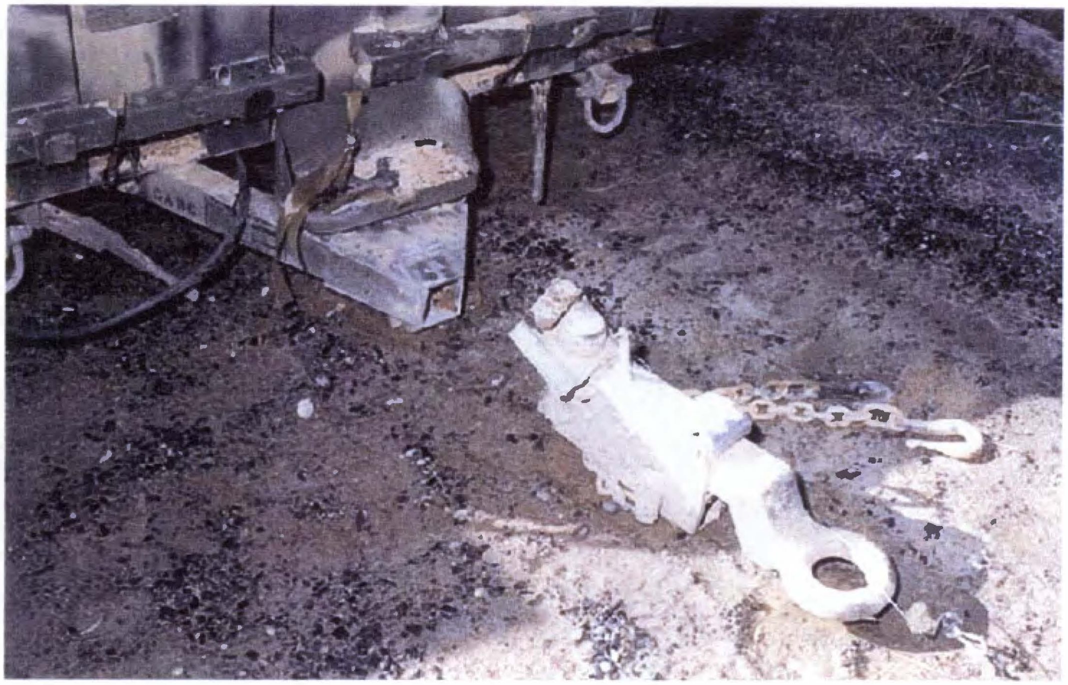

Figure 1.3: Broken drawbar.

free from the HMMWV and is a serious safety hazard. Due to this hazard, the Army temporarily removed six thousand trailers from service and parked them in the desert at the Yuma Proving Grounds (YPG), as shown in Figure 1.4, until the drawbar was redesigned for increased durability. Due to its known durability problems, the HMT was selected as the test case for a physics of failure (PoF) project to show the advances in computer simulation of durability prediction (TTCP, 2001).

To create an accurate simulation and analysis, the trailer was first modeled using Pro/Engineer. In the computer aided drafting (CAD) model, each component of the trailer shares a common reference frame and parameters. The CAD model was then verified by a comparison of its geometry and mass properties to those of the actual trailer.

The CAD model of the HMT was then meshed and analyzed using NASTRAN

Figure 1.4: Trailers in desert.

finite element analysis (FEA) software to determine the vibrational modes of the trailer using an eigenmode analysis. The first non-rigid body mode is shown in Figure 1.5. The first mode is at 18.92 Hz, and is the roll motion of the trailer. The second mode is a yaw motion at 21.55 Hz, and the third mode is a pitch motion at 26.3 Hz.

The CAD model was also exported to the multibody dynamics analysis program Dynamic Analysis Design System software (DADS). DADS creates a simulation that uses a multibody dynamics approach to determine a time history of the forces and accelerations on the trailer. A rigid body model was created directly from the CAD model of the trailer. This model required additional information that did not appear in the CAD model, such as suspension and tire spring rates. As shown in Figure 1.6, the trailer model was combined with a model of a HMMWV tow vehicle and simulated using measured test course terrain data.

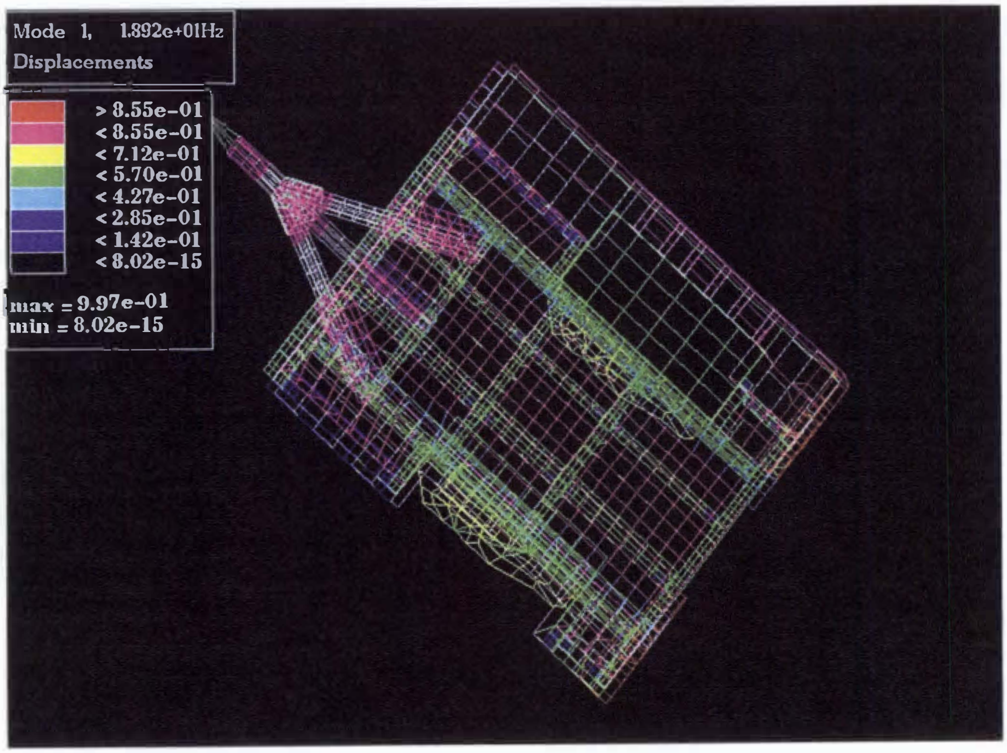

Figure 1.5: Vibration mode 1.

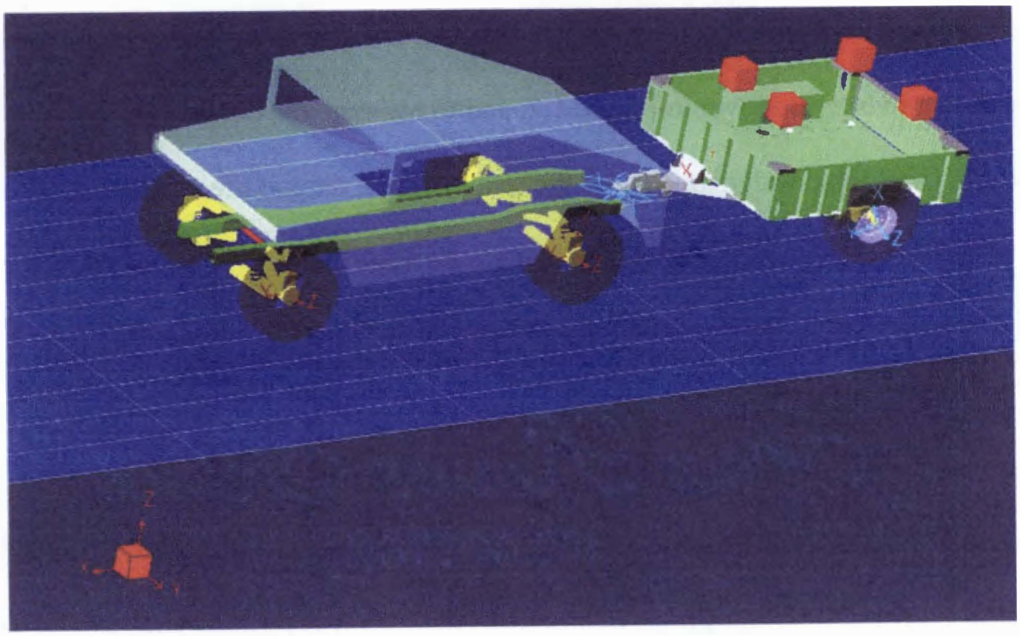

Figure 1.6: DADS model and simulation.

A flexible body model was then created from the rigid-body model by component mode synthesis (CMS) using a Craig-Bampton mode set (TTCP, 2001; Medepalli, 2000). The Craig-Bampton mode set (Craig and Bampton, 1968) utilizes the eigenmode solution of the constrained finite element model along with static correction modes, which represent the stiffness influence of the boundary conditions. For the flexible-body model, the three eigenmodes with the lowest natural frequencies were used. The modes are vertical and longitudinal bending and torsion. The eigenmodes are the vibrational modes of the trailer. Another simulation was run that analyzed the load history at the axles and lunette, and distributed inertial loading for the flexible body model.

The flexible body multibody dynamics model of the original trailer was simulated on several test courses at the Aberdeen Test Center (ATC). The dynamic load histories from the test course simulations and the Durability and Reliability Analysis Workspace (DRAW) (Iowa, 1998) software were used to predict the failure point on the drawbar, as shown in Figure 1.7, and to estimate the durability. The DRAW analysis includes dynamic stress computation and fatigue life prediction. The dynamic stress computation is based on linear elastic FEA and provides a nodal dynamic stress history. The dynamic stress history is used for the fatigue life prediction. The fatigue life prediction is divided into two parts: initiation and propagation. The fatigue crack initiation life prediction uses a multiaxial local strain approach, and failure is assumed to occur when the crack has reached 2mm in length. The fatigue crack propagation life prediction uses the FLAGRO software developed by NASA.

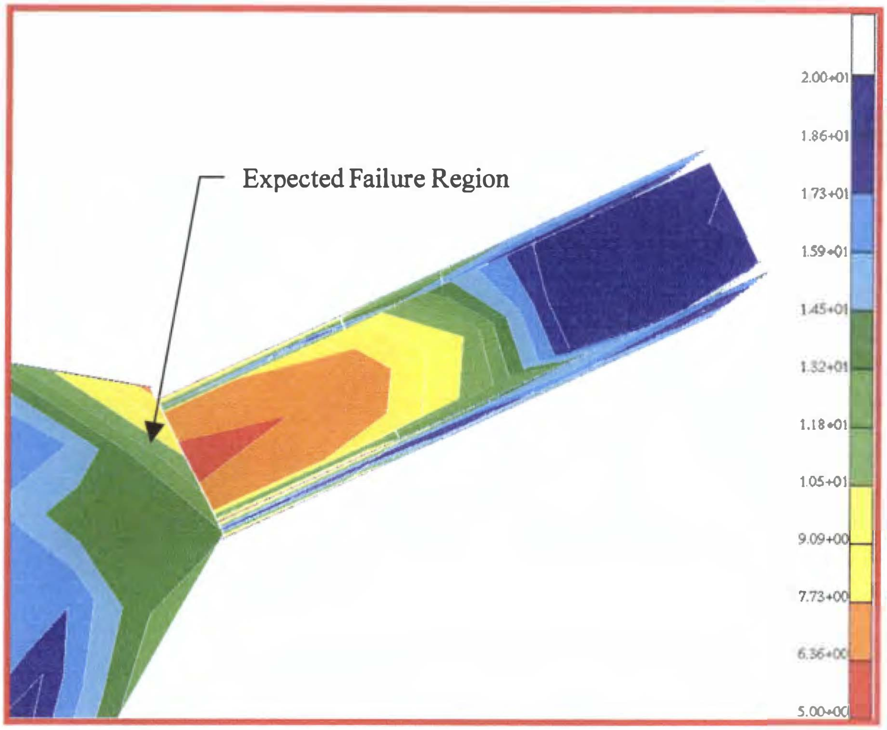

Figure 1.7: Drawbar life prediction using DRAW software.

To create an analysis and simulation, a representative re-creation of the vehicle and terrain must be made. The DADS program provides a representative vehicle simulation. A re-creation of the terrain must then be used in DADS to complete the simulation, so that it can provide a representation of the vehicles dynamic response that can be analyzed using known test data. Currently, experimental data for single test runs over several ATC test courses are used for the simulations.

The Army stores the terrain profile for each test course at the ATC in the form of a power spectral density (PSD) using the British Standard Institution BS 7853 and International Organization for Standardization ISO 8606, as shown in Figure 1.8. For the PSD to be used by DADS, it will have to be converted back to spatial data. This will give a statistically equivalent model for the course that was used to collect data for

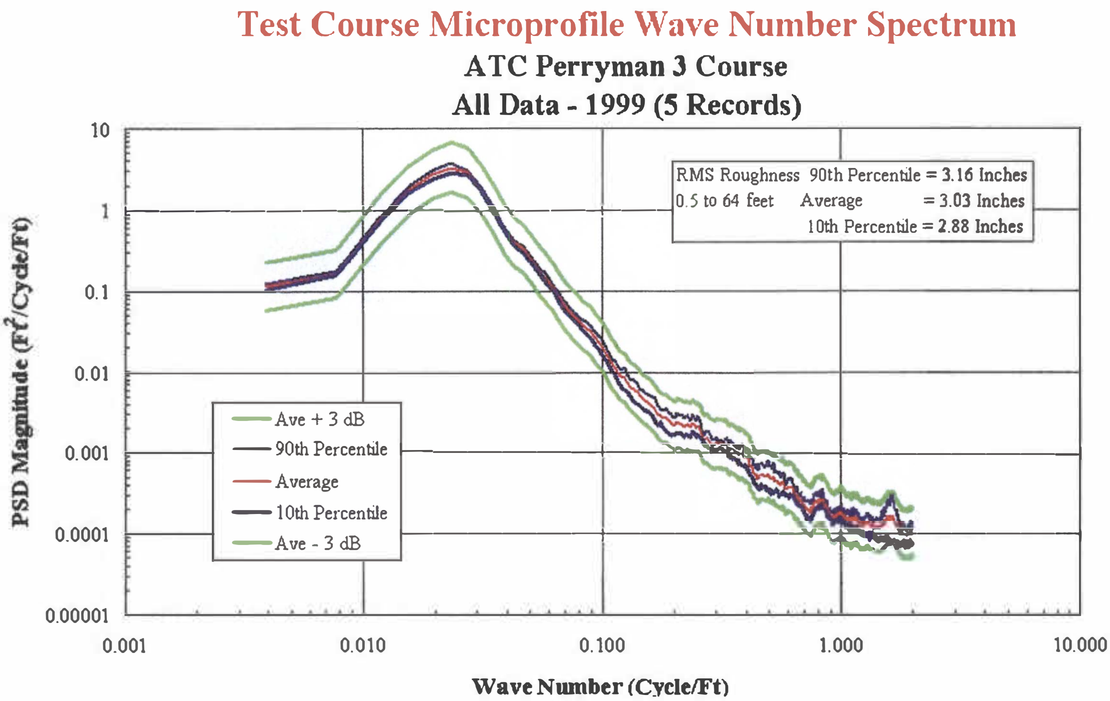

Figure 1.8: PSD from Perryman #3 test course.

the PSD. The conversion of the PSD to statistically equivalent spatial data is an initial step in determining if stored terrain data can be used with the DADS program.

1.1.1 Terrain Sensing

A second Army (PoF) project deals with life-consumption monitoring using the Terrain Sensor System/Vibration Severity Sensor (TSS/VSS) developed by the Defence Science and Technology Laboratory in the UK. It was noted in a recent task outcome report that "A process was developed to calculate life consumed (or damage accumulated) on a critical component of a U.S. Army trailer, based on real-time monitoring of the severity of the vibration experienced by the trailer." (TTCP, 2001)

The TSS/VSS attempts to calculate the damage to a vehicle indirectly, by using a single sensor (accelerometer) mounted to the axle of the tow vehicle, similar to Figure 1.9. The TSS/VSS monitors the cumulative time traveled on each of five terrain types (stopped, smooth, rough, off-road, and cross country), which are recorded by a controller located in the cab of the vehicle, as shown in Figure 1.10.

The signal from the accelerometer is filtered at a pass-band of 1 to 20 Hz. The peak accelerations are averaged over 10 to 20 seconds and then recorded as one of the five terrain types (TTCP, 2001). The five terrain types selected for the use by the TSS/VSS for the life prediction are classified by BS 7853, which is identical to ISO 8606. This standard defines terrain types based on the road's PSD and spatial frequency.

The data collected by the TSS/VSS is analyzed by a simple algorithm that calculates "trailer damage per time on an equivalent terrain class." (TTCP, 2001) The limitations of this type of system are that monitoring the life consumption from a single sensor is inaccurate and that one or more vehicles have to be tested until failure to determine the vehicle's life. The TTCP report states "The TSS/VSS was not designed to determine the actual terrain or speed, which is not important for this life-consumption monitoring application." The TTCP report also states "Given its actual function, the TSS name is a misnomer because the system does not sense the terrain, but the severity of the vibration loads." This system is the current state of the art in ground vehicle life consumption monitoring and is currently being tested in Europe (TTCP, 2001).

The dynamic vehicle model and use of terrain data are the two elements needed to evaluate life consumption during the initial design process. This information about

Figure 1.9: TSS/VSS accelerometer mounting location.

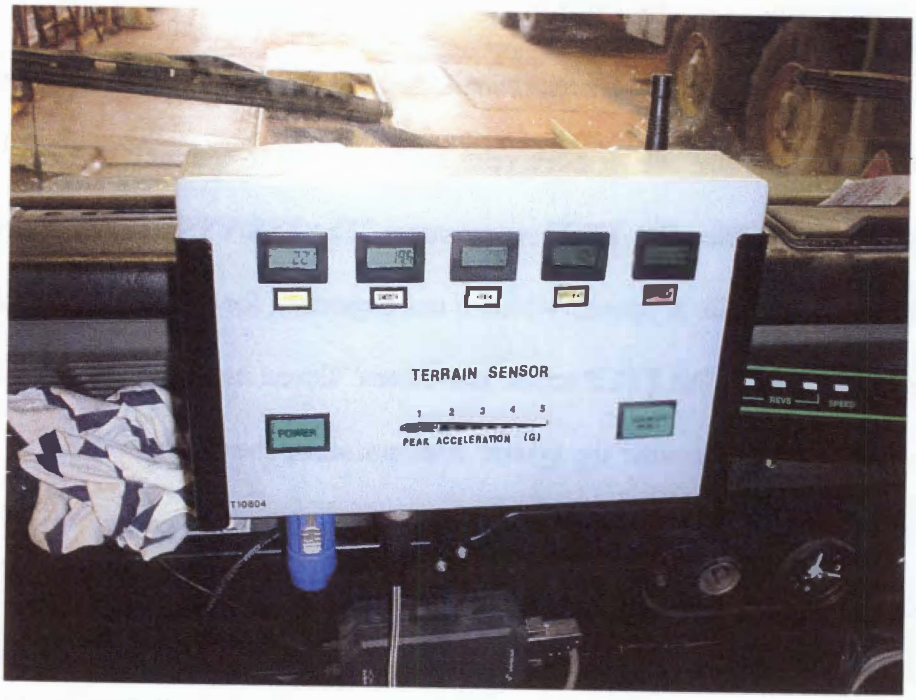

Figure 1.10: TSS/VSS controller located in cab of vehicle.

the data and model creation will lead to the ability to monitor the strain at the failure location directly, as the TSS/VSS attempts to do indirectly.

1.3 Project Objectives

This project is a step in the process of life consumption monitoring that will determine if vehicle failure due to fatigue can be predicted, and therefore prevented, and will answer the question "Can a model and accelerometer measurements be used to predict the life of the trailer?" In the future, this modeling process could eventually be used to determine the useable life of other vehicles during the initial design process, as well as for determining and preventing future failures. This research will investigate the use of models and simulation to determine the life of a vehicle during the design process and to analyze future failures.

1.4 Project Scope

This research has a scope of work that aims to advance the current technology of vehicle life-consumption monitoring. Data from the HMT being driven over known test courses will be analyzed. The experimental data for the Perryman #3 test course will be filtered at frequencies appropriate for the data collection methods and for use in comparison to the HMT simulation results. The univariate statistics of the data will be determined.

The experimental data from the HMT traversing the Belgian Block and Perryman #3 test courses at 15 mph, with the surge brake both enabled and disabled, will be used for the analysis to determine if the surge brake has an effect on life of the

HMT and is required in the DADS simulation. This will also determine if design improvements need to be made to the trailer's braking system. This analysis will use multivariate regression and principal component analysis (PCA). The data used in the current DADS simulation will be for the Perryman #3 test course. The simulation results using the Perryman #3 test data will be compared to the data of the 15 mph run with the surge brake enabled. This comparison will validate the use of the simulation.

The number and location of appropriate sensors for monitoring life-consumption of the HMT drawbar will also be determined by regression analysis of the collected data. The data collected from the Belgian Block and the Perryman #3 courses at 15 mph will be used to determine if the sensor and data collection procedure used in the TSS/VSS is appropriate for use with the HMT.

The appropriate signal processing and model type will be determined. The use of an appropriate model will provide accurate monitoring of the strain at the predicted point of failure. Appropriate signal processing will limit the amount of processed information, while maintaining accuracy.

An analysis of the measured terrain profiles that are stored as PSDs will be performed. The analysis will consist of determining if the PSDs can be actively used to create an appropriate simulation of the terrain type. The method of actively re-creating the terrain data will be written into a Fortran subroutine that will be the basis for another student's research that will implement the subroutine in the DADS simulation to eliminate the need for measured terrain data in the simulation.

Chapter 2 Literature Review

2.1 Terrain Monitoring

The TTCP report (2001) 'Physics of Failure Approach to Life Consumption Monitoring' details the use of the TSS/VSS for life consumption monitoring. The TSS/VSS falls short by not accounting for the accelerations that correlate directly to the loads that are causing the trailer failure. The TSS/VSS may monitor the severity of vibration, but it still has to categorize the vibration as a terrain type. The use of the terrain type does not differentiate between differences in vibrations within that category. A well-placed accelerometer or group of accelerometers could estimate the damage directly. This would produce a more accurate estimate of life consumption.

2.2 Durability Analysis

Srikantan, Yerrapalli, and Keshtkar (2000) discuss vehicle durability and fatigue analysis, using data from proving ground testing. They discuss the differences between yield strength based durability analysis and fatigue analysis. Fatigue analysis reduces the design cycle and produces a more optimally designed structure. The authors concentrate on the design of truck body structures and the severe duty cycles that accompany them. The loads from proving ground tests of similar vehicles are used in simulations to determine the fatigue life of the vehicle. The simulation used to calculate fatigue is MSC/FATIGUE while the stresses are determined using MSC/NASTRAN. When fatigue life design criteria are met a prototype is then built and tested. If the design criteria are not met the prototype is modified. The results from a correlation study showed the analytical strains from FEA and proving ground tests correlated very well.

Medepalli and Rao (2000) discuss the prediction of road loads for fatigue design. They discuss the use of computer simulations to predict road loads early in the design process, before a prototype vehicle is built. Medepalli and Rao outline and validate a process for the prediction of road loads. The computer simulation used was created using ADAMS. ADAMS is similar to DADS in its rigid and flexible body dynamic analysis. The results obtained from the simulation were then correlated to measured road loads. The results showed that the flexible body models correlated more closely to the measured road loads. The results also showed that the predicted and measured loads were correlated very well.

Kim, Yim, and Kim (2002) also outline a method for simulating vehicle dynamics loads, but they add durability estimation. For their multibody dynamic analysis they use DADS and a flexible body model. The model was for a transit bus. For their dynamic stress analysis MSC/NASTRAN was used. The fatigue life was then calculated using a local strain approach. From the fatigue life analysis, it was determined that the majority of the fatigue damage occurred over a frequency range that depended on the terrain traveled (service or accelerated test course). This shows that the actual service environment can be simulated instead of using an accelerated testing environment. Since the durability results for the actual service environment can be obtained using a simulation, they can be determined early in the design process.

Zhang, Chuckpaiwong, Liang, and Seth (2002) discuss a method for determining a fatigue model from accelerated life testing (ALT). The models used are inverse power law (IPL) and generalized Erying (GE) models. The models can then be used to determine life estimations from ALT data. To use ALT models, some assumptions must be made. The first assumption is that only the accelerated stress should be applied while all other stresses are kept constant. The second assumption is that the failure mode should be the same for both accelerated and normal stress conditions. The third and fourth assumptions are that the accelerated test results should not be extrapolated to stress levels beyond the range of the model, and the model is applicable to the component being tested. The authors propose a modified model to solve the singularity problems associated with IPL models. When the stress is near zero (singularity) another main stress (thermal stress) is considered using the GE model. The authors then discuss the testing of a bearing to validate the proposed method. The model was created using two ALT runs and validated with three other ALT runs. Thermal effects were accounted for during each test. The mean error was found to be 7.34% for the three verified stress levels.

Cuyper, Coppens, Leighfooghe, Swevers, and Verhaegen discuss system identification as it relates to the simulation of service loads on multi axial durability test rigs. Durability test rigs are used to simulate service loads in place of road testing, so that vehicle durability can be determined. The authors discuss several methods including: measurements of frequency response functions (FRF's), FRF averaging based on coherence, matrix inversion using singular value decomposition (SVD). The use of SVD makes the inversion more stable. The correlation between the calculated and target fast Fourier transforms (FFTs) of the signals to be used for testing is determined using principal component analysis (PCA). The authors also discuss two additional methods:

time domain modeling and a method that combines FRF and a non-linear calibration curve for axle force and shaker displacement. The time domain models discussed are input-output and state space models. The input-output model discussed is the autoregressive moving average model (ARMAX). The authors then discuss results obtained using a 12-poster test rig. The results show a successful reproduction of all FFTs of target signals.

2.3 Parameter Identification

Parametric modeling of a system is commonly used when a physical model is unavailable or impractical. Statistical models are the most widely used parametric models. The text by Neter, Kutner, Nachtsheim, Wasserman (1996) discusses linear statistical models including regression analysis and identification of relevant parameters. Hines (1998) discusses the use of PCA for parameter identification and regression analysis.

When parametrically modeling a system, the relevant parameters to be used in the model must be identified. Several techniques including PCA are available and widely used to determine the parameters to be used in a parametric model of the system.

Cho and Kim (2002) discuss indirect input force identification in multi-source environments using PCA on the output variables. Conventional transmissibility function approaches are only applicable when the number of independent excitation sources is just one. The method discussed by the authors extends to cases where the number of sources is greater than one. The authors validate their technique using numerical example of an Euler beam. The beam is excited at three points with two random sources and the responses were generated at 19 points. Their results showed low errors except near the resonant frequencies. The reason given for the error is that only one mode is predominant although the number of source is two. The errors for the PCA were much lower than for the transmissibility function.

Serban and Freeman (2001) discuss the identification of unknown values for the parameters used in the nonlinear models of multibody dynamic systems. These parameter values are often unavailable or difficult to measure. The authors use a numerical test based on the condition number of a matrix constructed using first-order derivative information. The method was validated using a pendulum, slider-crank, and HMMWV examples.

The literature reviewed discuss the current methods used for terrain monitoring, durability analysis, and parameter identification. Using parameter identification techniques, the appropriate sensors for monitoring the durability of the trailer can be made. Once the sensors are identified, appropriate methods for monitoring the durability of the trailer can then be determined.

Chapter 3 Method

In order to determine the most appropriate sensor for collecting data needed for predicting the fatigue life of the trailer, an analysis of experimental data was performed. The experimental data was taken from a HMT traveling over a known test course. The data was taken for 45 test runs at 8 speeds, over 6 test courses that have known terrain profiles, and with the trailer brakes both enabled and disabled. The data sets used in the current analysis are for the Belgian Block course at 15mph and the Perryman #3 course at 15mph, with the brakes both enabled and disabled.

The trailer was instrumented with 59 sensors, discussed in Chapter 4, which included strain gages, accelerometers, rate gyros, shock absorber displacements, brake pressures, and ground speed. The failure at the drawbar corresponds to the forces on the drawbar, which can be determined from the strain gage data. The failure location has also been determined by DRAW, as shown previously in Figure 1.8. This figure shows the failure region in red, which corresponds to the shortest life as shown on the legend.

Multivariate regressions (Neter et al., 1996) and principal component analysis (PCA) (Hines, 1998) will be used to determine which sensors most accurately reflect the loads on the drawbar at the failure point.

From the regression model created using the appropriate sensors, the fatigue life will be calculated using the Wave Analysis for Fatigue and Oceanography (WAFO) software package. WAFO (WAFO Group, 2000) uses a stress-based approach to fatigue life calculation, which is appropriate for the high cycle fatigue present in monitoring vehicle fatigue. WAFO uses the Wohler curve fit and the Palgrem-Miner rule to calculate fatigue damage from rainflow counting and the S-N curve, as described below in section 3.3.

Appropriate re-sampling of the data will be made using decimation and filtering will be made using a Butterworth filter. These techniques are discussed below in section 3.4. From the regression and fatigue calculations, an appropriate dynamic model will be made to determine the strain at the failure point from the series determined by the regression analysis.

3.1 Regression Analysis

Multivariate regressions are used for determining the linear relationship between a dependent variable (i.e. strain) based upon a set of independent variables (i.e. data channels). Regression analysis is used for description, control, and prediction of data. To determine the relationship between the input data and the strain, at the expected point of failure, a regression analysis was performed. The linear regression model has the general form:

$$Y = \beta_0 + \mathbf{X}^T \beta + \varepsilon = \beta_0 + X_1\beta_1 + X_2\beta_2 + \cdots + \varepsilon \tag{3.1}$$

where Y is the response (output) variable, $\mathbf{X}$ is the independent (input) matrix, β_i are the model parameters, X_i are the independent (input) variables, and ε is an error term.

Interaction effects can also be added to the regression model. An interaction effect is the effect one predictor variable X_1 has on the interaction between another predictor variable X_2 and the response variable Y. With the addition of pair-wise interaction effects, the regression model has the addition of all possible pairs if predictor variables are multiplied together and added to **X**. The linear regression model with interaction terms has the form:

$$Y = \beta_0 + \mathbf{X}^T \beta + \varepsilon = \beta_0 + X_1\beta_1 + X_2\beta_2 + X_1X_2\beta_{12} + \cdots + \varepsilon\,. \tag{3.2}$$

The goodness-of-fit for a regression model can be measured by the coefficient of determination, R^2, which is simply the proportion of variance between the measured and predicted values of the response variable, Y. It reflects the ratio of the regression sum of squares to the total sum of squares, and is given by:

$$R^2 = \frac{\sum_{i=1}^{n}(Y_{hi} - Y_m)^2}{\sum_{i=1}^{n}\left[(Y_{hi} - Y_m)^2 + (Y_i - Y_{hi})^2\right]} \tag{3.3}$$

where the regression sum of squares is the squared sum of the differences between the fitted value, Y_{hi}, and the mean of the fitted values, Y_m, for n observations and the error sum of squares is the squared sum differences between the observation, Y_i, and the mean of the fitted values, Y_m. The total sum of squares measures the uncertainty of predicting Y, when the predictor variables are not considered. The total sum of squares is the sum of both the error and regression sum of squares. It measures the variation in the measured values, Y_i, when the predictor variables X are considered. The closer the value of R^2 is to unity, the closer the observations Y are to the regression model and the greater the degree of linear association between the input variables, **X**, and the predicted response variable, Y.

The R^2 value is a measurement of the goodness of fit of the model, but it is also necessary to determine the accuracy of the regression model in terms of error in prediction. The error can be determined by simply comparing the predicted values from the model with the data it is predicting. This gives an average error that can be used to determine the accuracy of the model. The accuracy is usually tested by dividing the data set into halves. One half of the data set is used to create the model and the second half is used for testing the model.

3.2 Principal Component Analysis (PCA)

Principal component analysis identifies variables or groups of variables that represent the behavior of the system. Each principal component (PC) is a linear combination of the original data and thus forms a vector basis for the data. The transformed vectors are uncorrelated and orthogonal, which allow them to be used in regressions without collinearity problems, effectively removing interactions.

Since there are an infinite number of ways to construct the vector basis, the principal component technique defines the basis to be constructed such that the first principal component describes the direction of maximum variance, and each succeeding principal component is defined to be orthogonal to all previous principal components and to have the maximum variance of all remaining choices. By neglecting the PCs that do not contain a significant amount of variability, a systematic reduction in the size of the input data can be made without losing significant information in the data.

In the context of this analysis, the input space X, which consists of all the accelerometer, rate gyro, linear position and brake pressure data, is transformed into an orthogonal space Z using a transformation matrix α:

$$\{z\} = [\alpha]\{x\} \tag{3.4}$$

This transformation is performed sequentially by first creating a variable z_1 that is a linear combination of the input data channels, x_j, and has maximum variance with respect to the data.

$$z_1 = \alpha_{11}x_1 + \alpha_{12}x_2 + \cdots + \alpha_{1p}x_p = \sum_{j=1}^{p} \alpha_{1j}x_j \tag{3.5}$$

A second variable, z_2, is then created. This variable has maximum variance with respect to the remaining data, and is uncorrelated (ie. orthogonal) to z_1.

$$z_2 = \alpha_{21}x_1 + \alpha_{22}x_2 + \cdots + \alpha_{2p}x_p = \sum_{j=1}^{p} \alpha_{2j}x_j \tag{3.6}$$

This process continues until p uncorrelated principal components are found and are arranged in order of decreasing variance. The values of the PC scores show how each input variable is weighted. The percent explained by each principal component shows how much variance is explained in by each PC.

$$\%\text{explained} = \frac{\text{variance}_j}{\sum_{j=1}^{p} \text{variance}_j} \cdot 100\% \tag{3.7}$$

The principal components are calculated from the covariance matrix. The principal components are the eigenvectors of the covariance matrix with the first eigenvector corresponding to the largest eigenvalue (λ) and therefore the most variance. The latent variables are the eigenvalues of the covariance matrix. The eigenvectors are orthogonal, and the sum of the eigenvalues equals the total variance of the original data. From the eigenvalues the amount of information explained by each PC can be computed.

$$\%\text{explained} = \frac{\lambda_j}{\sum_{j=1}^{p} \lambda_j} \cdot 100\% \tag{3.8}$$

Singular value decomposition (SVD) is used for PCA because it is a method of calculating the eigenvectors and eigenvalues that is considered to be computationally efficient and stable. SVD decomposes a matrix X into a diagonal matrix L that contains the singular values which are the square roots of the eigenvalues of X^TX and are arranged in decreasing order, an orthogonal vector space A of the standardized PC scores, and an orthogonal vector space U of right singular values which are the eigenvectors, PCs, and result in the same matrix as the eigenvector matrix of the covariance.

$$\{X\} = \{A\}\{L\}\{U\}^T \tag{3.9}$$

The PC scores can be calculated by multiplying A by L.

$$\{z\} = \{A\}\{L\} \tag{3.10}$$

3.3 Fatigue Life Calculation

To develop an equation for damage at a given stress level, as it relates to the S-N curve, the techniques of rainflow counting will be combined with the Wohler fit to the S-N curve and the Palmgren-Miner fatigue damage rule. Rainflow counting (WAFO Group, 2000; Dowling, 1999) is used to divide variable amplitude loading into a series of cycles of maximums, M_k, and minimums, m_k^{RFC}, that give the amplitude for a given cycle, s_k^{RFC}:

$$s_k^{RFC} = M_k - m_k^{RFC} \tag{3.11}$$

The S-N curve is determined experimentally by testing material samples at a constant cyclic stress, S, until failure. The number of cycles until failure, N, are recorded and plotted against the corresponding stress for each test. The Wohler curve fits the S-N curve as a function N(s), where s is a given stress amplitude.

$$N(s)=K^{-1}s^{-\beta} \text{ for } s > s_\infty \text{ and } \infty \text{ for } s \leq s_\infty \tag{3.12}$$

The Palmgren-Miner linear damage accumulation theory states that damage is the sum of the number of cycles to failure at each stress level. Failure occurs when $D(t) = 1$.

$$D(t) = \sum_{t_k \leq t} \frac{1}{N(s_k)} \tag{3.13}$$

Combining the Wohler curve (3.12) and the Pamlgren-Miner rule (3.13) with the rainflow cycle distribution, we have an equation for damage at a given stress level, as it relates to the fit of the S-N curve.

$$D(t) = K \sum_{t_k \leq t} s_k^{\beta} \tag{3.14}$$

Using the amplitudes from the rainflow cycle, s_k^{RFC}, we have the following damage estimation for a given S-N curve and loading.

$$D(t) = K \sum_{t_k \leq t} (s_k^{RFC})^{\beta} \tag{3.15}$$

3.4 Decimation and Filtering

The decimation function in Matlab is used to filter and re-sample the data at a given level, R, which is 1/R times the original sample rate, Fs. The function uses an eighth order Chebyshev type-1 low pass filter with a cutoff frequency set at the 80 % of the new Nyquist frequency, 0.8*(Fs/2)/R. Once the data is filtered it is re-sampled to the given level.

The filter used for further filtering of the data was an 8 pole low pass digital Butterworth filter. The filter was applied with a zero-phase forward and reverse digital filter. This results in no phase distortion and magnitude modified by the square of the filter's magnitude response.

Chapter 4 Data Collection and DADS Validation

4.1 Test Setup

The data used for the analysis of the HMT; was collected by the United States Army at the U.S. Army Aberdeen Test Center (ATC). The data was collected for 45 test runs at 8 speeds, over 6 test courses that have known terrain profiles, and with the trailer brakes both enabled and disabled. The trailer was instrumented with 59 sensors, listed in Table 4.1, that included strain gages, accelerometers, rate gyros, shock absorber displacements, brake pressures, and ground speed.

The strain gauge rosettes were located at several points on the trailer. The strain gauge rosettes monitored strains in the transverse, 45 degree, and longitudinal directions. A total of eight strain gauge rosettes were used. Four of the strain gauge rosettes were located on the bottom of the drawbar. The analyses in this dissertation used the data from one rosette located on the bottom of the drawbar near the failure point, as shown in Figure 4.1.

Four single axis accelerometers were located at the frame attachment point for both the curbside (CS) and roadside (RS) suspension road arms, or close to the axle location on the road arms. The axis of the axle accelerometers changes due to movement of the suspension.

Seven tri-axial and four single axis accelerometers were used during the trailer testing. As can be seen in Figure 4.2, one of the tri-axial accelerometers was located on

Table 4.1: Data acquisition system channel assignments.

Channel #	Description	
5	Bottom Drawbar Center	Transverse strain
6		45 degree strain
7		Longitudinal strain
8	Bottom Drawbar Center Aft	Transverse strain
9		45 degree strain
10		Longitudinal strain
11	Bottom Drawbar Curbside Edge	Transverse strain
12		45 degree strain
13		Longitudinal strain
14	Bottom Drawbar Curbside Aft Edge	Transverse strain
15		45 degree strain
16		Longitudinal strain
17	Top Triangle Plate Corner	Transverse strain
18		45 degree strain
19		Longitudinal strain
20	Bottom Triangle Plate Corner	Transverse strain
21		45 degree strain
22		Longitudinal strain
23	Left Angle Plate Lower	Vertical strain
24		45 degree strain
25		Longitudinal strain
26	Left Angle Plate Upper	Vertical strain
27		45 degree strain
28		Longitudinal strain
29	Curbside Axle Acceleration	
30	Curbside Frame Acceleration	
31	Roadside Axle Acceleration	
32	Roadside Frame Acceleration	

Table 4.1: Continued.

33	Lunette Acceleration	Vertical (z)
34		Transverse (y)
35		Longitudinal (x)
36	Tongue Acceleration	Vertical (z)
37		Transverse (y)
38		Longitudinal (x)
39	Trailer CG Acceleration	Vertical (z)
40		Transverse (y)
41		Longitudinal (x)
42	Curbside Acceleration Forward	Vertical (z)
43		Transverse (y)
44		Longitudinal (x)
45	Curbside Acceleration Aft	Vertical (z)
46		Transverse (y)
47		Longitudinal (x)
48	Roadside Acceleration Forward	Vertical (z)
49		Transverse (y)
50		Longitudinal (x)
51	Roadside Acceleration Aft	Vertical (z)
52		Transverse (y)
53		Longitudinal (x)
54	Trailer CG	Vertical (z)
55		Transverse (y)
56		Longitudinal (x)
57	Curbside Shock Displacement	
58	Roadside Shock Displacement	
59	Longitudinal Ground Speed	
60	(not used)	
61	Master Cylinder Brake Pressure	

Table 4.1: Continued.

62	Curbside Wheel Brake Pressure
63	Roadside Wheel Brake Pressure

Figure 4.1: Strain gage rosette at failure location.

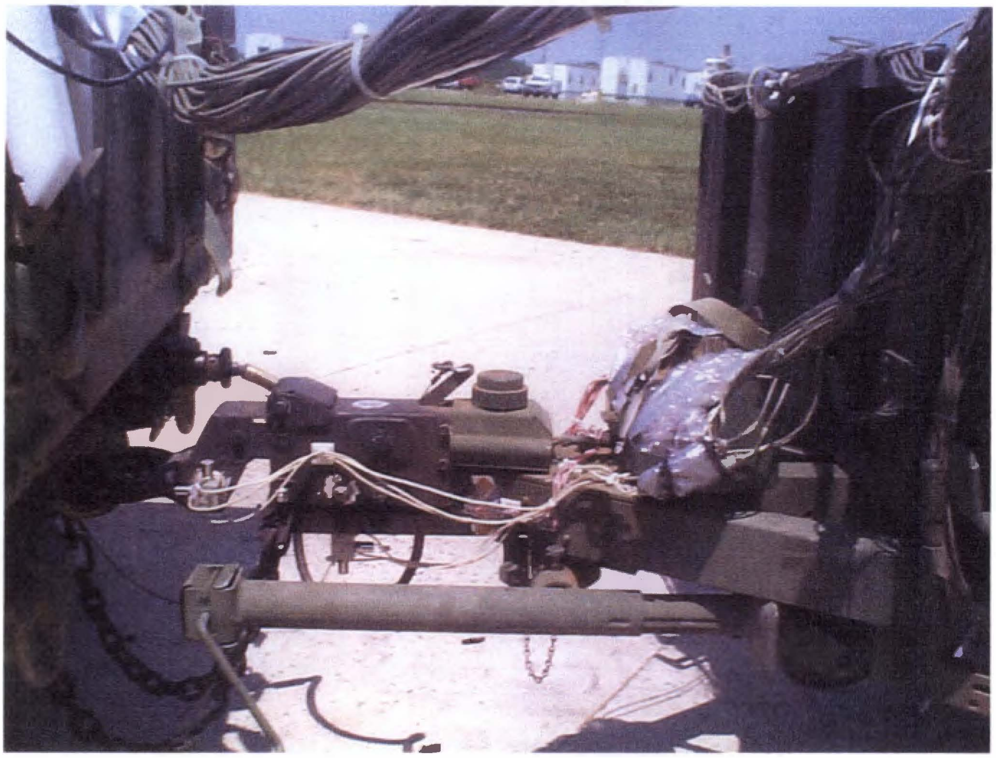

Figure 4.2: Accelerometers and strain gages on drawbar of HMT.

the lunette, and another on the trailer tongue. Significant differences between these two sets of transducers should only exist for experimental runs where the surge brake was active. Four tri-axial accelerometers were located at the corners of the cargo box, as shown in Figure 4.3. A rate gyro was used to measure the roll, pitch and yaw rates at the CG of the trailer, with a final tri-axial accelerometer to measure center of gravity (CG) accelerations, as shown in Figure 4.4.

Linear displacement transducers were used to measure shock absorber displacements and three pressure transducers were used to monitor brake pressures. The pressure transducers were located at the master cylinder, left wheel cylinder, and right wheel cylinder, respectively.

Figure 4.3: HMT testing instrumentation.

Figure 4.4: Tri-axial accelerometer and rate gyro at trailer CG location.

4.2 Test Data

The data used for the analysis in this dissertation was for the tests on the Belgian Block and Perryman #3 courses. The data collected over the two courses was for the brakes both enabled and disabled at a speed of 15 mph. The filenames for the test runs used, are shown in Table 4.2.

The Belgian Block Course is paved with uneven granite blocks that simulate a cobblestone road. The granite blocks are on average 13 cm (5 in) square. The course varies with a peak of approximately 8 cm (3 in). The course is approximately 1.2 km (0.75 mi) in length. The data from this course was used because it creates a random vehicle motion.

The Perryman #3 course is a cross-country course. It is a rough course composed of native soil that includes Sassafras loam and Sassafras silt loam. Dust is severe when the course is dry. Much of the course is rough due to many years of testing tank-type vehicles.

The data was collected at a frequency of 1262.626 Hz. The data was filtered with low-pass anti-aliasing filters. The cutoff frequency of the filter differed by the type of sensor being used on that channel, as shown in Table 4.3. The data was then stored in a comma delimited format with 59 columns, one for each data channel. The data files were stored in the format shown in Table 4.4.

Table 4.2: Test matrix data file names.

Course / Speed	Brakes	Test Run
Belgian Block / 15 mph	Off	Run010
	On	Run013
Perryman #3 / 15 mph	Off	Run055
	On	Run052

Table 4.3: Analog low-pass anti-aliasing cutoff frequencies.

Transducer Type	Filter Cutoff Frequency
Strain gauge	100 Hz
Accelerometer	200 Hz
Rate gyro	20 Hz
Linear position	20 Hz

Table 4.4: Experimental data file format.

Col #	Description	Units	Col. #	Description	Units
1	Time	sec	31	Lunette Accel (T)	g's
2	Btm Drwbr Cntr (T) strain	μ inch	32	Lunette Accel (L)	g's
3	Btm Drwbr Cntr (45) strain	μ inch	33	Tongue Accel (V)	g's
4	Btm Drwbr Cntr (L) strain	μ inch	34	Tongue Accel (T)	g's
5	Btm Drwbr Cntr Aft (T) strain	μ inch	35	Tongue Accel (L)	g's
6	Btm Drwbr Cntr Aft (45) strain	μ inch	36	Trailer CG Accel (V)	g's
7	Btm Drwbr Cntr Aft (L) strain	μ inch	37	Trailer CG Accel (T)	g's
8	Btm Drwbr CS Edge (T) strain	μ inch	38	Trailer CG Accel (L)	g's
9	Btm Drwbr CS Edge (45) strain	μ inch	39	CS Forward Accel (V)	g's
10	Btm Drwbr CS Edge (L) strain	μ inch	40	CS Forward Accel (T)	g's
11	Btm Drwbr CS Edge Aft (T) strain	μ inch	41	CS Forward Accel (L)	g's
12	Btm Drwbr CS Edge Aft (45) strain	μ inch	42	CS Aft Accel (V)	g's
13	Btm Drwbr CS Edge Aft (L) strain	μ inch	43	CS Aft Accel (T)	g's
14	Top Triang Plate Corner (T) strain	μ inch	44	CS Aft Accel (L)	g's
15	Top Triang Plate Corner (45) strain	μ inch	45	RS Forward Accel (V)	g's
16	Top Triang Plate Corner (L) strain	μ inch	46	RS Forward Accel (T)	g's
17	Btm Triang Plate Corner (T) strain	μ inch	47	RS Forward Accel (L)	g's
18	Btm Triang Plate Corner (45) strain	μ inch	48	RS Aft Accel (V)	g's
19	Btm Triang Plate Corner (L) strain	μ inch	49	RS Aft Accel (T)	g's
20	Left Angle Plate Lower (V) strain	μ inch	50	RS Aft Accel (L)	g's
21	Left Angle Plate Lower (45) strain	μ inch	51	Trailer CG Pitch Rate	deg/sec
22	Left Angle Plate Lower (L) strain	μ inch	52	Trailer CG Roll Rate	deg/sec
23	Left Angle Plate Upper (V) strain	μ inch	53	Trailer CG Yaw Rate	deg/sec
24	Left Angle Plate Upper (45) strain	μ inch	54	CS Shock Absorber Disp	Inches
25	Left Angle Plate Upper (L) strain	μ inch	55	RS Shock Absorber Disp	inches
26	CS Axle Accel (V)	g's	56	Surge Brake Pressure	psi
27	CS Frame Accel (V)	g's	57	CS Wheel Brake Pressure	psi
28	RS Axle Accel (V)	g's	58	RS Wheel Brake Pressure	psi
29	RS Frame Accel (V)	g's	59	Long. Ground Speed	mph
30	Lunette Accel (V)	g's			

4.3 Data Reduction Results

Representative data reduction results are presented for data collected on the Perryman cross-country #3 course at a nominal speed of 15 mph with the surge brakes activated and deactivated, respectively. The data has been decimated to a sampling frequency that is close to twice the cutoff frequencies listed in Table 4.3, for each sensor type. Strain gauge data is only shown for the failure location, bottom drawbar center aft. All other data channels are shown, except for ground speed. The statistics for the data were then calculated, as requested by the U.S. Army. The statistics calculated included the average, standard deviation, root mean square (RMS), +peak, -peak, +99.9%, -99.9%, +99%, -99%, +90%, and -90%.

4.3.2 Strain Data

The statistics for strain are shown in Table 4.5 and Figures 4.5 through 4.9. Table 4.6 shows the statistics for the principal strains. The experimental principal strain statistics are shown, due to the fact that the NASTRAN analysis of the DADS simulation returns principal strains. The principal strains will be used to validate the simulation.

From Table 4.5 and the figures, it can be seen that the longitudinal strain has a much greater amplitude than the other strains. From the Tables 4.5 and 4.6, the peak and percentile strains for the first principal strain, ε_1, match the positive portions of the transverse and longitudinal strains. The peak and percentile strains for the second principal strain, ε_2, match the negative portions of the transverse and longitudinal strains. From Figure 4.10, it can be seen that the longitudinal strain amplitude is well above the transverse strain amplitude. The longitudinal strain is also perpendicular to the direction of crack growth, determined from the broken drawbar, at the failure point. The longitudinal strain is the primary contributor to the positive and negative peaks in the principal strains. From Table 4.6 and Figure 4.10, it can be seen that the first principal strain only accounts for the positive strains in the longitudinal direction, and the second the negative. Therefore, if the only one principal strain is used for calculation, either the positive or negative portion of the strains will be ignored, and will reduce the peak to valley strain values of the cycle. From this, it can be determined that the longitudinal

Table 4.5: Strain amplitude distribution data.

Description	Ave	Std Dev	RMS	+Peak	- Peak	+99.9	-99.9	+99	-99	+90	-90	Brakes
Btm Cntr Aft (T)	0.903	61.25	61.25	180	-189	176	-187	132	-167	80.5	-75.3	ON
(45)	-32.6	59.48	67.82	136	-232	135	-225	120	-177	39.65	-107	
(L)	-37.2	178.1	181.9	505	-648	495	-627	442	-473	176	-256	
Btm Cntr Aft (T)	0.692	65.27	65.27	233	-255	221	-240	155	-180	81.9	-81.5	OFF
(45)	-16.3	66.48	68.44	235	-297	227	-283	154	-185	64.8	-97.3	
(L)	-2.75	191	191	728	-770	704	-749	514	-477	238	-226	

Table 4.6: Principal strain amplitude distribution data.

Description	Ave	Std Dev	RMS	+Peak	- Peak	+99.9	-99.9	+99	-99	+90	-90	Brakes
Btm Cntr Aft (ε_1)	79.6	86.59	118	506	-39.8	498	-27.6	443	-16.9	179	3.9	ON
(ε_2)	-116	104	156	-12.59	-648	-13.5	-627	-16.1	-474	-25.5	-258	
(α)	0.019	0.253	0.253	0.783	-0.78	0.77	-0.76	0.69	-0.68	0.33	-0.28	
Btm Cntr Aft (ε_1)	99.59	106	146	728	-39.2	705	-27.6	515	-8.36	241	11.89	OFF
(ε_2)	-102	103	144	-0.66	-770	-4.54	-749	-7.31	-478	-17.2	-232	
(α)	0.023	0.258	0.259	0.783	-0.79	0.781	-0.78	0.721	0.7	0.313	-0.27	

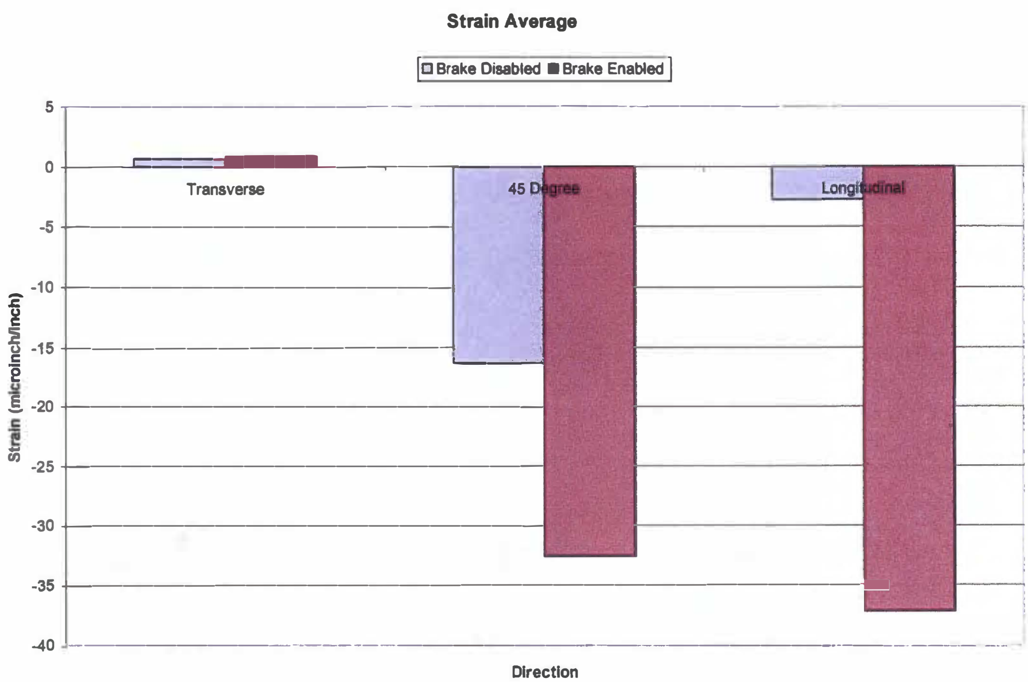

Figure 4.5: Longitudinal strain averages for each rosette direction.

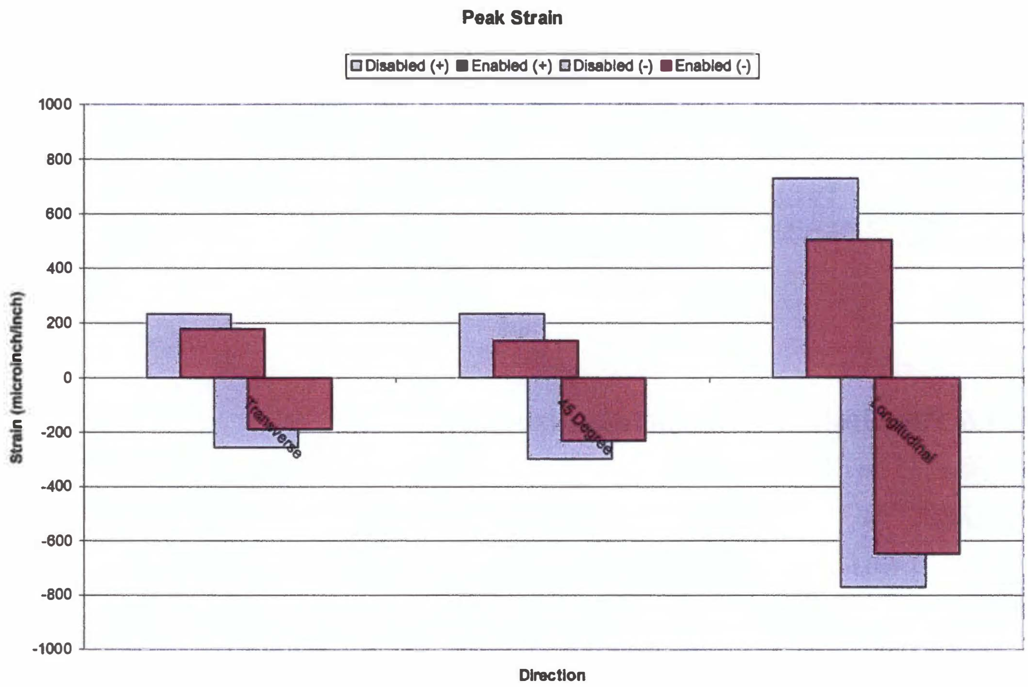

Figure 4.6: Longitudinal strain peaks for each rosette direction.

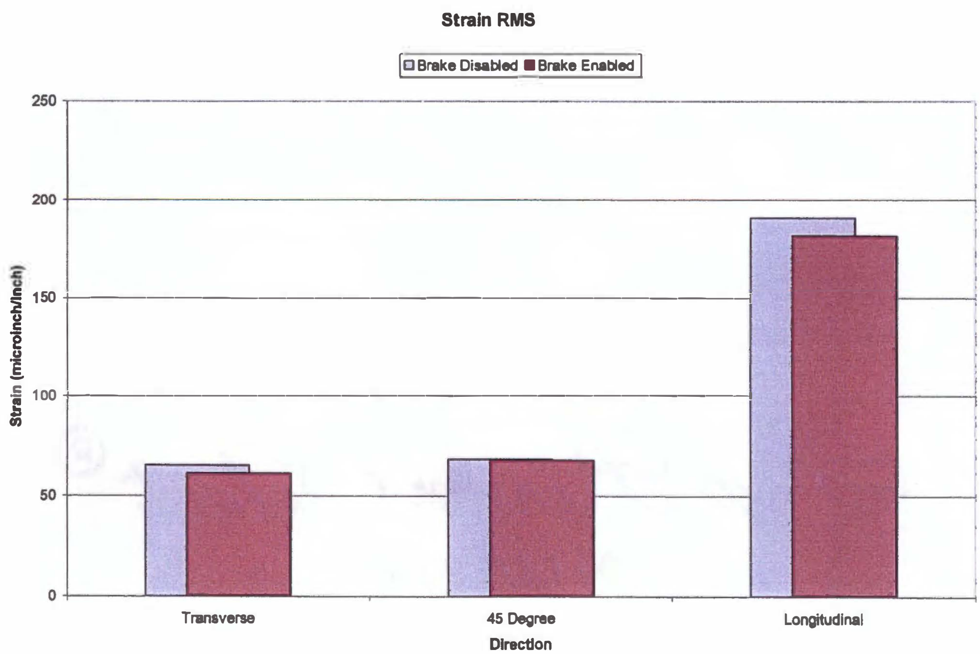

Figure 4.7: Longitudinal strain RMS for each rosette direction.

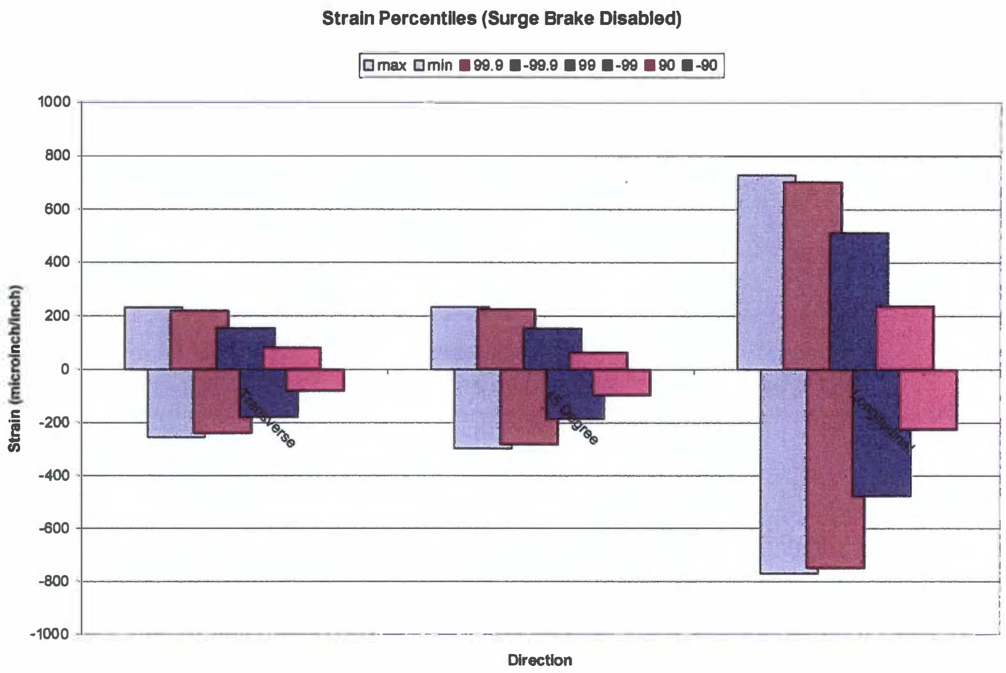

Figure 4.8: Long. strain percentiles for each rosette direction (brakes disabled).

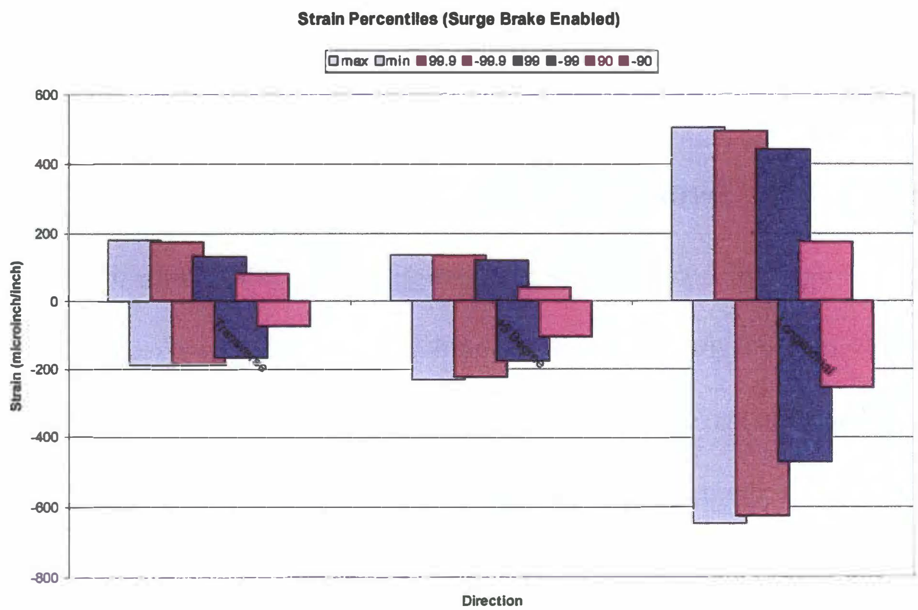

Figure 4.9: Long. strain percentiles for each rosette direction (brakes enabled).

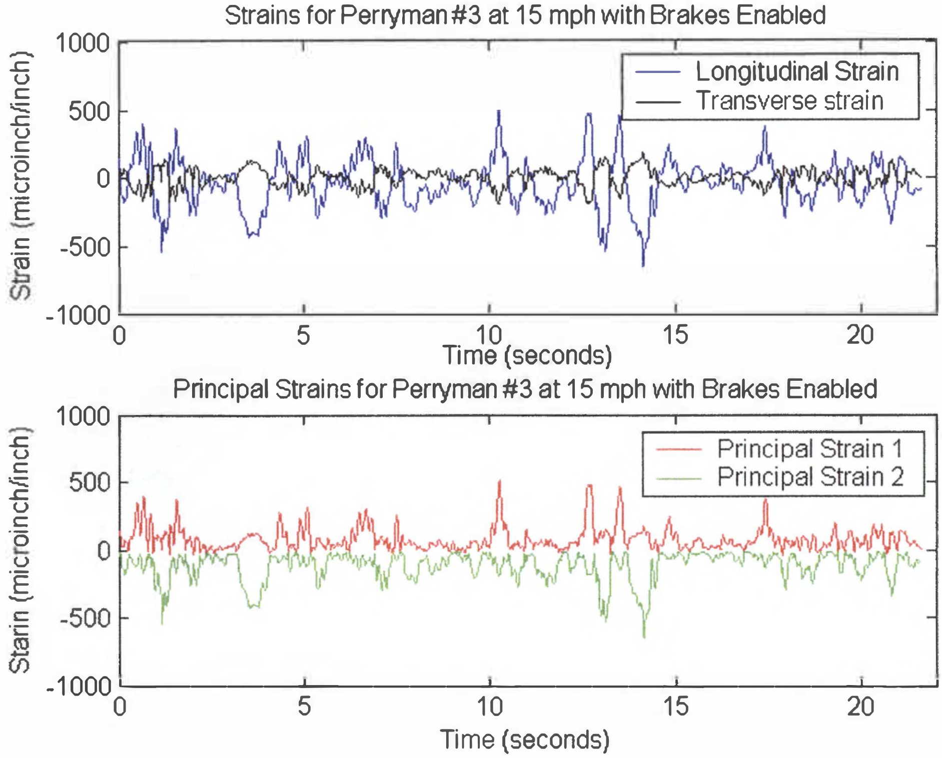

Figure 4.10: Comparing strain and principal strain.

strain or the combined first and second principal strains should be used for any fatigue life predictions.

4.3.3 Accelerometer Data

Statistics about the accelerometer data amplitude distribution for the Perryman #3 test course at 15 mph are given in Tables 4.7 and 4.8 for the brakes disabled, and enabled respectively. The statistics can be seen graphically in Figures 4.11 through 4.25. As expected the mean acceleration are less than 0.25 g. The RMS values are greater for the test data with the brakes enabled than the test data with the brakes disabled. The minimum values are lower for all trailer locations for the test data with the brakes

Table 4.7: Acceleration amplitude distribution data (brakes disabled).

Description	Ave	Std Dev	RMS	+Peak	-Peak	+99.9	-99.9	+99	-99	+90	-90
Lunette (V)	0.12168	0.4581	0.4332	9.5711	-6.713	2.4536	-3.396	0.9296	-0.972	0.5233	-0.271
(T)	-0.075	0.3101	0.319	12.632	-8.396	2.4542	-2.975	0.5986	-0.735	0.0754	-0.231
(L)	-0.0889	0.1779	0.1989	4.0817	-4.615	1.0331	-1.193	0.3298	-0.548	0.0693	-0.256
Tongue (V)	-0.0525	0.4156	0.4189	13.57	-6.954	1.996	-3.129	0.7836	-1.199	0.357	-0.453
(T)	-0.185	0.1688	0.2504	2.5198	-2.636	1.142	-1.176	0.2237	-0.629	-0.032	-0.34
(L)	-0.0053	0.1311	0.1312	1.9064	-1.041	0.661	-0.585	0.3064	-0.352	0.138	-0.161
CG (V)	0.1415	0.3706	0.3967	2.2667	-2.208	1.6796	-0.887	1.2249	-0.666	0.6607	-0.295
(T)	-0.0683	0.118	0.1363	0.7149	-0.594	0.4068	-0.467	0.2534	-0.352	0.0749	-0.209
(L)	0.0299	0.121	0.1266	1.6047	-0.479	0.636	-0.399	0.3406	-0.269	0.1781	-0.118
CS For. (V)	0.0317	0.3561	0.3575	4.3396	-3.145	1.88	-1.615	0.961	-0.815	0.4544	-0.371
(T)	0.0499	0.1613	0.1689	1.5647	-1.258	0.9982	-0.728	0.4733	-0.366	0.2247	-0.128
(L)	0.0808	0.2411	0.2543	1.8408	-1.099	1.3538	-0.716	0.7839	-0.512	0.3503	-0.2
CS Aft (V)	-0.0208	0.662	0.6623	4.1594	-2.302	3.2007	-1.793	2.1049	-	0.7118	-0.779
(T)	0.1244	0.3633	0.3834	5.6734	-4.693	2.0413	-1.754	1.1053	1.432-	0.515	-0.264
(L)	-0.1234	0.2317	0.2625	1.5709	-1.232	1.0813	-0.908	0.5811	0.799	0.1405	-0.390
									-0.639		
RS For (V)	0.0553	0.4088	0.4125	6.2374	-3.551	2.0098	-2.037	1.0706	-0.909	0.544	-0.408
(T)	-0.0394	0.1727	0.1171	1.5752	-1.381	0.9449	-0.84	0.4047	-0.478	0.15	-0.234
(L)	-0.0745	0.2486	0.2596	1.975	-1.936	1.1045	-0.863	0.6167	-0.657	0.2317	-0.365
RS Aft (V)	0.0075	0.6042	0.6042	3.1227	-2.227	2.3379	-1.563	1.7719	-1.345	0.7346	-0.699
(T)	0.1265	0.3075	0.3325	4.2607	-3.694	1.864	-1.409	0.9809	-0.642	0.4597	-0.204
(L)	0.0394	0.2106	0.2142	1.3207	-0.732	1.0818	-0.579	0.65451	-0.432	0.3096	-0.194
CS Axle (V)	0.0852	0.4934	0.5007	4.3174	-3.36	2.7369	-1.972	1.5695	-1.07	0.6409	-0.459
CS Frame (V)	-0.0525	0.4021	0.4055	1.8081	-1.272	1.6858	-1.094	1.2094	-0.947	0.4166	-0.523
RS Axle (V)	-0.0301	0.3931	0.3943	2.2952	-2.017	1.7752	-1.456	1.1079	-0.908	0.4299	-0.497
RS Frame (V)	-0.0261	0.3909	0.3917	1.6563	-1.128	1.4053	-1.035	1.1184	-0.935	0.4417	-0.481

Table 4.8: Acceleration amplitude distribution data (brakes enabled).

Description	Ave	Std Dev	RMS	+Peak	-Peak	+99.9	-99.9	+99	-99	+90	-90
Lunette (V)	0.2202	0.6183	0.6521	21.071	-13.44	4.802	-5.761	1.5933	-1.45	0.6616	-0.202
(T)	-0.1545	0.5104	0.5332	15.779	-20.02	4.5127	-4.447	1.0028	-1.346	0.0511	-0.366
(L)	0.0399	0.6974	0.6985	19.735	-29.83	5.7253	-7.924	1.5271	-1.671	0.2877	-0.217
Tongue (V)	0.13324	0.6087	0.6231	10.218	-12.37	4.929	-4.901	1.5916	-1.559	0.5915	-0.306
(T)	0.14123	0.2694	0.3041	6.8436	-7.215	2.2118	-1.804	0.8591	-0.576	0.3469	-0.069
(L)	0.13663	0.2205	0.2594	3.4864	-3.999	1.9519	-1.549	0.7293	-0.412	0.3091	-0.05
CG (V)	-0.1242	0.4284	0.446	4.5005	-7.643	2.5262	-1.976	1.1257	-1.112	0.3346	-0.578
(T)	-0.0395	0.1547	0.1597	0.9022	-1.751	0.5993	-0.930	0.3599	-0.442	0.1384	-0.207
(L)	0.1465	0.1861	0.2368	3.447	-3.808	1.7097	-1.096	0.6771	-0.255	0.311	-0.019
CS For. (V)	-0.1274	0.4411	0.4591	4.3337	-7.979	2.3179	-2.677	1.0904	-1.29	0.3406	-0.566
(T)	0.021	0.2111	0.2121	3.1715	-2.835	1.1754	-1.185	0.6102	-0.556	0.2416	-0.192
(L)	0.1736	0.3394	0.3812	5.0471	-6.094	2.6709	-2.045	1.1309	-0.645	0.4848	-0.148
CS Aft (V)	0.0349	0.7652	0.766	8.4154	-6.358	5.4353	-3.009	2.3397	-1.709	0.834	-0.771
(T)	-0.0232	0.5302	0.5307	6.2574	-8.565	3.6121	-3.545	1.3968	-1.564	0.4568	-0.484
(L)	-0.0918	0.3226	0.3354	4.8301	-4.944	2.3277	-2.099	0.8744	-0.817	0.2134	-0.396
RS For (V)	-0.0498	0.5111	0.5135	8.202	-9.584	2.807	-2.972	1.3539	-1.406	0.4688	-0.56
(T)	0.1679	0.224	0.2799	3.7841	-4.518	1.3926	-1.066	0.7736	-0.445	0.4001	-0.057
(L)	-0.1321	0.3325	0.3485	4.3677	-7.58	2.2229	-2.075	0.7561	-0.903	0.1827	-0.439
RS Aft (V)	-0.1377	0.6953	0.7088	10.413	-3.875	5.4252	-2.643	1.8761	-1.662	0.6125	-0.876
(T)	0.139	0.4711	0.4912	9.1632	-8.374	3.4472	-3.448	1.4288	-1.771	0.531	-0.246
(L)	0.1491	0.2769	0.3144	4.6166	-3.07	2.1879	-1.412	0.9581	-0.446	0.434	-0.111
CS Axle (V)	-0.0911	0.5322	0.534	4.1965	-2.985	2.9817	-2.303	1.5491	-1.344	0.4993	-0.669
CS Frame (V)	-0.0405	0.4357	0.4376	3.5915	-2.647	2.5291	-1.442	1.2945	-1.021	0.4558	-0.522
RS Axle (V)	-0.024	0.423	0.4236	4.7063	-3.578	3.0029	-1.643	1.2476	-0.909	0.4925	-0.446
RS Frame (V)	0.0528	0.4271	0.4303	3.6333	-2.039	2.6487	-1.256	1.3515	-0.878	0.5483	-0.437

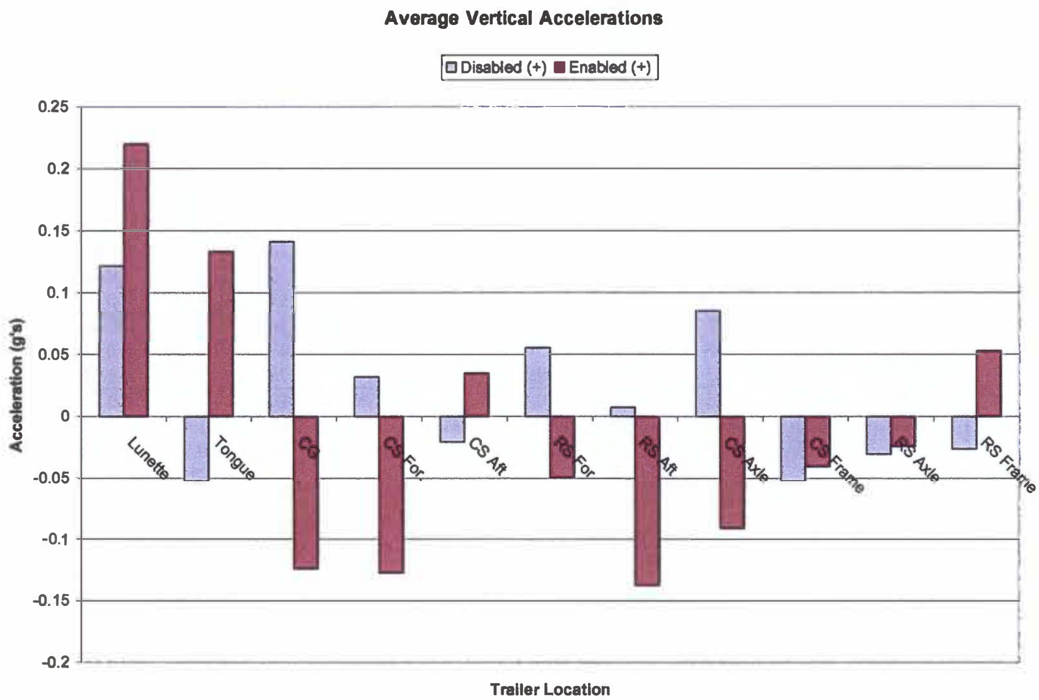

Figure 4.11: Average vertical accelerations for several trailer locations.

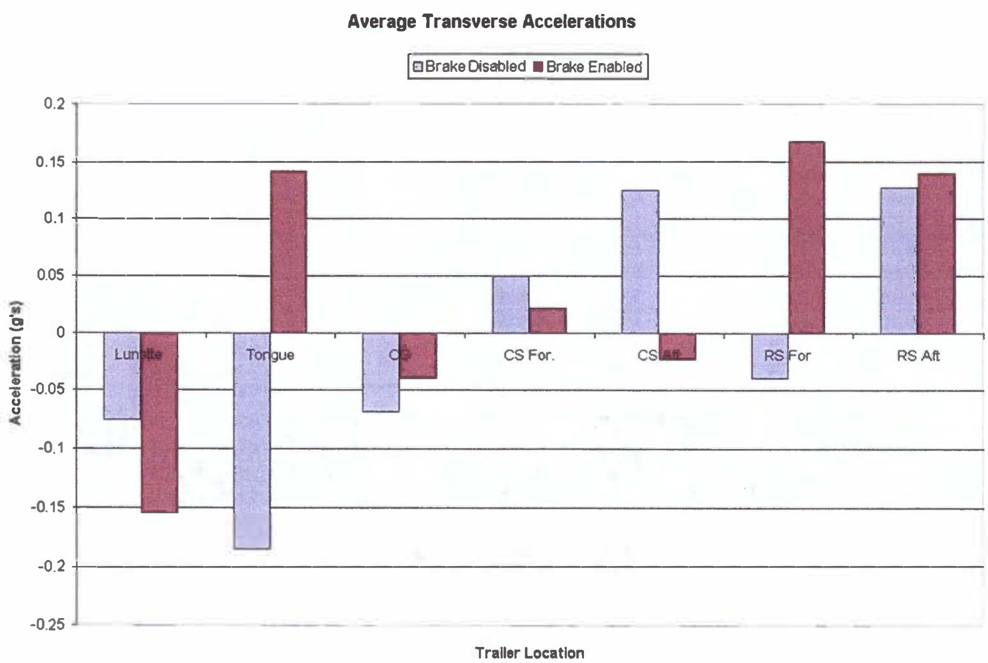

Figure 4.12 Average transverse accelerations for several trailer locations.

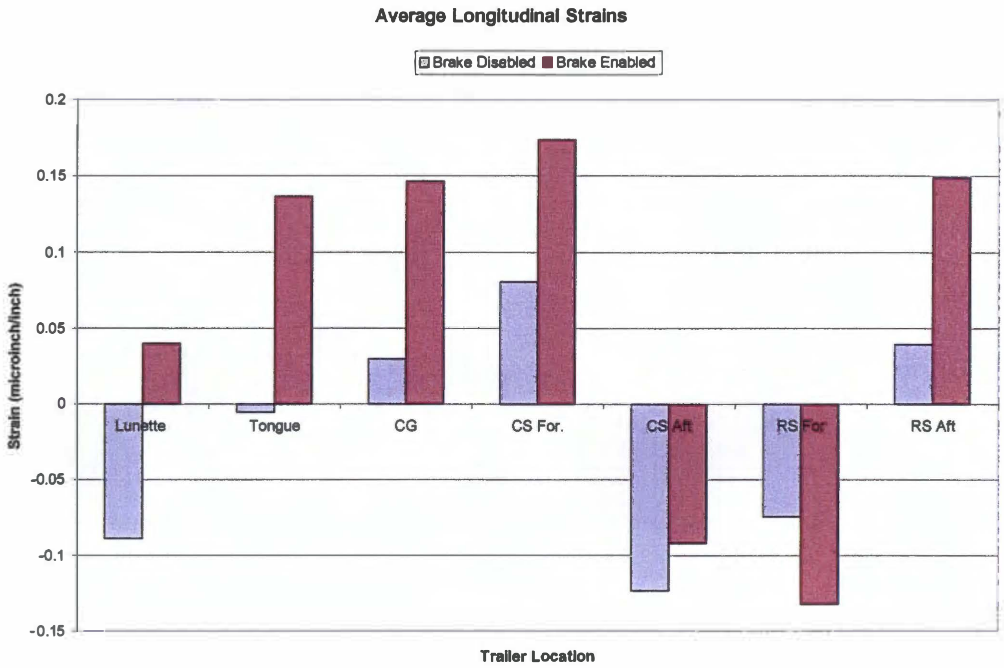

Figure 4.13: Average longitudinal accelerations for several trailer locations.

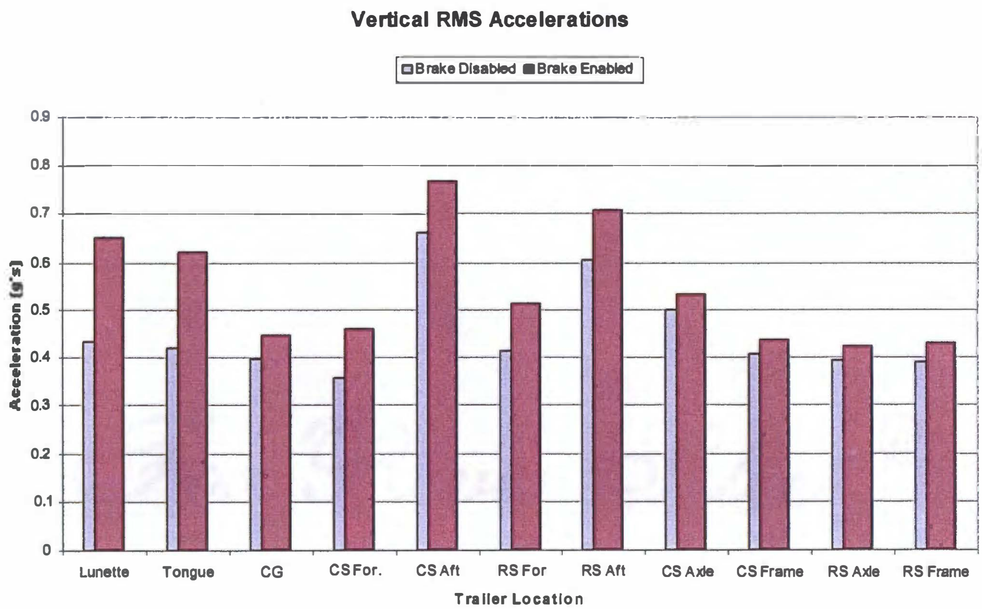

Figure 4.14: Vertical RMS accelerations for several trailer locations.

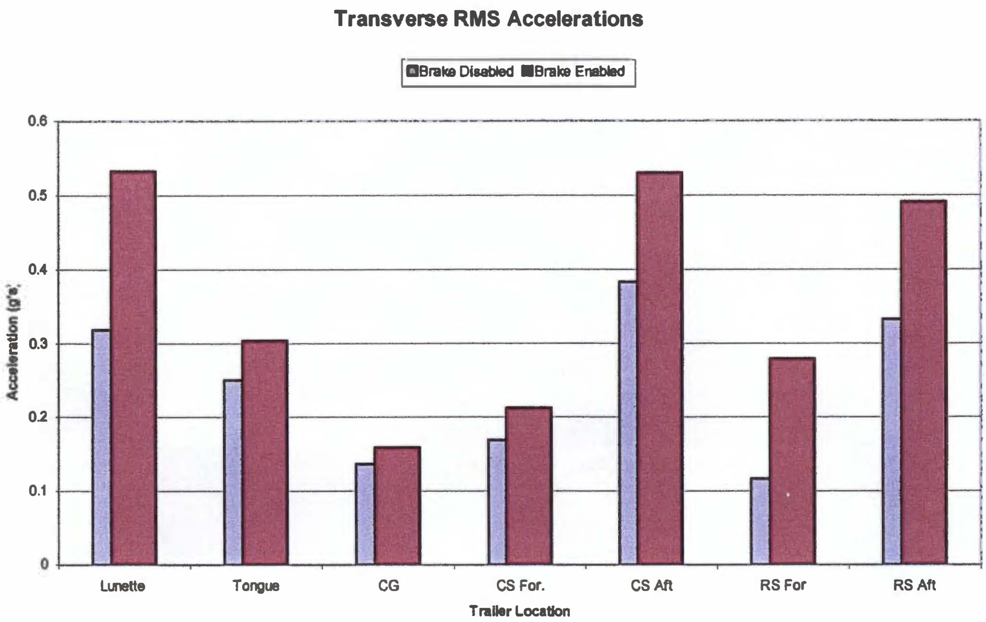

Figure 4.15: Transverse RMS accelerations for several trailer locations.

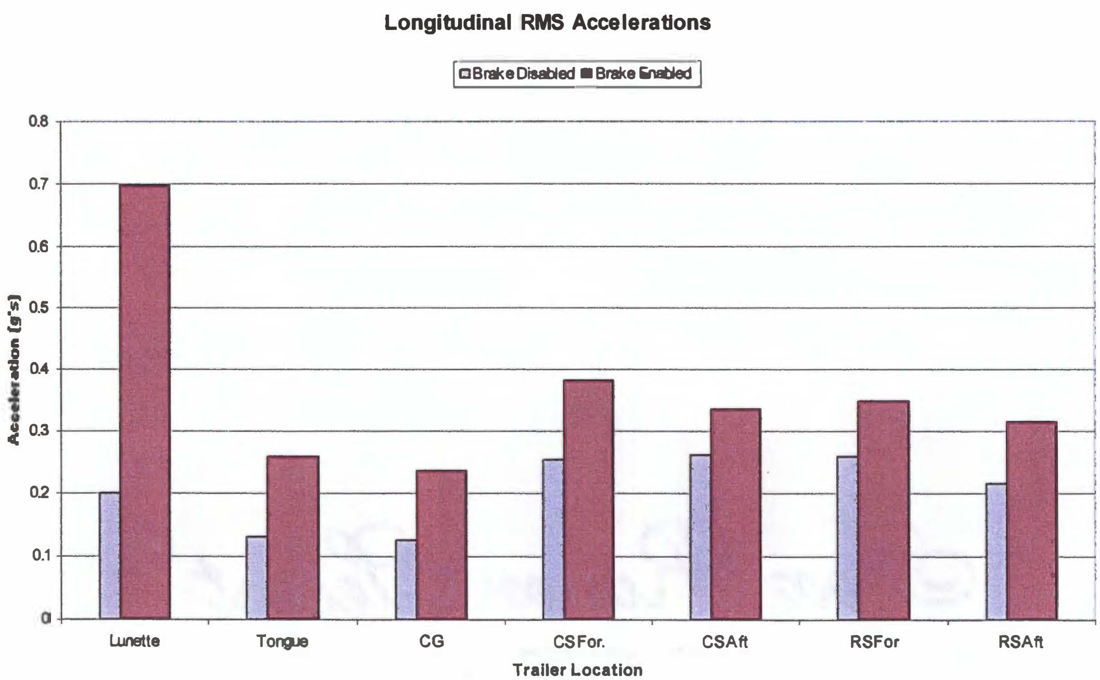

Figure 4.16: Longitudinal RMS accelerations for several trailer locations.

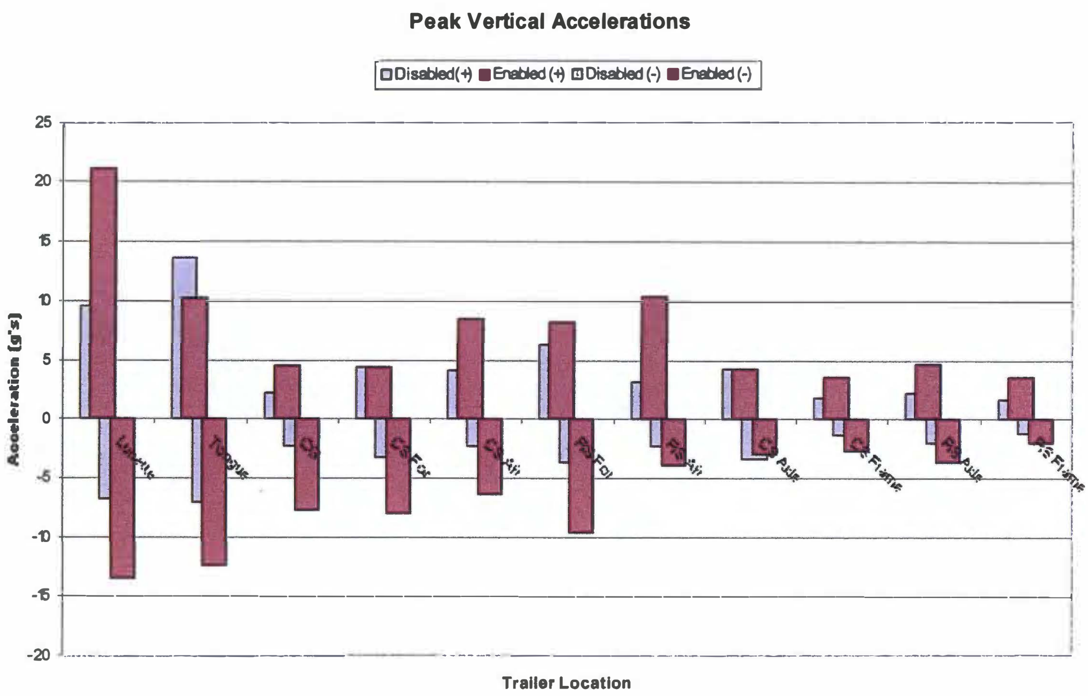

Figure 4.17: Peak vertical accelerations for several trailer locations.

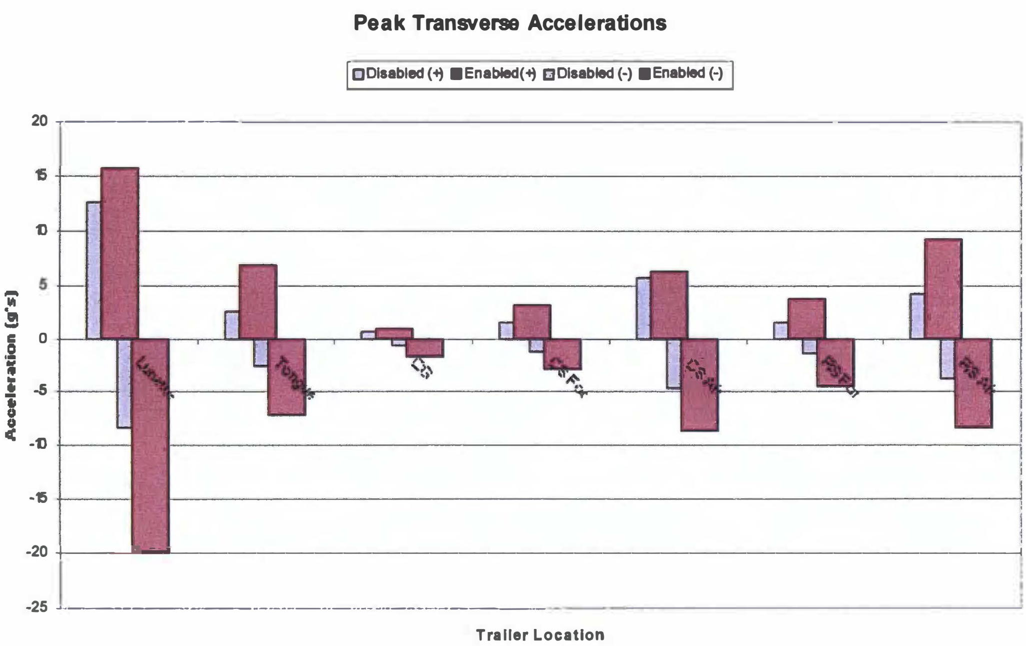

Figure 4.18: Peak transverse accelerations for several trailer locations.

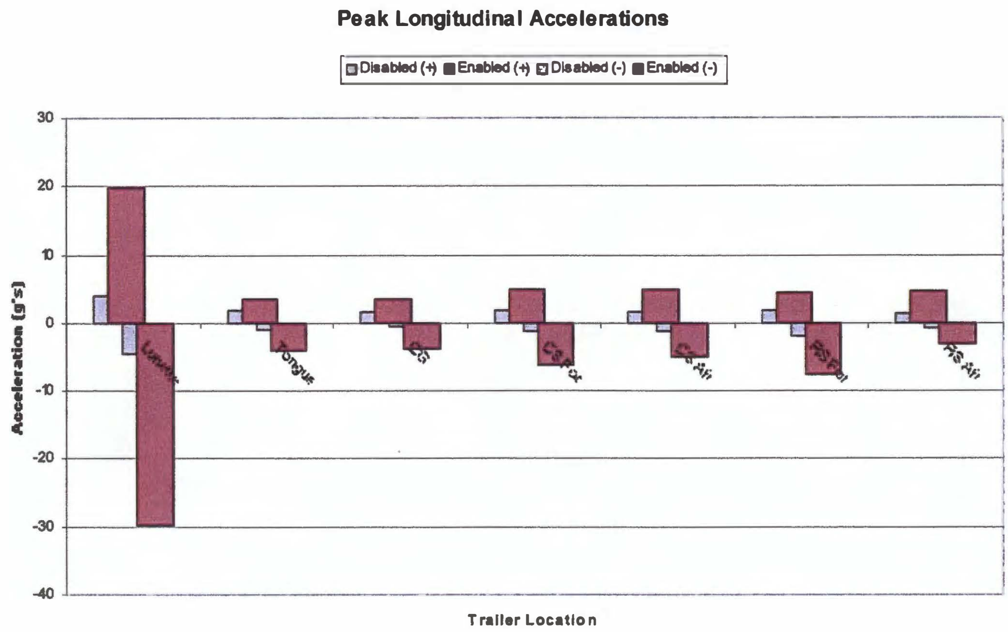

Figure 4.19: Peak longitudinal accelerations for several trailer locations.

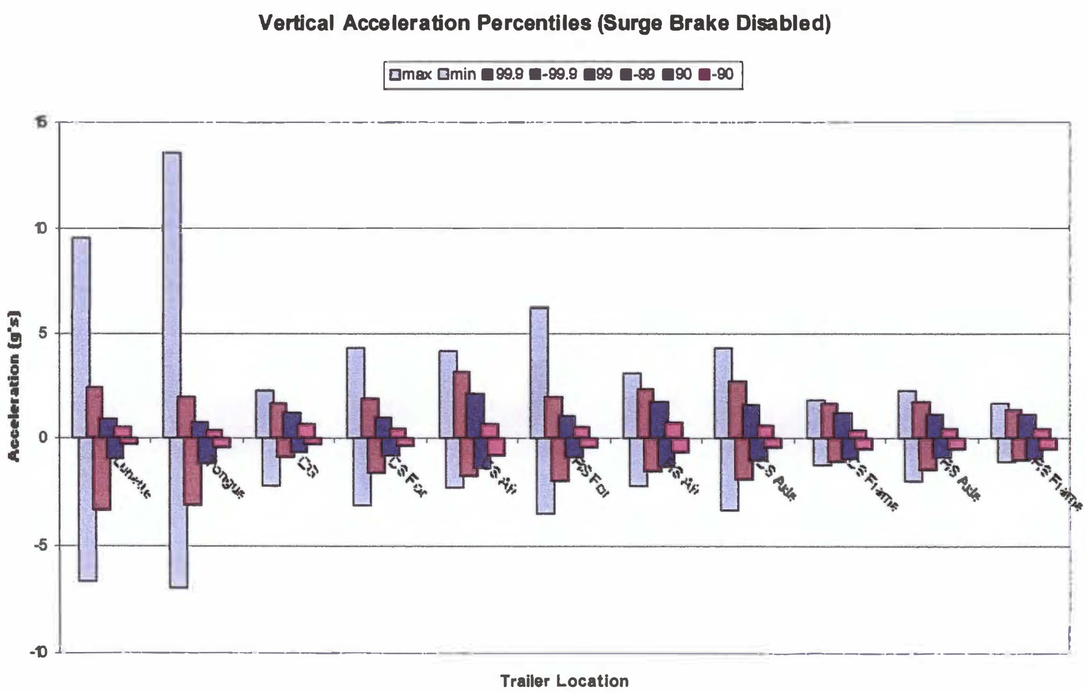

Figure 4.20: Vertical accel. statistics for several trailer locations (brakes disabled).

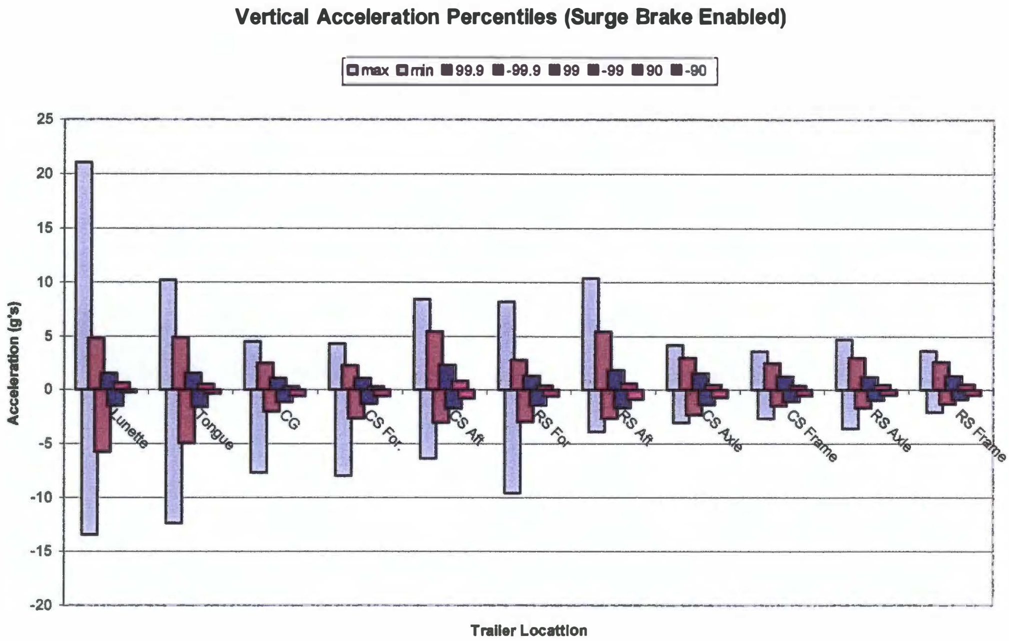

Figure 4.21: Vertical accel. statistics for several trailer locations (brakes enabled).

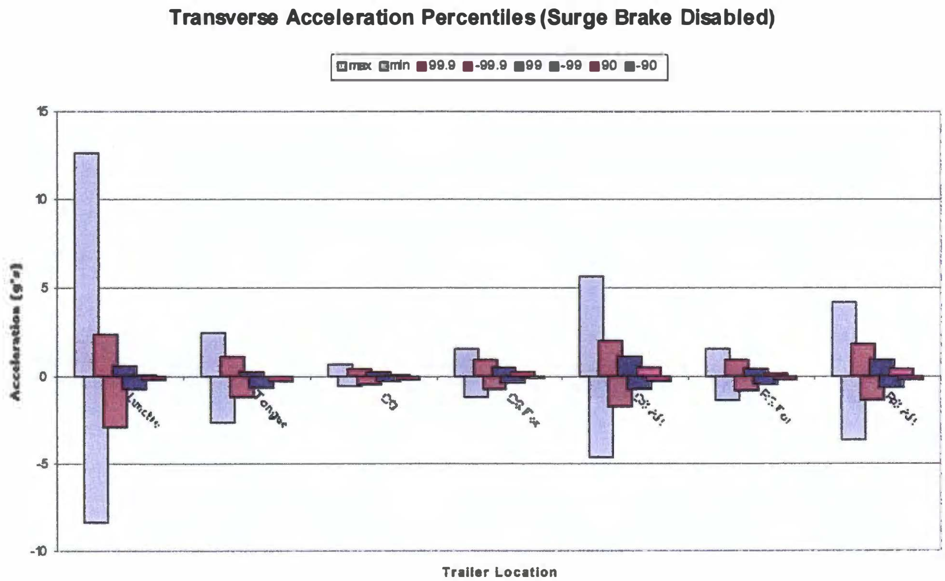

Figure 4.22: Transverse accel. statistics for several trailer locations (brake disabled).

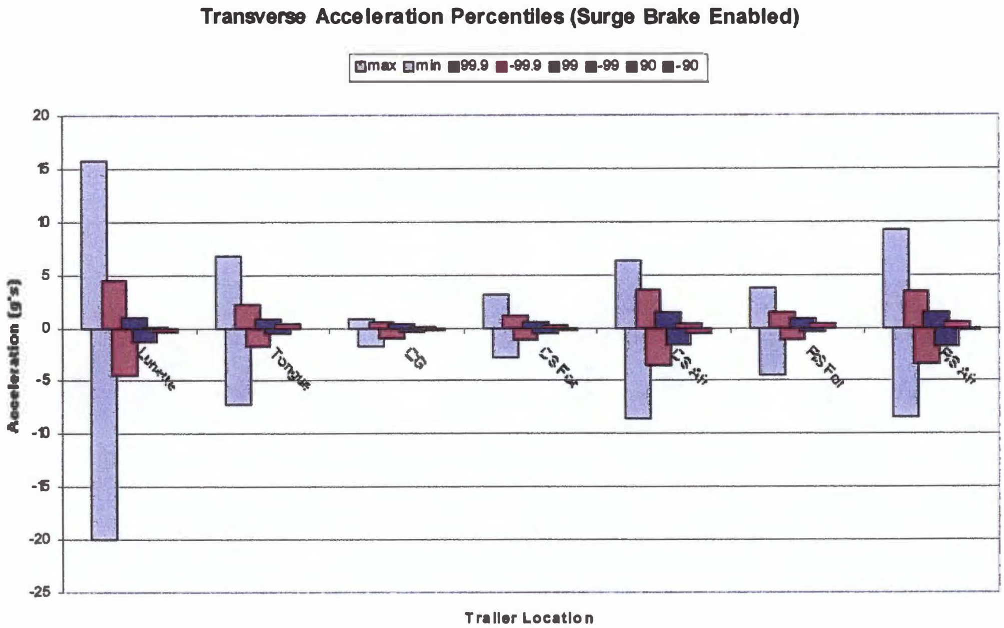

Figure 4.23: Transverse accel. statistics for several trailer locations (brake enabled).

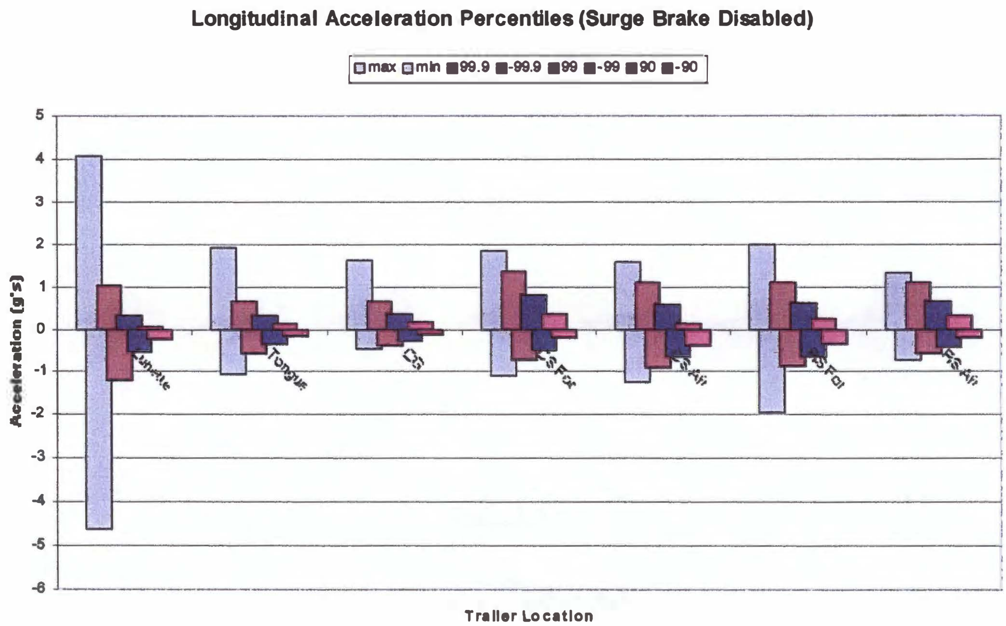

Figure 4.24: Long. accel. statistics for several trailer locations (brake disabled).

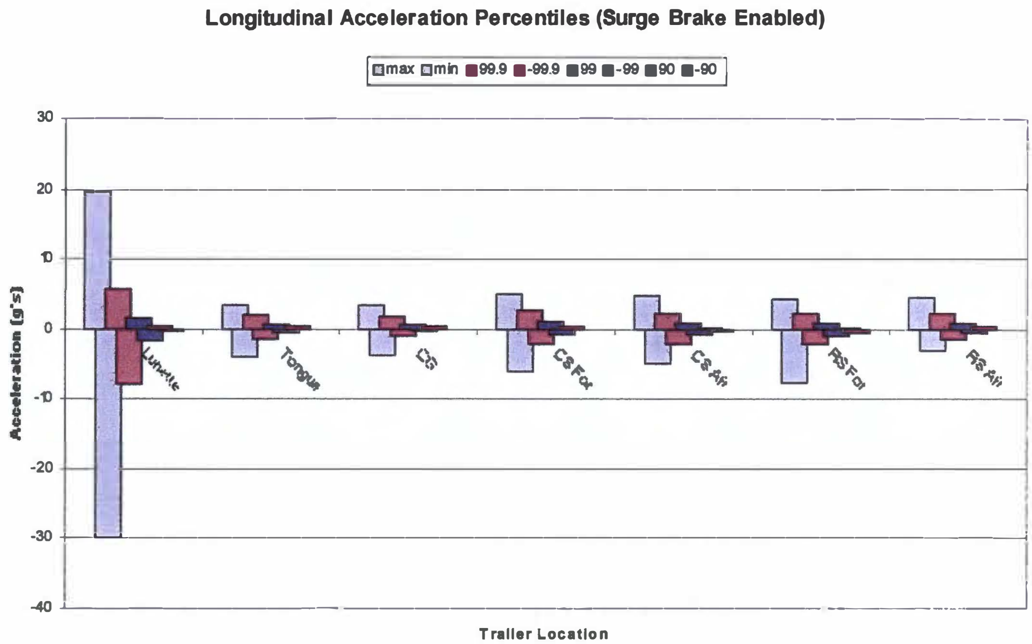

Figure 4.25: Long. accel. statistics for several trailer locations (brake enabled).

enabled and the maximum values are greater for all locations, except the tongue, for the brakes enabled case.

4.3.4 Rate-gyro Data

Statistics about the rate-gyro data amplitude distribution for the Perryman #3 test course at 15 mph are given in Tables 4.9 and 4.10 for the brakes disabled, and enabled respectively. The statistics can be seen graphically in Figures 4.26 through 4.28. From the tables and figures, it can be seen that the CG pitch rate was significantly higher than the CG roll and yaw rates for the brakes both disabled and enabled.

Table 4.9: Rate-gyro distribution data (brakes disabled).

Description	Ave	Std Dev	RMS	+Peak	-Peak	+99.9	-99.9	+99	-99	+90	-90
CG Pitch Rate	0.5326	19.625	19.626	75.409	-74.89	73.886	-74.23	53.694	-47.98	25.099	-20.37
CG Roll Rate	0.2818	5.8499	5.852	28.269	-21.98	27.15	-21.57	12.766	-13.87	7.5439	-7.346
CG Yaw Rate	-0.238	3.8906	3.8965	12.066	-10.37	11.649	-10.36	8.8219	-8.525	4.9595	-4.928

Table 4.10: Rate-gyro distribution data (brakes enabled).

Description	Ave	Std Dev	RMS	+Peak	-Peak	+99.9	-99.9	+99	-99	+90	-90
CG Pitch Rate	0.5062	21.129	21.13	86.102	-86.51	82.994	-83.46	65.056	-55.19	24.919	-22.35
CG Roll Rate	0.1854	6.816	6.817	26.256	-28.47	25.406	-26.22	16.541	-16.64	8.6564	-8.413
CG Yaw Rate	-0.033	4.5215	4.5206	16.61	-13.42	15.613	-11.70	11.204	-9.906	6.0071	-5.589

Figure 4.26: Trailer CG pitch rate statistics.

Figure 4.27: Trailer CG roll rate statistics.

Figure 4.28: Trailer CG yaw rate statistics.

4.3.5 Linear Displacement Transducer Data

Statistics about the rate-gyro data amplitude distribution for the Perryman #3 test course at 15 mph are given in Tables 4.11 and 4.12 for the brakes disabled, and enabled respectively. The statistics can be seen graphically in Figures 4.29 and 4.30. From the tables and figures, it can be seen that both the CS and RS shock displacements were greater for the test data for the brakes enabled than for the brakes disabled test data.

Table 4.11: Linear displacement distribution data (brakes disabled).

Description	Ave	Std Dev	RMS	+Peak	-Peak	+99.9	-99.9	+99	-99	+90	-90
CS Shock Displacement	0.0305	0.24631	0.2481	0.8698	-0.703	0.86805	-0.692	0.82091	-0.618	0.3067	-0.254
RS Shock Displacement	0.0132	0.2217	0.222	0.7777	-0.555	0.77536	-0.552	0.70989	-0.533	0.2702	-0.25

Table 4.12: Linear displacement distribution data (brakes enabled).

Description	Ave	Std Dev	RMS	+Peak	-Peak	+99.9	-99.9	+99	-99	+90	-90
CS Shock Displacement	0.0538	0.2594	0.2649	1.1323	-0.7	1.0674	-0.691	0.845	-0.57	0.35244	-0.246
RS Shock Displacement	0.0258	0.2417	0.243	1.0241	-0.571	0.9407	-0.558	0.7497	-0.542	0.33093	-0.252

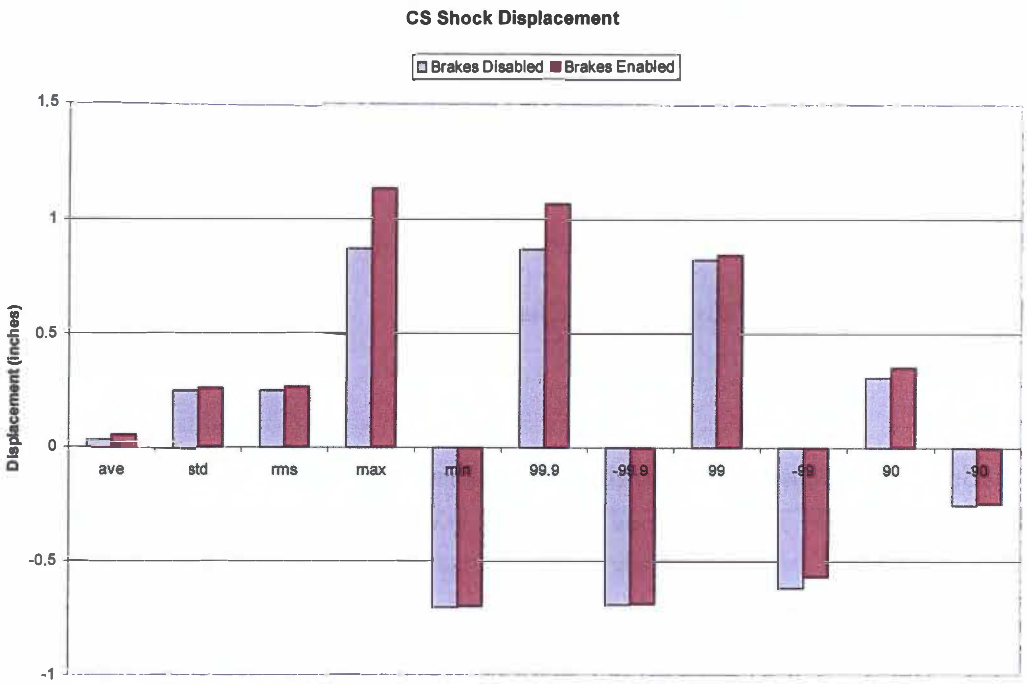

Figure 4.29: Trailer CS shock displacement statistics.

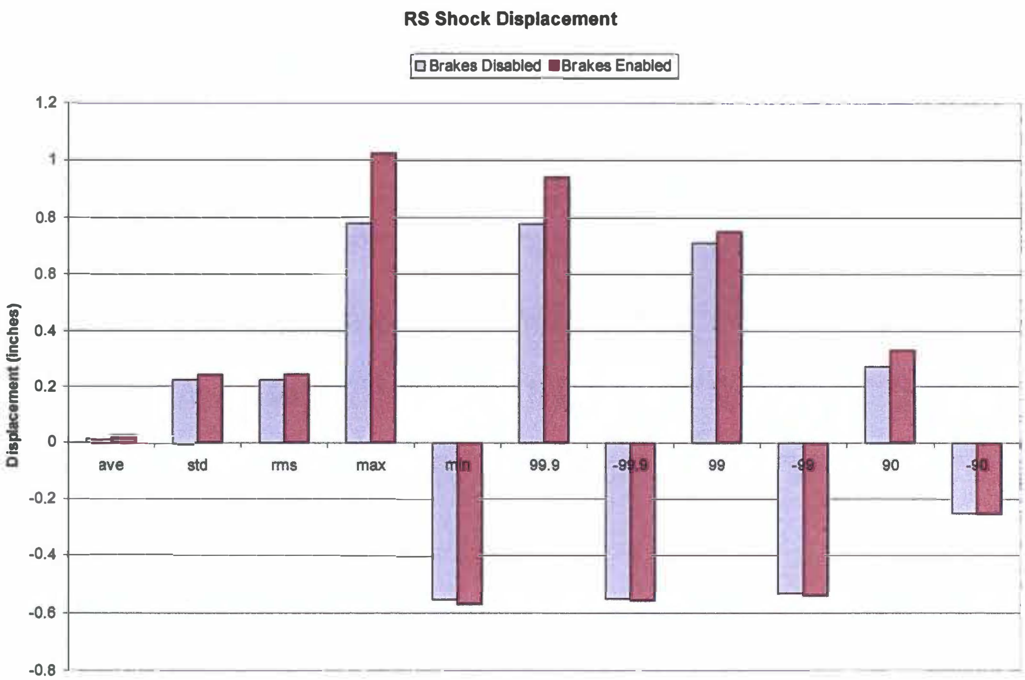

Figure 4.30: Trailer RS shock displacement statistics.

4.3.6 Pressure Transducer Data

Statistics about the rate-gyro data amplitude distribution for the Perryman #3 test course at 15 mph are given in Tables 4.13 and 4.14 for the brakes disabled, and enabled respectively. The statistics can be seen graphically in Figures 4.31 through 4.33. The surge brake statistics will be discussed in Chapter 5.

Table 4.13: Brake pressure distribution data (brakes disabled).

Description	Ave	Std Dev	RMS	+Peak	-Peak	+99.9	-99.9	+99	-99	+90	-90
Master Cylinder Pressure	9.4367	0.4364	9.4468	11.717	8.1985	11.372	8.3904	10.855	8.6425	9.9773	8.9646
CS Wheel Brake Pressure	-1.495	0.5439	1.5905	3.8995	-2.072	2.8229	-1.951	1.7807	-1.745	-1.562	-1.62
RS Wheel Brake Pressure	1.1399	0.3615	1.1958	5.283	0.5786	4.6211	0.733	3.1368	0.91659	1.1409	1.048

Table 4.14: Other amplitude distribution data (brakes enabled).

Description	Ave	Std Dev	RMS	+Peak	-Peak	+99.9	-99.9	+99	-99	+90	-90
Master Cylinder Pressure	6.1166	72.906	73.159	622.15	-22.07	611.6	-21.71	413.97	-21.06	51.59	-20.49
CS Wheel Brake Pressure	2.3007	67.735	67.772	581.19	-24.25	569.13	-24.06	385.65	-23.71	39.852	-23.03
RS Wheel Brake Pressure	3.2322	71.075	71.145	609.93	-24.41	598.56	-24.23	404.17	-23.78	41.719	-23.1

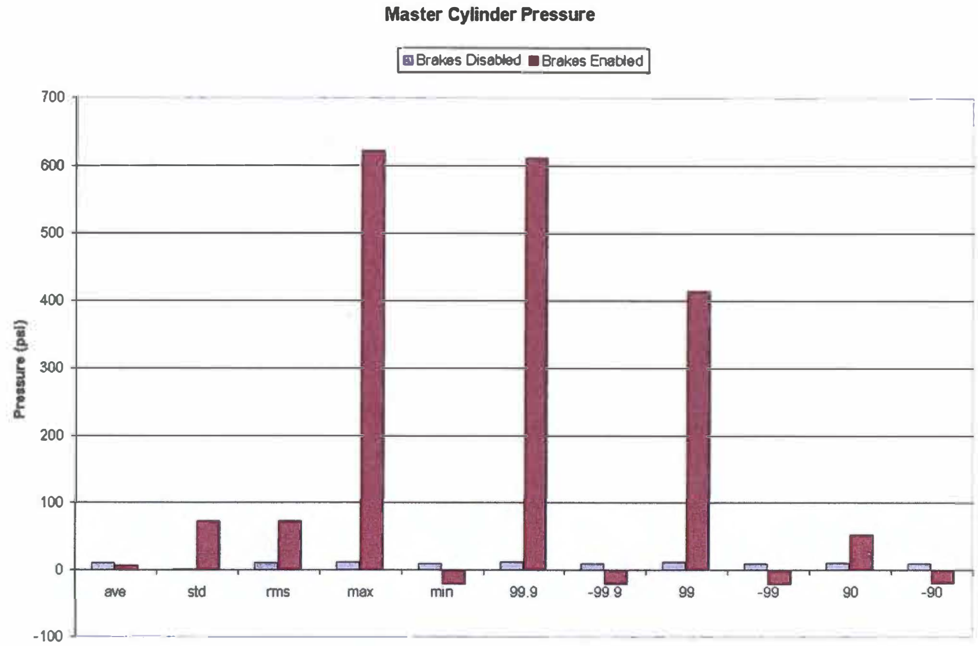

Figure 4.31: Trailer master cylinder pressure statistics.

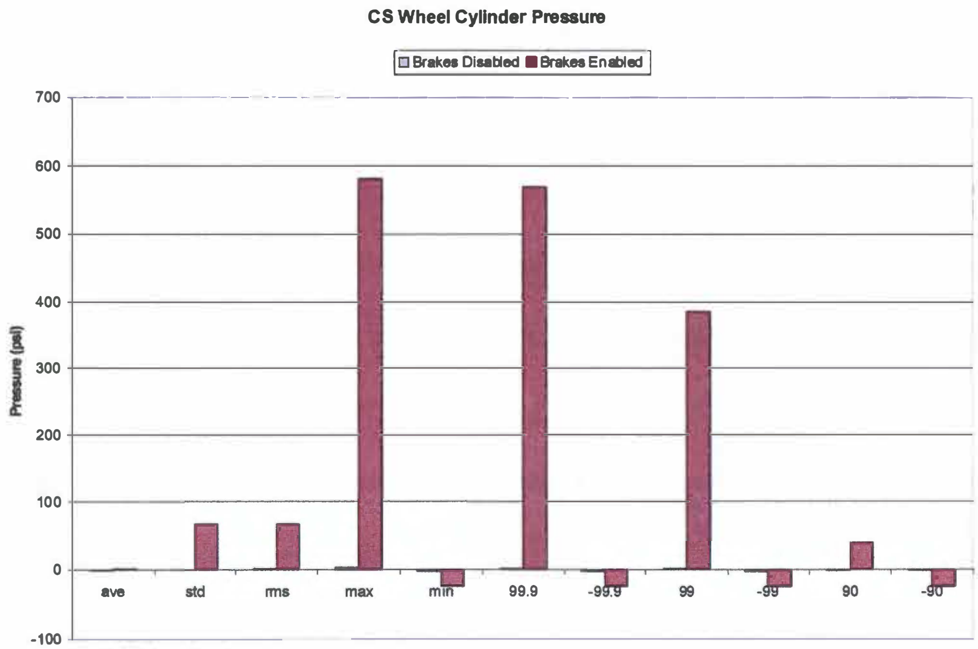

Figure 4.32: Trailer CS wheel cylinder pressure statistics.

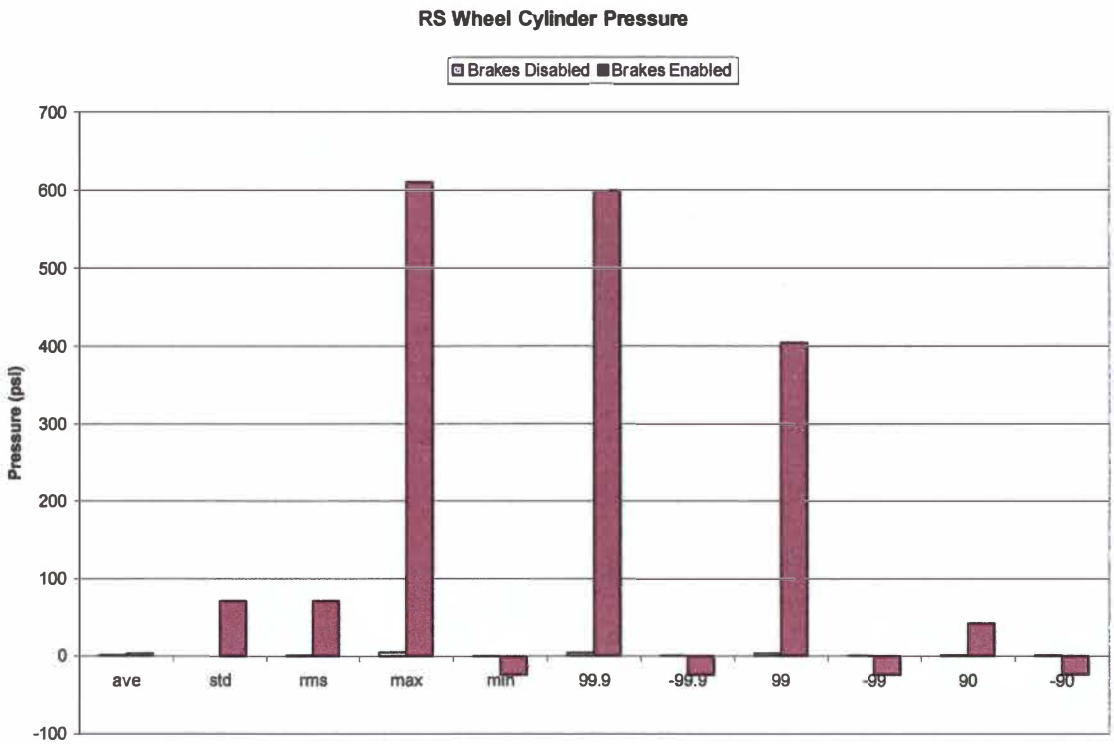

Figure 4.33: Trailer RS wheel cylinder pressure statistics.

4.4 DADS Validation

Rigid and flexible body DADS simulations were made of the Perryman #3 course at 15 mph. The loads from DADS were then used by NASTRAN to calculate the principal strains at various locations on the trailer. One of the locations was at the failure point on the drawbar. The statistics for 15 seconds of data for the experimental and simulated strains, for both the rigid and flexible body models can be found in Table 4.15 and Figures 4.34 and 4.35. It is important to recognize that the experimental and simulated data were not taken at the same point on the test course. From the table and figures, it can be seen that the flexible body model more closely represents the

Table 4.15: DADS validation statistics.

	Principal Strain 1			Principal Strain 2		
Statistics	**Exp.**	**Rigid**	**Flexible**	**Exp.**	**Rigid**	**Flexible**
Mean	94.7697	523.2	285.1	-99.6982	-68.72	-106
Standard Deviation	102.3792	590.1	135	96.3041	65.94	42.18
RMS	139.5106	788.4728	315.4487	138.6049	95.2253	114.0718
Maximum	605.2628	2390	956	-5.186	89.46	55.78
Minimum	-39.1682	-918	-318	-770.1156	-289.3	-306.9
Range	644.431	3308	1274	775.3016	378.76	362.68

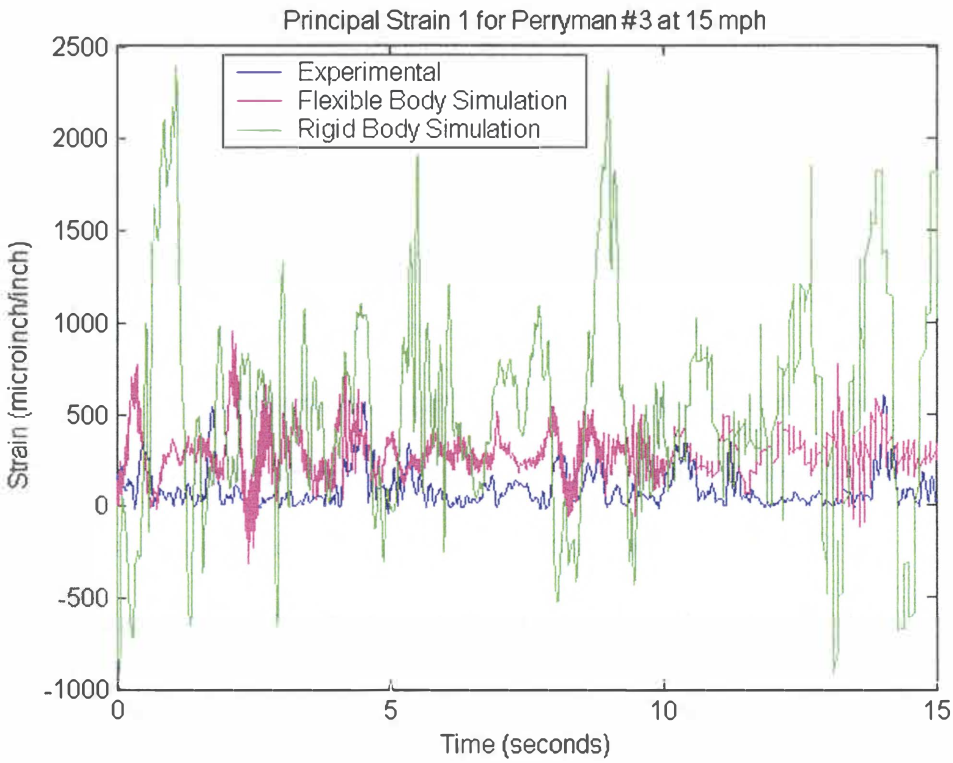

Figure 4.34: Principal strain 1 for experimental and simulated data.

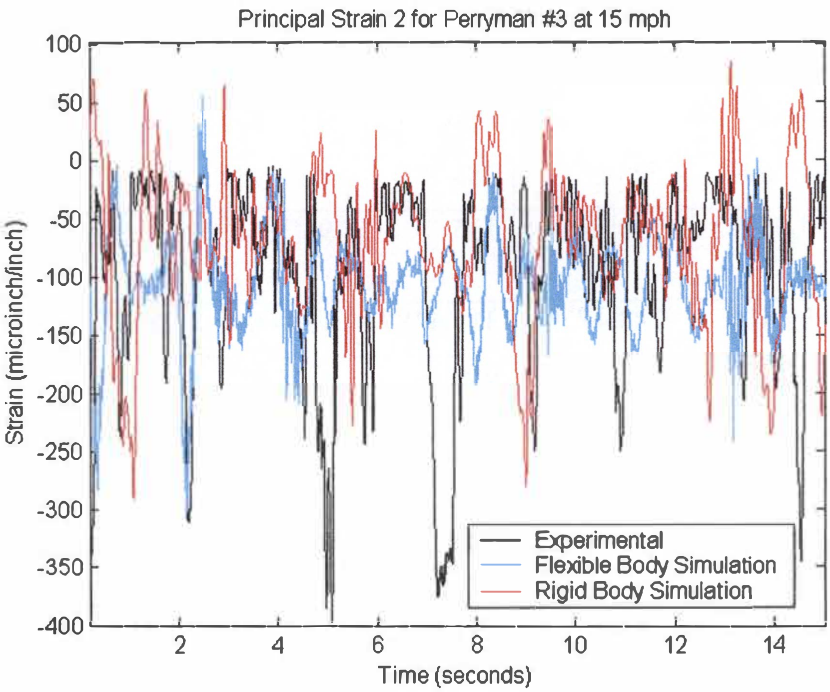

Figure 4.35: Principal strain 2 for experimental and simulated data.

experimental data in the time domain. For principal strain 1, the flexible body model has a magnitude that is double the experimental data, as reflected in all the statistics. The data from the flexible body model more closely represents the experimental data for principal strain 2, with a reduction in the standard deviation and range. The time data from the model does not adequately represent the experimental data.

To further examine the models, the frequency content must be analyzed. From Figures 4.36 and 4.37 it can bee seen that the PSDs of the rigid and flexible body models have higher magnitudes, but the models do adequately represent the frequency content of the experimental strain data, except for a peak at 30 Hz for the flexible body model. The rolloff after 40 Hz for the simulated data is a function of the sampling frequency and not the model.

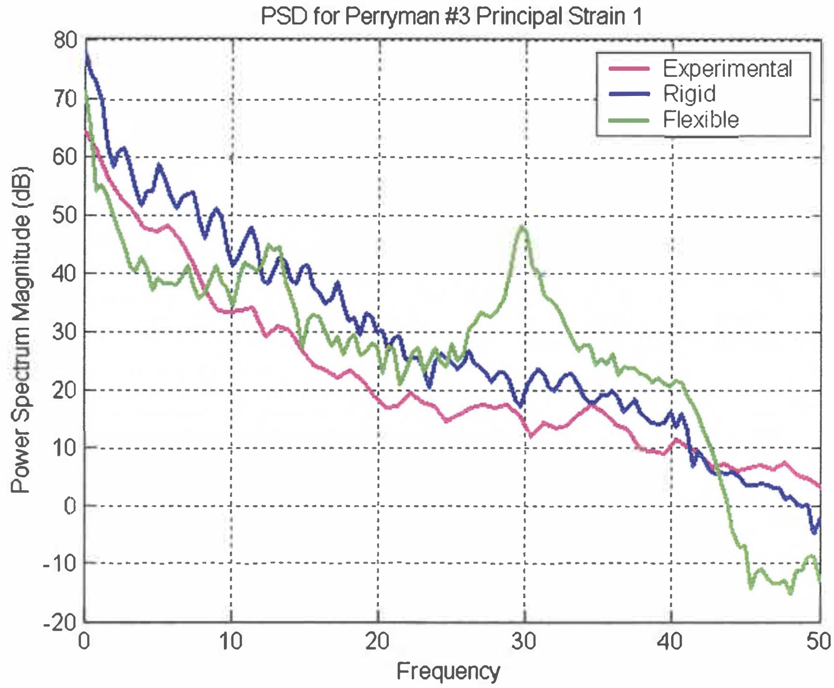

Figure 4.36: PSD of principal strain 1 for experimental and simulated data.

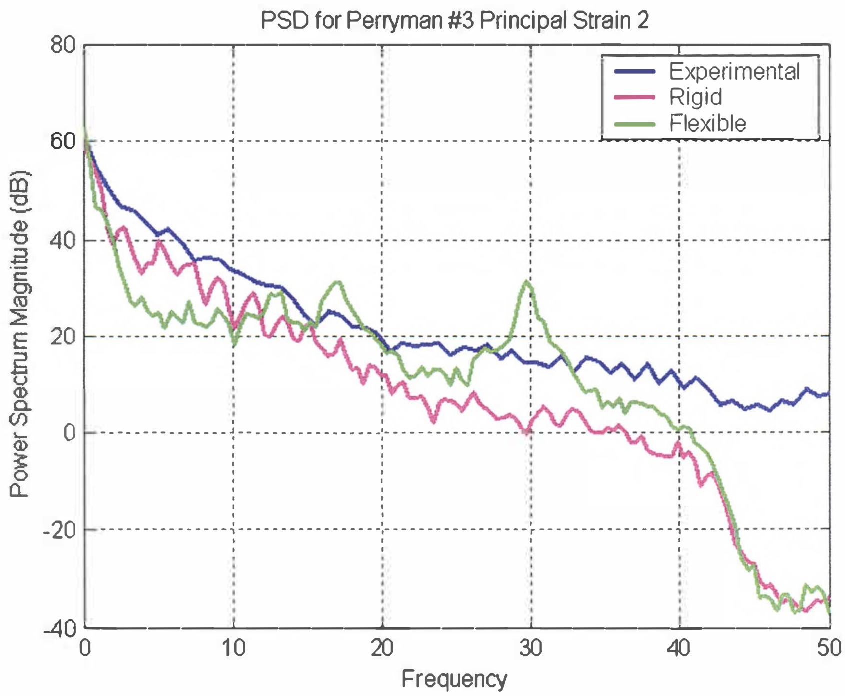

Figure 4.37: PSD for principal strain 2 for experimental and simulated data.

Chapter 5 PSD Conversion

5.1 Introduction

The PSD is a widely recognized means of representing random processes in the frequency domain. For terrain monitoring, it compresses the spatial data of the profilometer by representing it as a PSD magnitude vs. wavelength. The vertical axis of the PSD has units of elevation cubed per cycle, while the horizontal axis has units of cycles per unit length. For the PSD to be used by DADS, it will have to be converted back to spatial data. This will give a normally distributed model for the course that was used to collect data for the PSD. The conversion of the PSD to data in the spatial domain, that has an equivalent frequency content to the original data set, is an initial step in determining if stored terrain data can be used with the DADS program.

5.2 PSD

A PSD is the representation of the frequency, ω, content of a time, t, signal *W(t)* (Ljung and Glad, 1994). The Fourier transform of the signal, *W*(ω), can be used to calculate the PSD.

$$W(\omega) = \int_{-\infty}^{\infty} W(t) e^{-i\omega t} dt \tag{5.1}$$

The Fourier transform is a complex number having a magnitude and a phase. The magnitude is the square root of the sum of the squares of the real and imaginary parts of the transform.

$$|W(\omega)| = \sqrt{\mathrm{Re}(W(\omega))^2 + \mathrm{Im}(W(\omega))^2} \tag{5.2}$$

The phase angle, $\phi(\omega)$, is the inverse tangent of the ratio of the imaginary and real parts of the transform.

$$\phi(\omega) = \tan^{-1} \frac{\mathrm{Im}(W(\omega))}{\mathrm{Re}(W(\omega))} \tag{5.3}$$

For signals with finite energy, the PSD can be defined as the square of the magnitude of the Fourier transform.

$$\Phi_{\omega} = |W(\omega)|^2 \tag{5.4}$$

This value is then usually divided by product of the sampling frequency, f_s, and signal length L. Other denominators may be used, since they are scaling factors.

$$\Phi_{\omega} = \frac{|W(\omega)|^2}{f_s \cdot L} \tag{5.5}$$

The energy of the signal, Φ_{ω}, has dimensions of power/frequency and is measured between ω_1 and ω_2.

$$PSD = \int_{\omega_1}^{\omega_2} \Phi_{\omega}(\omega) d\omega \tag{5.6}$$

5.3 PSD Conversion Method

To return the PSD to a statistical equivalent of the original data, the PSD must first be multiplied by the denominator that was originally used, which is f_s*L.

$$|W(\omega)|^2 = f_s \cdot L \cdot \Phi_{\omega} \tag{5.7}$$

The square root of the converted data can be taken and the Fourier transform inversed. If the length of the signal, L, cannot be determined from the stored PSDs, the product of the sampling frequency, f_s, and the window size, T, will be used for L. This modifies the denominator in equation 5.7.

$$|W(\omega)|^2 = f_s \cdot T \cdot \Phi_\omega \tag{5.8}$$

Since only the magnitude of the Fourier transform is used when calculating the PSD; the phase angles, $\phi(\omega)$, for the data points are lost. Without the phase angles an inverse Fourier transform cannot be used to return the data to its original form. To eliminate this problem, a set of random phase angles, between zero and one, must be created to reconstruct a statistical equivalent of the Fourier transform of the original data. The phase angles are then applied to both the real and imaginary parts of the signal.

$$\mathrm{Re}(W(\omega)) = \sqrt{f_s \cdot T * \Phi(\omega)} * \cos(\phi(\omega)) \tag{5.9}$$

$$\mathrm{Im}(W(\omega)) = -\sqrt{f_s \cdot T * \Phi(\omega)} * \sin(\phi(\omega)) \tag{5.10}$$

$$W(\omega) = \mathrm{Re}(W(\omega)) + \mathrm{Im}(W(\omega)) \tag{5.11}$$

An inverse Fourier transform can then be performed to get a statistical equivalent of the original data $W(t)$. The inverse of the Fourier transform is calculated by:

$$W(t) = \frac{1}{2\pi} \int_{\infty}^{\infty} W(\omega)^{i\omega t}\, d\omega \tag{5.12}$$

The subroutines used by DADS must be written in Fortran. A subroutine, shown in Figure 5.1, was created in Fortran to inverse the PSD, for later used in DADS. This subroutine uses a window size of 2048 and a sampling frequency of 4 samples/ft. Since the signal length is not known for the known ATC PSDs, the window value is also used as the signal length.

The subroutine first reads in the PSD data. Each data point is then multiplied by the denominator, f_s*T, and the square root of the product is taken. A random number is then created using the random number generator in Fortran. The random number is then

```
SUBROUTINE IPSD(YPSD,X,Y,Z)
! J. ANDREW RIDNOUR
! 7-19-01
! DECLARATIONS
INTEGER P
REAL X, Y, YPSD(2048),YMAGBK(2048), PHI, YIMAGRE(2048), PI, B, YIMAGPHI(4096)
PARAMETER(T=2048,PI=3.14159,fs=4)
EXTERNAL TIME
! Return to time domain
!
! Reconsrutuct magnitude using matrix of random phase angles
!
DO 10 P= 1,T
  YMAGBK(P)=SQRT(fs*T*YPSD(P))
        B=RAND(0)
        PHI=2*PI*B
        YIMAGRE(P)=(YMAGBK(P))*COS(PHI)
        A=YIMAGRE(P)
        C=-YMAGBK(P)*SIN(PHI)
        YIMAGPHI(2*P-1)=A
        YIMAGPHI(2*P)=C
10 CONTINUE
! Inverse FFT
! From Numerical Recipies Second Edition
CALL FOUR1(YIMAGPHI,2048,-1)
YIMAGPHI=YIMAGPHI/2048
Z=YIMAGPHI(1)
RETURN
END
```

Figure 5.1: PSD conversion Fortran subroutine.

multiplied by 2π, to generate the phase angle. The phase angle is then applied to the real and imaginary parts of the signal using the cosine and sine functions, respectively, which allow the Fourier transform to be inversed. The inverse FFT routine from the Numerical Recipes Book (Press et al., 1992) is then used to inverse the Fourier transform.

5.4 PSD Conversion Results

PSDs of terrain data from both the Belgian Block and Perryman #3 test courses were used to test the PSD inversion method and routine. The univariate statistics for the reconstructed data are shown in Table 5.1. The reconstructed terrain data is shown in Figures 5.2 and 5.3 for the Belgian Block and Perryman #3 test courses, respectively. For the Belgian Block test course, the difference between the original and reconstructed mean, standard deviation, and range, was 1.481E-5 ft (14.55 %), 0.00194 ft (3.20 %), and 0.3845 ft (73.97 %), respectively. For the Perryman #3 data, the difference between the original and reconstructed mean, standard deviation, and range, was -0.0005 ft (38.46 %), 0.0766 ft (4.765 %), and 0.9029 ft (16.476 %), respectively. The difference in the mean values was expected since the terrain data is randomly reconstructed. The small differences in standard deviation were also expected since the standard deviation relates to the variation in the data. The large differences in range are due to the fact the signal length for the PSD was not known, and was assumed to be the window. This is acceptable since the main goal is to represent the frequency content of the original data. Once the PSD subroutine is implemented in DADS, simulation results will be available to determine the effect of the reduction in range.

Table 5.1: Univariate statistics for terrain data.

	Perryman #3		Belgian Block	
	Original	**Reconstructed**	**Original**	**Reconstructed**
Mean	-0.0013	-0.0018	1.0181E-4	8.7E-5
Standard Dev.	0.2358	0.3124	0.06284	0.0609
Range	1.6076	0.7047	0.5198	0.1353

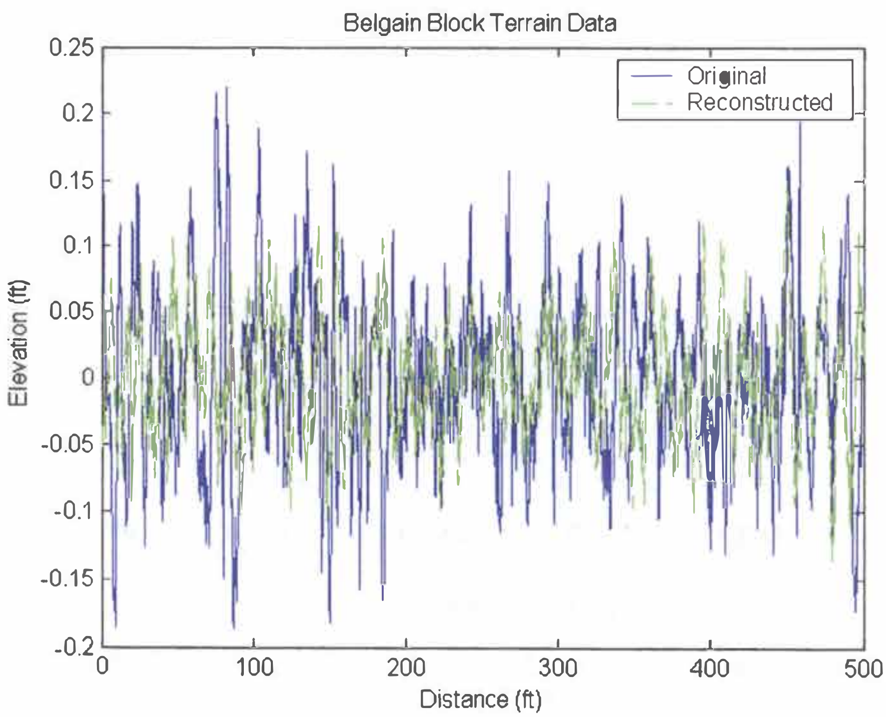

Figure 5.2: Belgian Block terrain data.

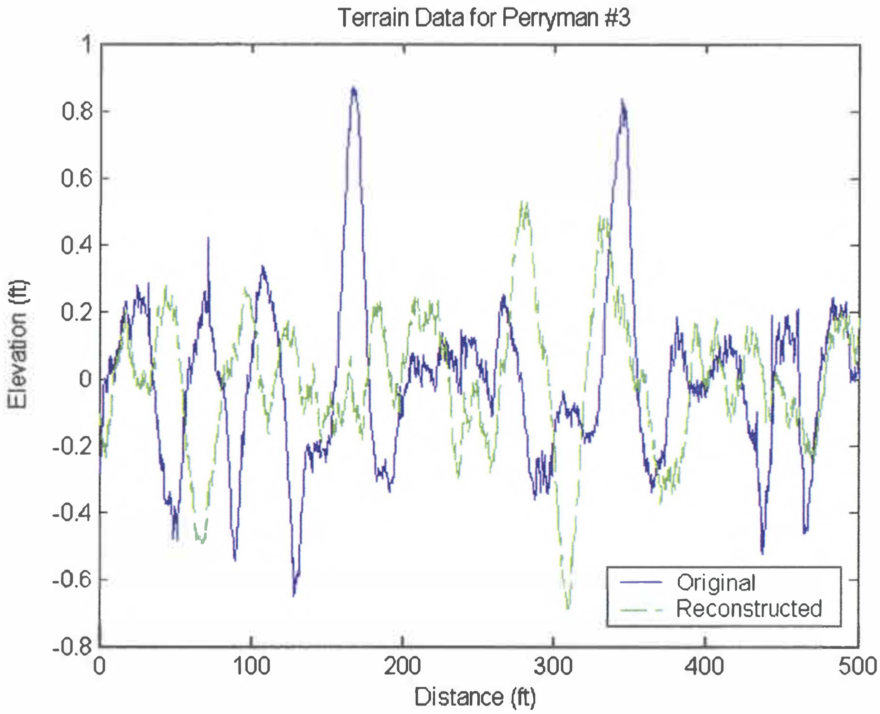

Figure 5.3: Perryman #3 terrain data.

The frequency of the terrain that is transferred to the trailer is thought to be more important in determining the durability. To check the frequency content of the re-created signal, the FFT and PSD of the original and reconstructed signals were compared, as shown in Figures 5.4 through 5.7. From the figures it can be seen that the terrain data can be reconstructed with an equivalent of the frequency content of the original terrain data.

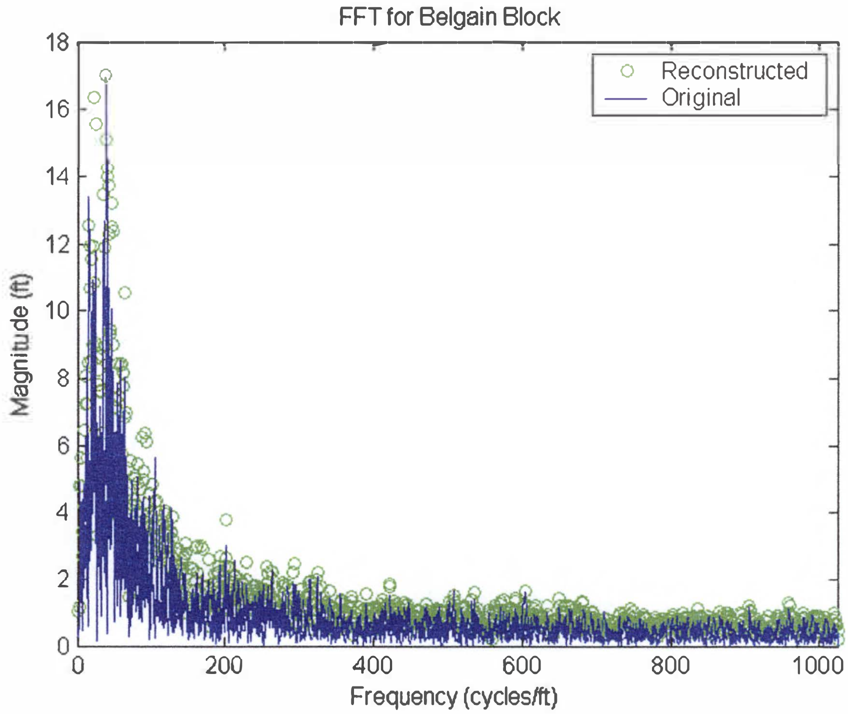

Figure 5.4: Belgian Block FFT.

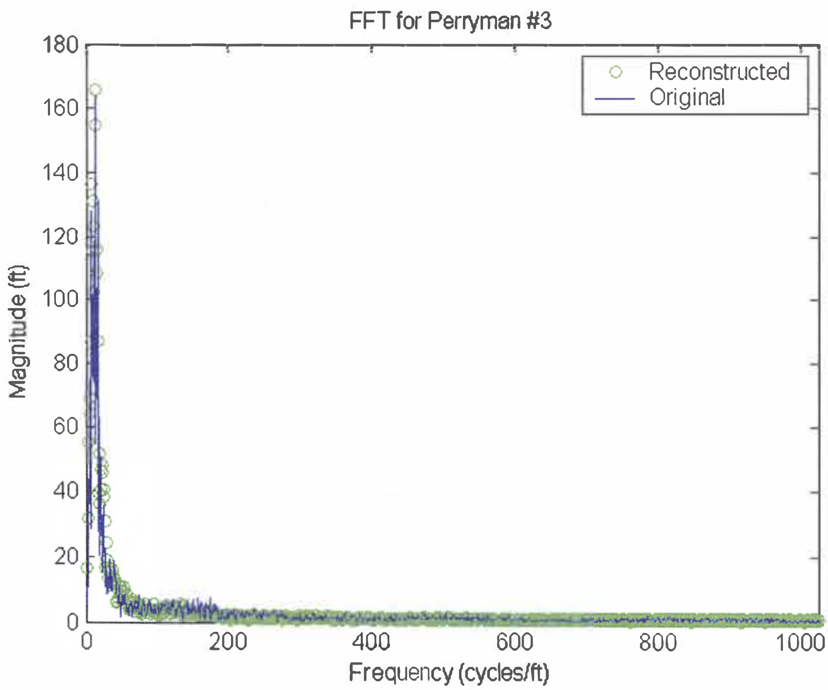

Figure 5.5: Perryman #3 FFT.

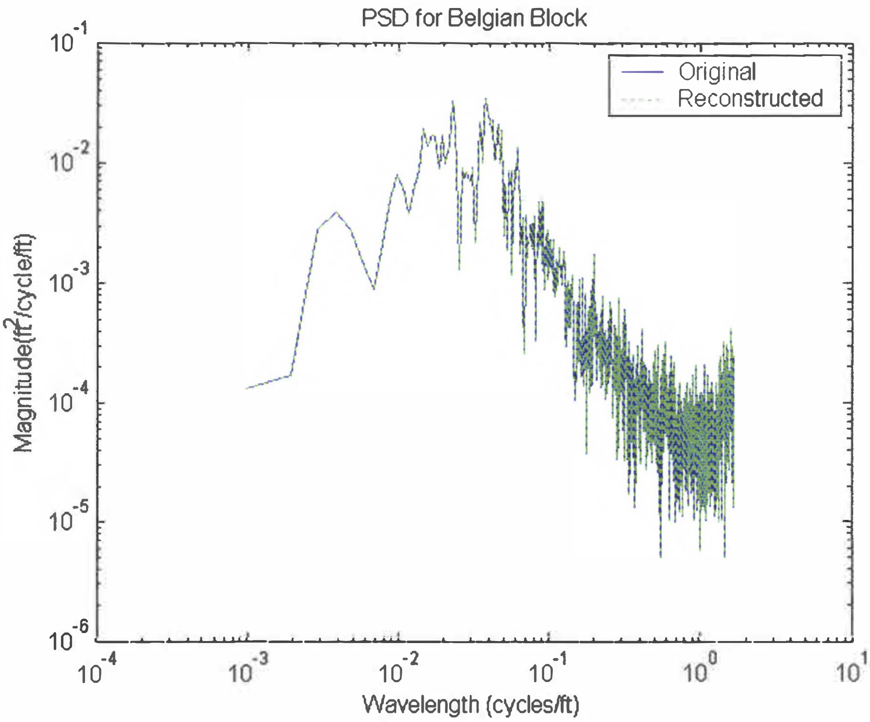

Figure 5.6: Belgian Block PSD.

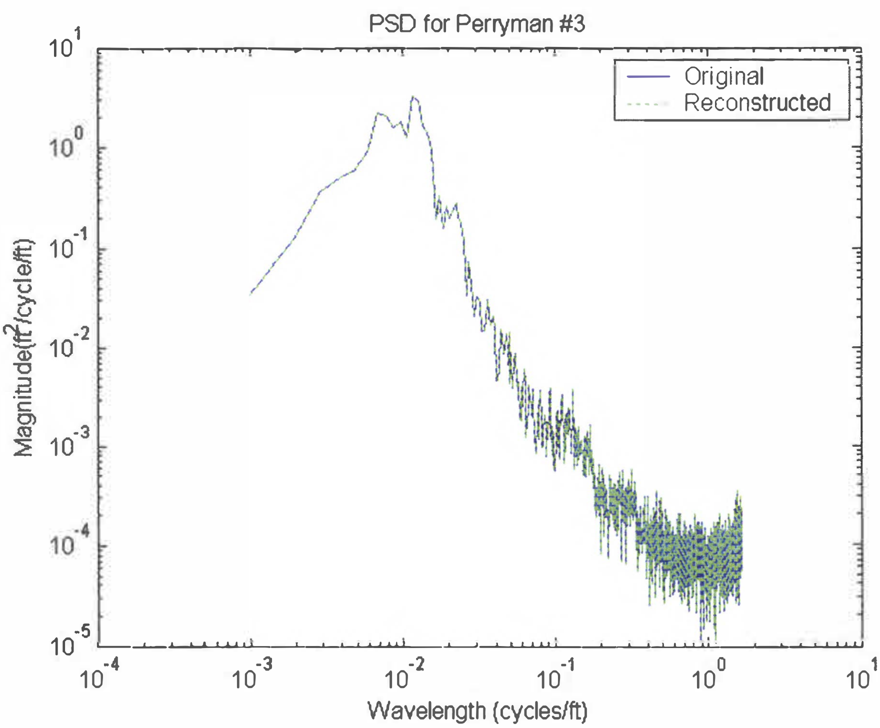

Figure 5.7: Perryman #3 PSD.

Chapter 6 Surge Brake Analysis

To optimize the current DADS model, it is important to determine which sensor data variables are not relevant to the strains at the location of the drawbar failure. By determining the non-relevant variables, they can be eliminated. Of particular interest, in this case, are the surge brake pressures on the trailer. In the current study, it was suspected that the hydraulic surge brake was contributing to fatigue failures of the trailer drawbar. By determining if the brake pressure variables are relevant, having a significant effect on the strains, we can determine if the brake activation has an effect on the life of the trailer. If the brake pressure variables do not have an effect on the strains, a model of the brake is not required in the simulation.

The trailer was instrumented and tested at the U.S. Army Aberdeen Test Center (ATC). Testing was performed, both with a normally operational surge brake system, and with the system physically disabled. Of interest in this chapter, are the statistical effects of the braking system on the trailer drawbar strains in the region of failure.

6.1 Hydraulic Surge Brake Operation

Hydraulic surge brakes are actuated by a force acting on the trailer hitch between the tow vehicle and trailer. Only negative forces, due to braking or deceleration of the tow vehicle, or in some instances backing in reverse, can actuate the brake system. A typical surge brake hitch assembly is shown in Figure 6.1. When actuated, the lunette translates with respect to the housing and presses on the brake cylinder, causing hydraulic pressure to be transmitted to the drum brakes. The damper controls the rate of actuation,

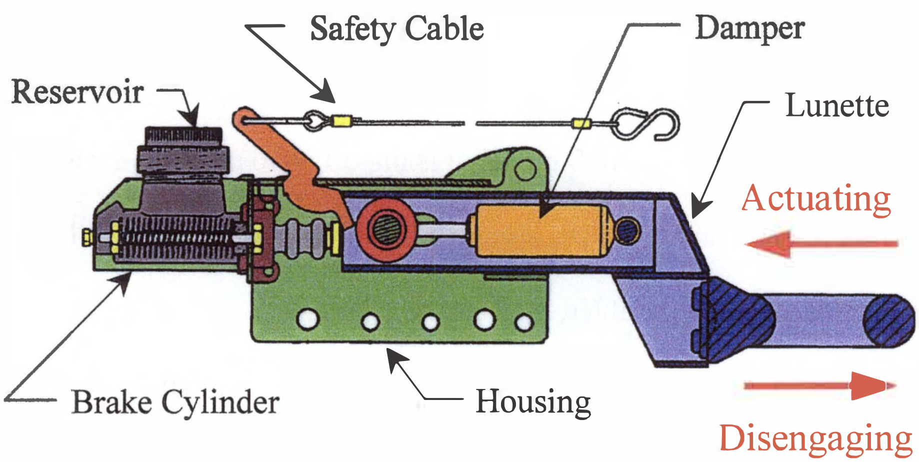

Figure 6.1: Typical hydraulic surge brake hitch assembly

both engaging and disengaging, so that the brakes do not operate as a 'bang-bang' system.

6.2 Test Data

Both the Belgian Block and Perryman #3 for runs with the brakes both enabled and disabled was used for this analysis. A listing of the instrumentation channels from the test data appears in Table 6.1. For the purposes of this study, the data channels were divided into three groups; input channels, output channels, and ignored channels. The output channels consisted of the strain gauge rosette located closest to the predicted point of failure. This is identified as the bottom drawbar center-aft rosette in the table. Other strain gauge channels, as well as the tow vehicle speed were ignored. This left the accelerometers, rate gyros, pressure transducers, and position transducers to represent the input variables to the system.

Table 6.1: Listing of Data Acquisition Channels and Grouping.

#	Description	Group	#	Description	Group
1	Time	Ignored	31	**Lunette Trans. Accel.**	**Input**
2	Btm Drwbr Cntr (T) Strain	Ignored	32	**Lunette Long. Accel.**	**Input**
3	Btm Drwbr Cntr (45) Strain	Ignored	33	**Tongue Vert. Accel.**	**Input**
4	Btm Drwbr Cntr (L) Strain	Ignored	34	**Tongue Trans. Accel.**	**Input**
5	**Btm Drwbr Cntr Aft (T) Strain**	**Output**	35	**Tongue Long. Accel.**	**Input**
6	**Btm Drwbr Cntr Aft (45) Strain**	**Output**	36	**CG Vert. Accel.**	**Input**
7	**Btm Drwbr Cntr Aft (L) Strain**	**Output**	37	**CG Trans. Accel.**	**Input**
8	Btm Drwbr CS Edge (T) Strain	Ignored	38	**CG Long. Accel.**	**Input**
9	Btm Drwbr CS Edge (45) Strain	Ignored	39	**Curbside Front Vert. Accel.**	**Input**
10	Btm Drwbr CS Edge (L) Strain	Ignored	40	**Curbside Front Trans. Accel.**	**Input**
11	Btm Drwbr CS Edge Aft (T) Strain	Ignored	41	**Curbside Front Long. Accel.**	**Input**
12	Btm Drwbr CS Edge Aft (45) Strain	Ignored	42	**Curbside Rear Vert. Accel.**	**Input**
13	Btm Drwbr CS Edge Aft (L) Strain	Ignored	43	**Curbside Rear Trans. Accel.**	**Input**
14	Top Triang Plate Corner (T) Strain	Ignored	44	**Curbside Rear Long. Accel.**	**Input**
15	Top Triang Plate Corner (45) Strain	Ignored	45	**Roadside Front Vert. Accel.**	**Input**
16	Top Triang Plate Corner (L) Strain	Ignored	46	**Roadside Front Trans. Accel.**	**Input**
17	Btm Triang Plate Corner (T) Strain	Ignored	47	**Roadside Front Long. Accel.**	**Input**
18	Btm Triang Plate Corner (45) Strain	Ignored	48	**Roadside Rear Vert. Accel.**	**Input**
19	Btm Triang Plate Corner (L) Strain	Ignored	49	**Roadside Rear Trans. Accel.**	**Input**
20	Left Angle Plate Lower (V) Strain	Ignored	50	**Roadside Rear Long. Accel.**	**Input**
21	Left Angle Plate Lower (45) Strain	Ignored	51	**Pitch Rate**	**Input**
22	Left Angle Plate Lower (L) Strain	Ignored	52	**Roll Rate**	**Input**

Table 6.1: Continued.

23	Left Angle Plate Upper (V) Strain	Ignored	53	**Yaw Rate**	**Input**
24	Left Angle Plate Upper (45) Strain	Ignored	54	**Curbside Shock Length**	**Input**
25	Left Angle Plate Upper (L) Strain	Ignored	55	**Roadside Shock Length**	**Input**
26	**Curbside Axle Vert. Accel.**	**Input**	56	**Master Cylinder Press.**	**Input**
27	**Curbside Frame Vert Accel**	**Input**	57	**Curbside Brake Press.**	**Input**
28	**Roadside Axle Vert. Accel.**	**Input**	58	**Roadside Brake Press.**	**Input**
29	**Roadside Frame Vert. Accel.**	**Input**	59	Tow Vehicle Speed	Ignored
30	**Lunette Vert Accel**	**Input**			

Four test runs were used for analysis of the surge brake. The test runs were on the Belgian Block and Perryman #3 test courses with the tow vehicle/trailer speed at nominally 15 mph. Two test runs were performed on each test course. On one of the test runs for each course, the brake system was operating normally. On the second run, the brake system was disabled by fixing the lunette, preventing the actuation of the brake master cylinder.

The brakes pressure variables are for the master cylinder, RS wheel cylinder, and CS wheel cylinder. The strains are the transverse, 45 degree, and longitudinal strains for the center drawbar aft location. The brake pressure data from all four test runs, which includes the runs with the brakes disabled, was analyzed to look for errors and potential analysis problems.

6.2.1 Belgian Block

For the test data from the Belgian Block test course at 15 mph with the brakes enabled. Table 6.2 shows the brake pressures to be highly correlated. Although the CS wheel cylinder pressure has lower mean and minimum values than the RS wheel cylinder, indicating a possible bias in the system. Ideally, the losses between the master and wheel cylinders should be equivalent.

As you can see from Table 6.3 and Figure 6.2, the brake pressures are highly correlated and have the same changes in magnitude. Although the RS wheel cylinder pressure is not as highly correlated with the master cylinder, also indicating a possible bias in the system. The friction losses between the master and wheel cylinders should only cause a pressure drop between the master and wheel cylinders, and the wheel cylinders should have the same pressures.

For the test data from the Belgian Block at 15 mph with the brakes disabled, the wheel cylinder pressures were not constant, as shown in Table 6.4 and Figure 6.3. This was not expected since the surge brake was disabled and the brake pressures should remain constant. The variations in the master cylinder and RS wheel cylinder pressures were very small and can be contributed to the sensor noise in data collection. The CS wheel cylinder pressure variation was enough to affect the regression model, but not activate the brake. It cannot be determined if the variation in the CS wheel cylinder pressure was from the sensor, noise, or the brake dragging slightly. The surge brake was not activating since the master cylinder and RS wheel cylinder pressures remained constant. There was also a calibration problem as seen in Belgian Block at 15 mph with

Table 6.2: Statistics for brake pressures for Belgian Block at 15 mph with brakes enabled.

	Minimum (psi)	Mean (psi)	Maximum (psi)
Master Cylinder	-3.6135	7.7645	91.7407
CS Wheel Cylinder	-10.4465	2.1369	76.6134
RS Wheel Cylinder	-4.9795	4.9117	75.3901

Table 6.3: Correlation coefficient between brake pressures for Belgian Block at 15 mph with brakes enabled.

	Master Cylinder	CS Wheel Cylinder	RS Wheel Cylinder
Master Cylinder	1.0000	0.9889	0.9639
CS Wheel Cylinder	0.9889	1.0000	0.9857
RS Wheel Cylinder	0.9639	0.9857	1.0000

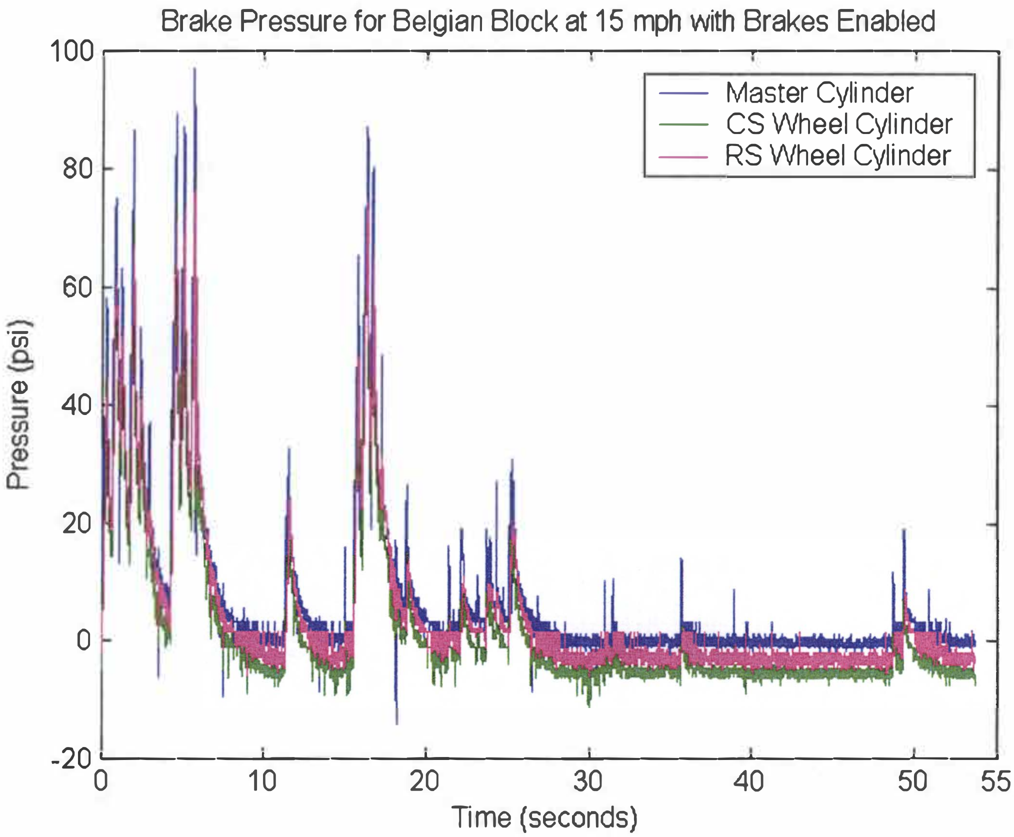

Figure 6.2: Surge brake response for Belgian Block at 15 mph with brakes enabled.

Table 6.4: Statistics for brake pressures for Belgian Block at 15 mph with brakes disabled.

	Minimum (psi)	Mean (psi)	Maximum (psi)
Master Cylinder	3.0166	3.5226	4.8359
CS Wheel Cylinder	-6.5763	-0.2867	4.5523
RS Wheel Cylinder	0.1862	1.5529	1.7714

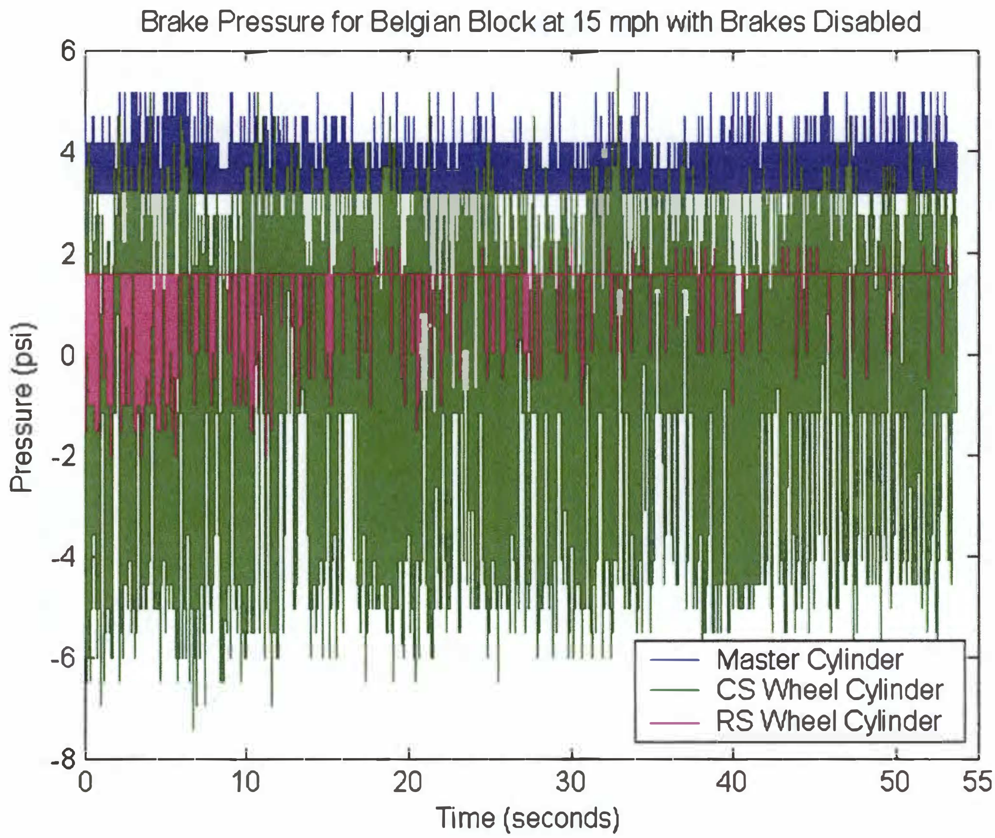

Figure 6.3: Surge brake response for Belgian Block at 15 mph with brakes disabled.

brakes enabled, as expected, since the runs with brakes disabled and enabled were consecutive, and had the same calibration. Due to the effect of the CS wheel cylinder pressure on the model, the brake pressure variables were then removed from the model. The errors in brake pressures also explain some of the results from the analysis of Belgian Block at 15 mph with brakes enabled, and validates the assumptions of errors in the pressure data.

6.2.2 Perryman #3

For the test data from the Perryman #3 test course at 15 mph with the brakes enabled, an analysis of the data shows, in Table 6.5, that there was a pressure loss (as would be expected) between the master and wheel cylinders, and there was also a calibration problem. As you can see from Table 6.6 and Figure 6.4, the brake pressures are well correlated and have the same changes in magnitude. The range for the wheel cylinder pressures is 89.647 psi and 98.77 psi for the CS and RS wheel cylinders, respectively. These values indicating a possible difference in actuation between the CS and RS wheel cylinders. The range for the master cylinder pressure was 110.122. The friction losses between the master and wheel cylinders should only cause a pressure drop between the master and wheel cylinders and the wheel cylinders should have the same pressures.

For the test data from the Perryman #3 test course at 15 mph with the brakes disabled, an analysis of the data shows, in Table 6.7, that the brake pressure did not remain constant, and there was also a calibration problem. The calibration problem would be expected since the Perryman #3 runs at 15 mph with the brakes both disabled and enabled were consecutive and had the same calibration.

It cannot be determined if the variation in the brake pressures were from the sensor, noise, or the brake dragging slightly. As you can see from Table 6.8 and Figure 6.5, the brake pressures are not very well correlated and do not have the same changes in magnitude, which would indicate the pressure variations are probably due to noise in the system and not partial actuation. These pressure variations could affect the regression

Table 6.5: Statistics for brake pressures for Perryman #3 test course at 15 mph with brakes enabled.

	Minimum (psi)	Mean (psi)	Maximum (psi)
Master Cylinder	-23.232	-13.1417	86.89
CS Wheel Cylinder	-21.9140	-16.1996	67.7330
RS Wheel Cylinder	-25.4010	-15.9754	73.3690

Table 6.6: Correlation coefficient between brake pressures for Perryman #3 test course at 15 mph with brakes enabled.

	Master Cylinder	CS Wheel Cylinder	RS Wheel Cylinder
Master Cylinder	1.0000	0.9886	0.9804
CS Wheel Cylinder	0.9886	1.0000	0.9963
RS Wheel Cylinder	0.9804	0.9963	1.0000

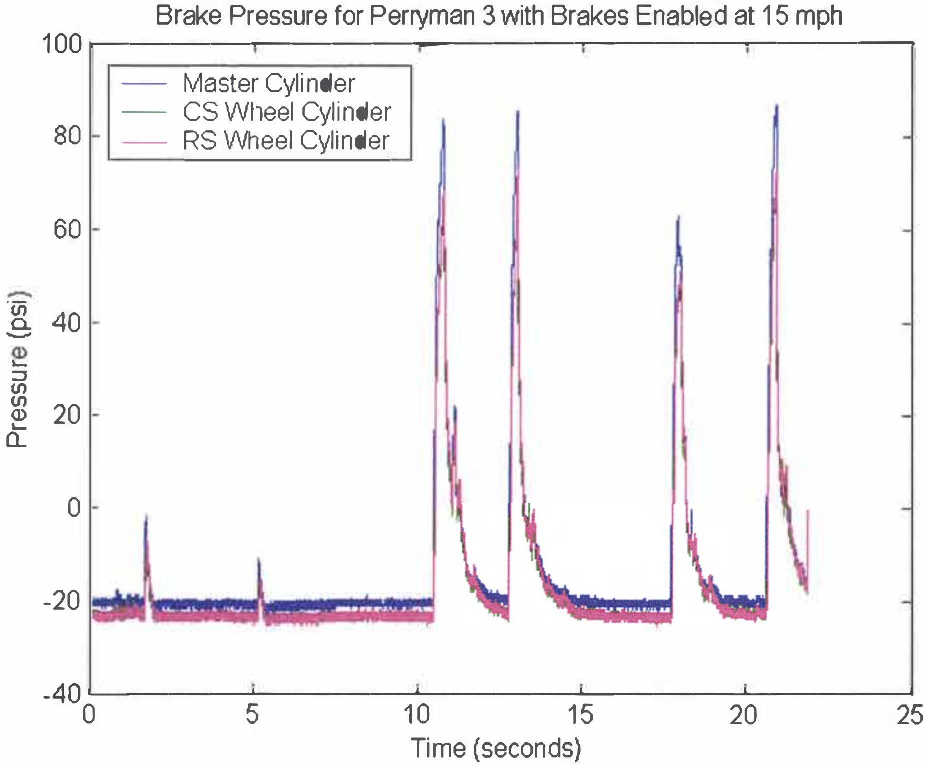

Figure 6.4: Surge brake response for Perryman #3 test course at 15 mph.

Table 6.7: Statistics for brake pressures for Perryman #3 at 15 mph with brakes disabled.

	Minimum (psi)	**Mean (psi)**	**Maximum (psi)**
Master Cylinder	6.6650	9.5471	12.146
CS Wheel Cylinder	-2.6010	-1.5177	4.19
RS Wheel Cylinder	0.0550	1.1530	6.165

Table 6.8: Correlation coefficient between brake pressures for Perryman #3 at 15 mph with brakes disabled.

	Master Cylinder	CS Wheel Cylinder	RS Wheel Cylinder
Master Cylinder	1.0000	0.346	0.242
CS Wheel Cylinder	0.346	1.0000	0.0587
RS Wheel Cylinder	0.242	0.0587	1.0000

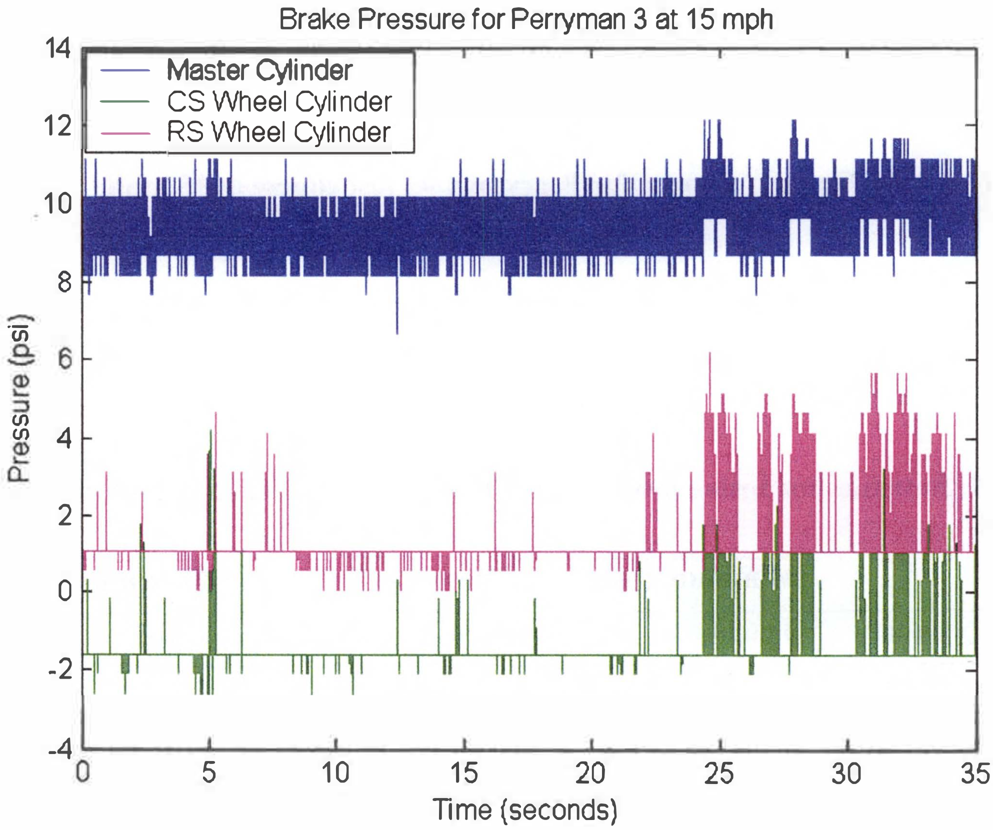

Figure 6.5: Surge brake response for Perryman #3 at 15 mph with brakes disabled.

model and the variables should be removed from the model. The range for the wheel cylinder pressures is 6.791 psi and 6.22 psi for the CS and RS wheel cylinders, respectively. These values indicate no brake actuation for both wheel cylinders.

6.3 Analysis Method

The four test runs measured by ATC need to be evaluated to compare the effects of the surge brake on the measured strain. Assuming that the brake torques, which are generated by the brake pressure, have a direct relationship to the measured strain, a regression model can be developed to represent this relationship. However, other measured responses, such as longitudinal acceleration may also affect the relationship. Given that 59 channels of data were measured for each run, and 33 of those were considered as input variables, the task of determining which of the data channels was relevant to the observed response (strain) and which were non-relevant was required to reduce the size of the dataset.

The non-relevant variables were determined by using principal component analysis and multivariate regression. Several regression models were created:

- Brakes enabled, brake pressure data included in regression.
- Brakes enabled, brake pressure data removed from regression.
- Brakes disabled, brake pressure data removed from regression.
- Concatenated dataset, combining both brakes enabled and disabled.

The regression models were developed using both the data as measured, and using the principal component variables, which form an uncorrelated, orthogonal set of predictor variables.

6.3.1 Regression Analysis for Belgian Block (Brakes enabled)

The non-relevant variables were determined by using multivariate regression. Regression analysis is used for description, control, and prediction of data. SAS and Matlab were used to perform the statistical analyses. The data was stored in a matrix form with one column for each data channel. To simplify the regression equations in SAS the channels used the variable names shown in Table 6.9.

A multivariate regression that included pairwise interaction effects was created to determine if there were any significant interactions between the input variables. The models for transverse, 45 degree, and longitudinal strain had overall R^2 values of 0.8666, 0.8952, and 0.9086, respectively.

Three regression models, without interaction effects, were created to initially determine which variables contained the least amount of significant information. The first strain model created was for the transverse strain. The variable for ground speed was eliminated before the models were created. Using a stepwise regression model we can see that the R^2 value for the model using all 33 independent variables is 0.7879 and with the brake pressure data eliminated the R^2 is 0.7832. It is interesting to note that if ground speed is eliminated, the R^2 value does not change. If the RS longitudinal lunette acceleration, CG pitch rate, CG roll rate, and CG yaw rate are also eliminated the R^2 value is 0.7716. This pattern continues throughout the model, with the reduction in variables not reducing R^2 by a significant amount by each reduction, until only highly correlated variables are left. Note that the R^2 value of the entire model decreased significantly with the removal of the terms for interaction effects.

Table 6.9: Column and variable numbers for data channels of reduced data sets.

Col	Var	Description	Units	Col	Var	Description	Units
1	F1	Btm Drwbr Cntr Aft ε (T)	μ inch	20	F20	CS Aft Accel (V)	g's
2	F2	Btm Drwbr Cntr Aft ε (45)	μ inch	21	F21	CS Aft Accel (T)	g's
3	F3	Btm Drwbr Cntr Aft ε (L)	μ inch	22	F22	CS Aft Accel (L)	g's
4	F4	CS Axle Accel (V)	g's	23	F23	RS Forward Accel (V)	g's
5	F5	CS Frame Accel (V)	g's	24	F24	RS Forward Accel (T)	g's
6	F6	RS Axle Accel (V)	g's	25	F25	RS Forward Accel (L)	g's
7	F7	RS Frame Accel (V)	g's	26	F26	RS Aft Accel (V)	g's
8	F8	Lunette Accel (V)	g's	27	F27	RS Aft Accel (T)	g's
9	F9	Lunette Accel (T)	g's	28	F28	RS Aft Accel (L)	g's
10	F10	Lunette Accel (L)	g's	29	F29	Trailer CG Pitch Rate	deg/sec
11	F11	Tongue Accel (V)	g's	30	F30	Trailer CG Roll Rate	deg/sec
12	F12	Tongue Accel (T)	g's	31	F31	Trailer CG Yaw Rate	deg/sec
13	F13	Tongue Accel (L)	g's	32	F32	CS Shock Disp	inches
14	F14	Trailer CG Accel (V)	g's	33	F33	RS Shock Disp	inches
15	F15	Trailer CG Accel (T)	g's	34	F34	Surge Brake Press.	psi
16	F16	Trailer CG Accel (L)	g's	35	F35	CS Wheel Brake Press.	psi
17	F17	CS Forward Accel (V)	g's	36	F36	RS Wheel Brake Press.	psi
18	F18	CS Forward Accel (T)	g's	37	F37	Long. Ground Speed	mph
19	F19	CS Forward Accel (L)	g's	38	off	Added Class Variable	n/a

The second strain model created was for the 45 degree strain. Using a stepwise regression model we can see that the R^2 value for the model using all 33 independent variables is 0.8016 and with the brake pressure data eliminated the R^2 is 0.7957. It is interesting to note that if ground speed is eliminated, the R^2 value does not change. If longitudinal lunette acceleration, transverse CS aft acceleration, CG pitch rate, CG roll rate, and CG yaw rate are also eliminated the R^2 value drops to 0.7862.

The third strain model created was for the longitudinal strain. Using a stepwise regression model we can see that the R^2 value for the model using all 33 independent variables is 0.8143 and with the brake pressure data eliminated the R^2 is 0.8081. If the CG roll and yaw rates are then eliminated, the R^2 drops to 0.8072. If longitudinal lunette acceleration, and CG pitch rate are also eliminated the R^2 value drops to 0.7951. If transverse lunette acceleration and longitudinal ground speed are eliminated, the R^2 drops to 0.7941.

A multivariate regression with interactions was again created with the brake pressure variables eliminated. The model for transverse, 45 degree, and longitudinal strains had overall R^2 values of 0.8577, 0.8818, and 0.8975, respectively. The fit of the regression models was also analyzed by looking at the residuals. Since the regression models for longitudinal strain are of particular interest in the prediction of fatigue life and failure of the trailer they will be used for the analyses.

As shown in Figure 6.6, the linear regression model that included the brake pressure data and interaction terms is an appropriate model. Comparing Figures 6.6 and 6.7, it can be seen that the removal of the brake pressure data had little effect on the fit

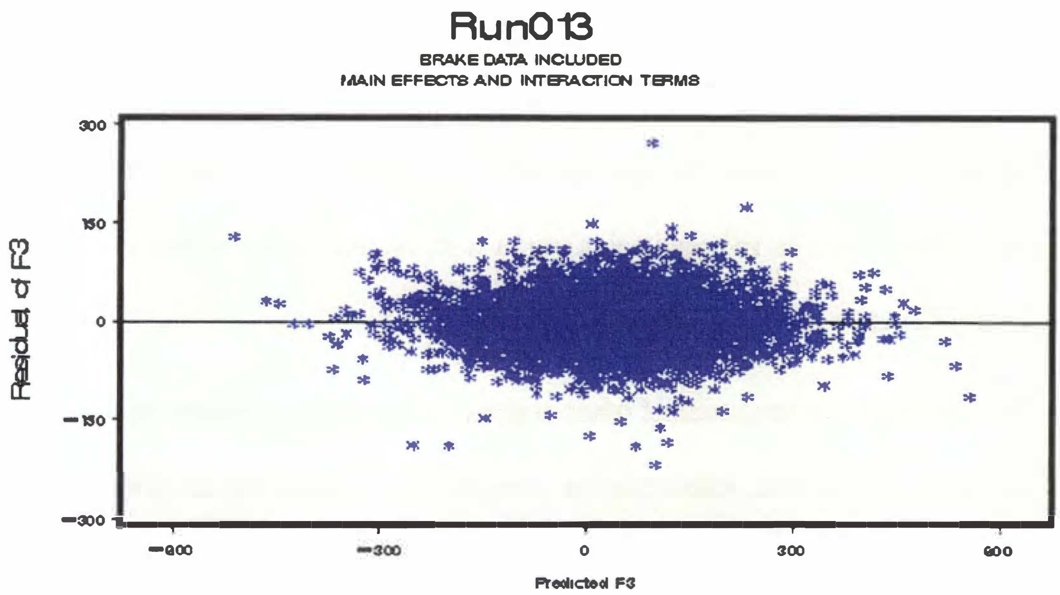

Figure 6.6: Residual plot for Belgian Block at 15 mph with brakes enabled longitudinal strain regression model, with interaction terms and brake pressure data included.

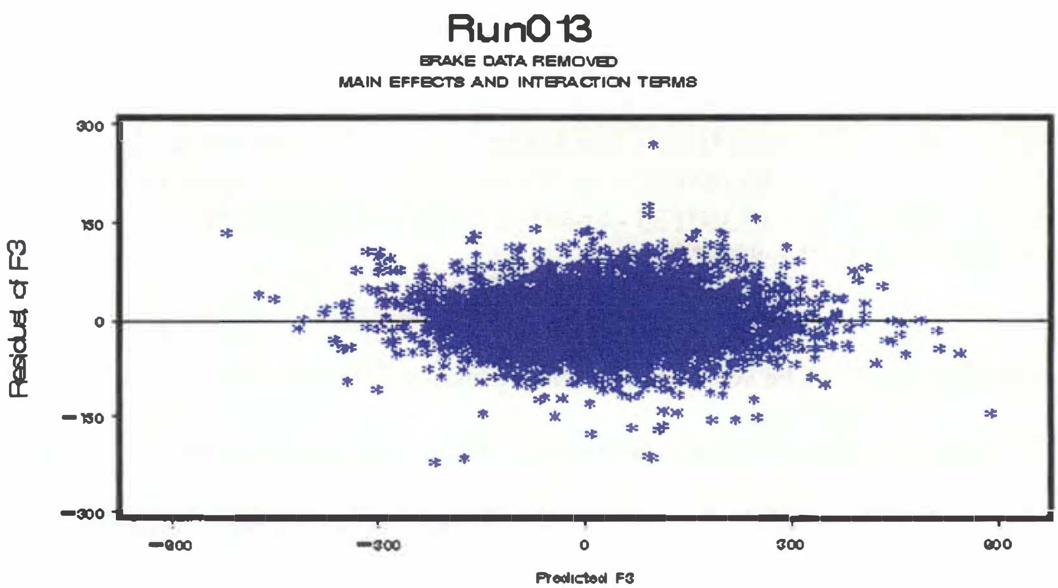

Figure 6.7: Residual plot for Belgian Block at 15 mph with brakes enabled longitudinal strain regression model, with interaction terms and brake pressure data removed.

of the regression model. From Figure 6.8 it can be seen that the linear model is also appropriate with the interaction terms removed, but the fit is not as accurate. Comparing Figure 6.8 and Figure 6.9, it can be seen that the removal of the brake pressure data also had little effect on the fit on the regression model with the interaction effects removed. Some outliers could be seen in all the residual plots.

The equations for longitudinal strain regression models for Belgian Block at 15 mph with the brakes enabled, without interaction effects included, and the brake pressure variables both included and removed are shown in Equations 6.1 and 6.2, respectively.

The predicted model is F3 = 221.3 + 0.662*F10 -261.0*F11 + 61.27*F12
+ 1696*F14 + 1715*F13 -236.1*F19 + 152.3*F20 + 36.11*F21 + 527.8*F15
-1926*F16 + 175.2*F17 -359.4*F18 + 317.8*F22 -269.3*F23 -425.0*F24 (6.1)
-55.99*F25 + 323.4*F26 + 95.04*F27 -2.095*F29 -631.7*F28 + 0.746*F30
-0.419*F31 + 84.63*F32 + 0.399*F33 -3.240*F37 + 13.32*F4 - 861.0*F5 +
10.83*F6 + 18.71*F8 -6.666*F9 -966.9*F7 + 0.895*F34 + 3.458*F35 -3.968*F36.

The predicted model is F3 = 232.4 + 3.034*F10 -250.9*F11 + 65.60*F12
+ 1711*F14 + 1662*F13 -301.9*F19 + 173.7*F20 + 15.64*F21 + 511.2*F15
-1918*F16 + 162.7*F17 -192.1*F18 + 356.5*F22 -252.4*F23 -548.0*F24 (6.2)
-46.33*F25 + 310.3*F26 + 90.16*F27 -2.021*F29 -575.0*F28 + 0.782*F30
-0.224*F31 + 95.16*F32 + 17.19*F33 -4.686*F37 + 14.48*F4 -888.7*F5 +
10.71*F6 + 19.24*F8 -6.318*F9 -976.4*F7.

From Equation 6.1, it can be seen that the brake pressure data parameters (F34, F35, F36) are small in comparison to the other parameters. The other parameters with large values do not drastically change when the brake pressure parameters are removed, as shown in Equation 6.2. The equations for models with interaction effects are not useful for comparison due to their length and complexity.

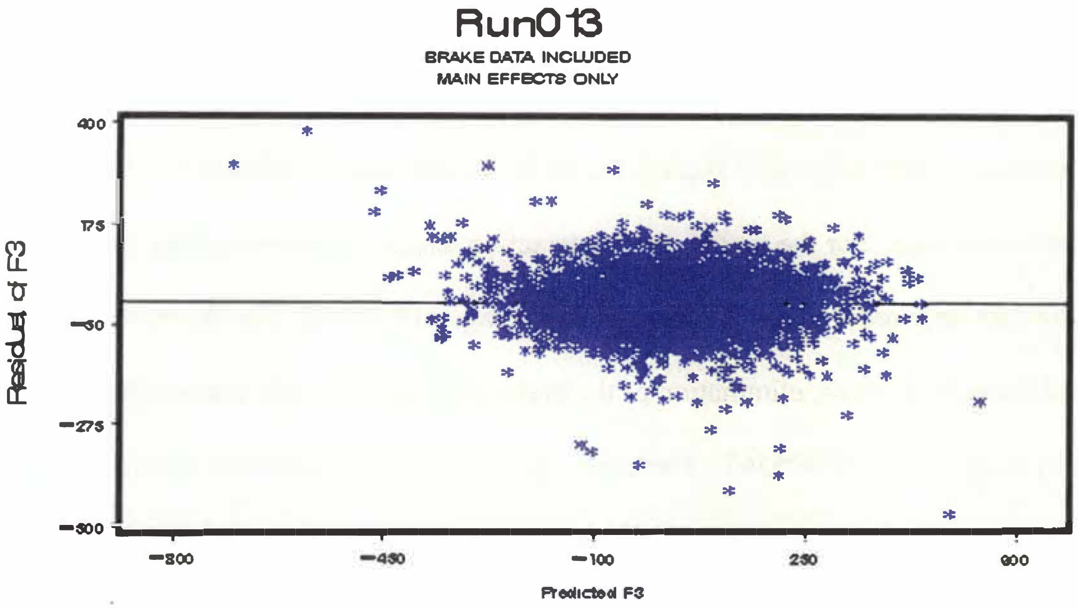

Figure 6.8: Residual plot for Belgian Block at 15 mph with brakes enabled longitudinal strain regression model, without interaction terms and brake pressure data included.

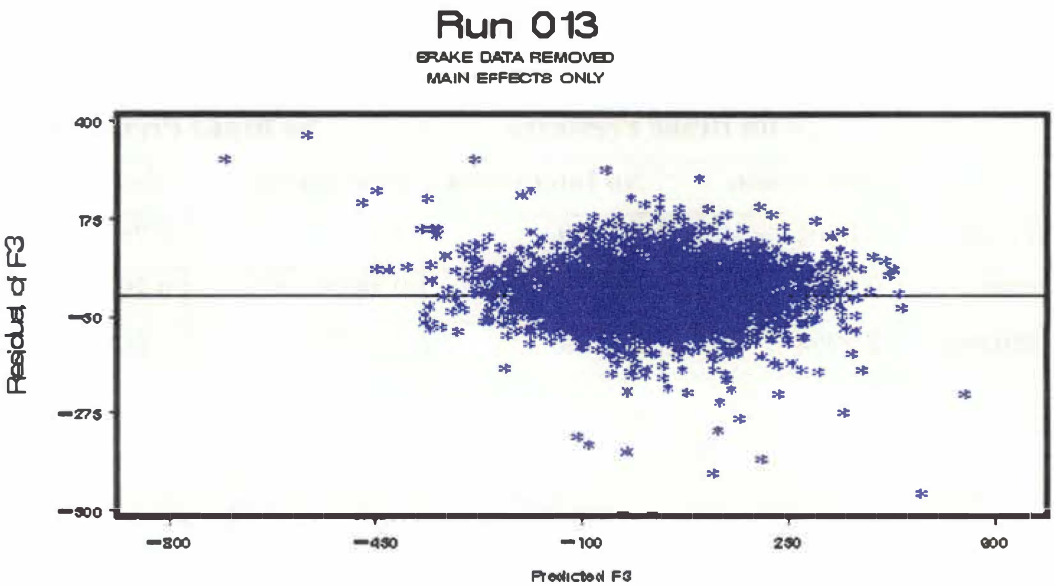

Figure 6.9: Residual plot for Belgian Block at 15 mph with brakes enabled longitudinal strain regression model, without interaction terms and brake pressure data removed.

As shown in Table 6.10, the models with interaction effects had higher R^2 values than the models without interaction terms. The R^2 values for the models with the brake pressure data included had only slightly higher R^2 values than the models without the brake pressure data. For the models with interaction terms, elimination of the brake pressure data only reduced the R^2 value by an average of 0.00967. For the models without interaction terms, elimination of the brake pressure data only reduced the R^2 value by an average of 0.005567. Therefore, the brake pressure data can be eliminated without having a significant effect on the model. This shows that the enabling or disabling of the surge brake does not have a significant effect on the life of the trailer.

Table 6.10: R^2 values for all models for Belgian Block at 15 mph with brakes enabled.

	With Brake Pressures		No Brake Pressures	
	Interaction	**No Interaction**	**Interaction**	**No Interaction**
Transverse	0.8666	0.7879	0.8577	0.7832
45 Degree	0.8926	0.8015	0.8818	0.7957
Longitudinal	0.9068	0.8143	0.8975	0.8081

6.3.2 Regression Analysis for Belgian Block (Brakes disabled)

A second analysis was performed to help explain and validate the findings from the analysis of Belgian Block at 15 mph with brakes enabled. For this analysis the data taken from the Belgian Block course with the surge brake disabled at 15 mph was used. This run was selected due to the fact it corresponds to Belgian Block at 15 mph with brakes enabled.

The initial analysis was performed using a multivariate regression without interactions for Belgian Block at 15 mph with brakes disabled. The results of the regression models for Belgian Block at 15 mph with brakes disabled are shown in Table 6.11. The results that are labeled 'with brake pressures' are only for showing the effect of the sensor error, since the brake pressures should have been constant and would have no effect on the regression model. Table 6.11 shows the R^2 values for the regression models for Belgian Block at 15 mph with brakes disabled, and the benefit of adding interaction terms to the models. The overall R^2 values for Belgian Block at 15 mph with brakes disabled were lower than the R^2 values for Belgian Block at 15 mph with brakes enabled, shown in table 6.10. The models for Belgian Block at 15 mph with brakes disabled that included interaction terms and no brake pressure data had overall R^2 values of 0.8049, 0.8133, and 0.8269, for transverse, 45 degree, and longitudinal strains, respectively. Without interaction terms the models for transverse, 45 degree, and longitudinal strains, had R^2 values of 0.7280, 0.7259, and 0.7373, respectively. The same models with interaction terms and brake pressure variables eliminated for Belgian Block at 15 mph with brakes enabled had overall R^2 values of 0.8577, 0.8818, and 0.8975, for transverse,

Table 6.11: R^2 values for all Belgian Block at 15 mph with brakes disabled regression models.

	With Brake Pressures		No Brake Pressures	
	Interaction	**No Interaction**	**Interaction**	**No Interaction**
Transverse	0.8121	0.7283	0.8049	0.7280
45 Degree	0.8206	0.7264	0.8133	0.7259
Longitudinal	0.8338	0.7383	0.8269	0.7373

45 degree, and longitudinal strains, respectively. Without interaction terms and brake pressure variables the models for Belgian Block at 15 mph with brakes enabled transverse, 45 degree, and longitudinal strains, had R^2 values of 0.7879, 0.7957, and 0.8081, respectively. The average difference in the overall R^2 value for the models with interaction terms and brake pressure variables removed between Belgian Block at 15 mph with brakes disabled and 13 was 0.06397 and 0.0668 for the models with no interaction terms and brake pressure variables removed. The equation for the longitudinal strain regression model for Belgian Block at 15 mph with brakes disabled, without interaction effects included, and the brake pressures removed is shown in Equation 6.3.

The predicted model is: $F3 = 221.0 + 34.90*F10 -329.2*F11 + 2410*F13 +1840*F14 + 522.9*F15 -4163*F16 + 48.82*F12 + 222.2*F17 - 598.7*F18 + 48.15*F19 + 14.13*F20 + 113.3*F21 + 596.0*F22 -229.2*F23 - 128.0*F24 +59.68*F25 + 55.26*F26 -107.1*F27 + 116.0*F28 -2.521*F29 + 0.434*F30 +0.0979*F31 + 113.6*F32 + 43.28*F33 -2.712*F37 + 12.18*F4 - 828.0*F5 +12.36*F6 -760.9*F7 + 20.62*F8 -10.34*F9.$ (6.3)

The fit of the regression models for the Belgian Block test data at 15 mph, with the brakes disabled, was also analyzed by looking at the residuals. Since the regression models for longitudinal strain are of particular interest in the prediction of fatigue life and failure of the trailer they again will be used for the analyses. Since the brake pressure should have been constant, containing no information, and the pressures would not have actuated the brake; the fit of the regression model was only analyzed for the models without brake pressure data. As shown in Figure 6.10, the linear regression model that included the interaction terms is an appropriate model. Comparing Figure 6.10 and Figure 6.11, it can be seen that the removal of the brake pressure data had little effect on the fit of the regression model. Some outliers could be seen in both models.

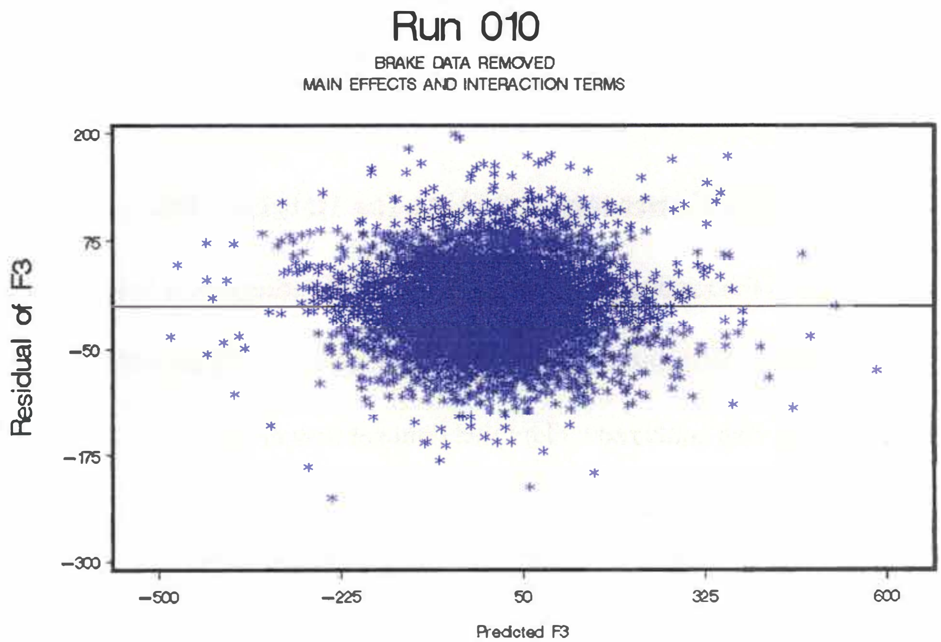

Figure 6.10: Residual plot for Belgian Block at 15 mph with brakes disabled longitudinal strain regression model, with interaction terms included and brake pressure data removed.

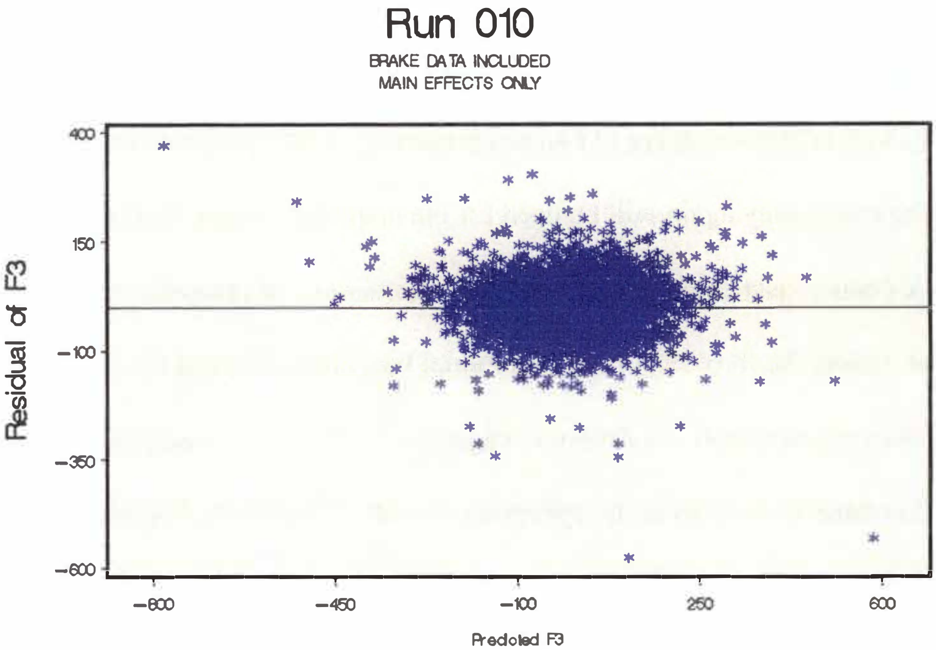

Figure 6.11: Residual plot for Belgian Block at 15 mph with brakes disabled longitudinal strain regression model, without interaction terms and brake pressure data removed.

6.3.4 Regression with Concatenated Data for Belgian Block

To determine if the reduced R^2 values were due to information lost with the surge brake disabled and if the disabling of the surge brake had a significant effect on the strains, a third data set was analyzed. The third data set was created by combining the data from both the Belgian Block tests at 15 mph, with brakes enabled and disabled. The brake pressures in Belgian Block at 15 mph with brakes disabled were all set to zero to minimize the effect of the error from the brake pressure data. The runs were also separated into classes based on whether the surge brake was enabled or disabled. By adding classes, the effect of the surge brake being enabled or disabled can be directly analyzed.

A multivariate regression with interactions was created for the third data set using all 33 independent variables and 1 classification variable. The models for transverse, 45 degree, and longitudinal strains had R^2 values of 0.8194, 0.8351, and 0.8512, respectively. The models showed significant interaction effects between the class variable and several other independent variables. With these interaction effects, the main effect of the classification variable could not be determined.

To determine the effect of the classification variable on the model, the classification variable was removed and another multivariate regression with interactions was created using all 33 independent variables. The models for transverse, 45 degree, and longitudinal strains had overall R^2 values of 0.8119, 0.8260, and 0.8430, respectively.

To determine the effect of the brake pressures on the model, the brake pressure variables were then removed from the model, leaving 30 independent variables. This yielded models for transverse, 45 degree, and longitudinal strains with overall R^2 values of 0.8106, 0.8243,and 0.8413, respectively.

The effect of the classification variable without the brake pressure variables was also studied by creating a multivariate regression and with interactions using the 30 independent variables left after the brake pressure variables were removed and the 1 classification variable. The models for transverse, 45 degree, and longitudinal strains had R^2 values of 0.8130, 0.8271,and 0.8442, respectively.

The equations for longitudinal strain regression models for Belgian Block at 15 mph with brakes disabled and enabled data without interaction effects that included the classification variable and the brake pressures both included and removed are shown in Equation 6.4 and Equation 6.5, respectively.

```
The predicted model is F3 = 211.0 -311.3*F11 + 29.36*F12 + 2104*F13
-119.1*F19 -405.1*F18 -3116*F16 + 190.2*F15 + 1809*F14 + 123.5*F17 +
95.51*F20 + 83.03*F21 + 445.3*F22 -155.7*F23 -55.40*F24 + 1.197*F25 +
213.9*F26 + 44.57*F27 -128.1*F28 -2.625*F29 + 0.752*F30 -0.493*F31 +
99.08*F32 + 36.42*F33 -1.683*F37 + 15.63*F4 -882.8*F5 + 11.75*F6
-930.4*F7 + 25.53*F8 -5.679*F9 + 7.530*F10 -61.15*(off='off') +
0.527*F34 + 3.781*F35 -3.706*F36 .
```
(6.4)

```
The predicted model is F3 = 203.2 -303.5*F11 + 30.98*F12 + 2055*F13
-185.3*F19 -306.5*F18 -3077*F16 + 138.8*F15 + 1820*F14 + 102.4*F17 +
105.7*F20 + 80.42*F21 + 486.8*F22 -138.5*F23 -95.27*F24 + 17.91*F25 +
208.6*F26 + 44.67*F27 -104.5*F28 -2.571*F29 + 0.782*F30 -0.363*F31 +
106.4*F32 + 46.60*F33 -2.085*F37 + 16.26*F4 -892.3*F5 + 11.64*F6
-940.1*F7 + 26.72*F8 -5.184*F9 + 10.66*F10 -52.68*(off='off') .
```
(6.5)

From Equation 6.4 you can see the brake pressure data parameters (F34, F35, F36) are small in comparison to the other parameters. The other parameters with large values do not drastically change when the brake pressure parameters are removed, as shown in Equation 6.5. The equations for longitudinal strain regression models for Belgian Block at 15 mph with brakes disabled and enabled data for Belgian Block at 15 mph, with brakes disabled and enabled data, without interaction effects or the classification variable and the brake pressures both included and removed are shown in Equation 6.6 and Equation 6.7, respectively.

```
The predicted model is F3 = 163.8 -309.0*F11 + 32.70*F12 + 2090*F13
-159.0*F19 -394.3*F18 -2935*F16 + 225.4*F15 + 1851*F14 + 116.9*F17 +
114.7*F20 + 76.95*F21 + 430.8*F22 -180.8*F23 -105.5*F24 -194.7*F25 +
250.2*F26 + 60.10*F27 -4.951*F28 -2.610*F29 + 0.707*F30 -0.519*F31 +
96.20*F32 + 37.81*F33 -1.952*F37 + 15.72*F4 -912.8*F5 + 12.77*F6
-969.2*F7 + 25.70*F8 -6.095*F9 + 6.964*F10 + 0.879*F34 + 2.993*F35
-3.282*F36 .
```
(6.6)

```
The predicted model is F3 = 162.4 -301.3*F11 + 33.47*F12 + 2039*F13
-226.0*F19 -292.7*F18 -2903*F16 + 169.9*F15 + 1855*F14 + 95.62*F17 +
123.6*F20 + 74.90*F21 + 474.6*F22 -161.2*F23 -143.5*F24 -161.0*F25 +
242.0*F26 + 58.99*F27 + 5.354*F28 -2.561*F29 + 0.739*F30 -0.389*F31 +
104.1*F32 + 47.79*F33 -2.310*F37 + 16.28*F4 -918.0*F5 + 12.58*F6
-974.1*F7 + 27.01*F8 -5.460*F9 + 10.35*F10 .
```
(6.7)

From Equation 6.6 it can be seen that the brake pressure data parameters (F34, F35, F36) are small in comparison to the other parameters. The other parameters with large values do not drastically change when the brake pressure parameters are removed, as shown in Equation 6.7. By comparing Equation 6.4 with Equation 6.6 and Equation 6.5 with Equation 6.7 it can be seen that the removal of the classification variable had little effect on the other model parameters. The equations for models with interaction effects are again not useful for comparison due to their length and complexity.

The fit of the regression models was also analyzed by looking at the residuals. Since the regression models for longitudinal strain are of particular interest in the prediction of fatigue life and failure of the trailer, they will be used for the analyses. As shown in Figure 6.12, the linear regression model with interaction terms that included the brake pressure data and the classification variable is an appropriate model. Comparing Figure 6.12 and Figure 6.13, it can be seen that the removal of the brake pressure data had little effect on the fit of the regression model. From Figure 6.14 it can be seen that the linear model is also appropriate with the classification term removed. Comparing Figure 6.14 and Figure 6.15, it can be seen that the removal of the brake pressure data also had little effect on the fit on the regression model with classification variable removed. Some outliers could be seen in all the residual plots.

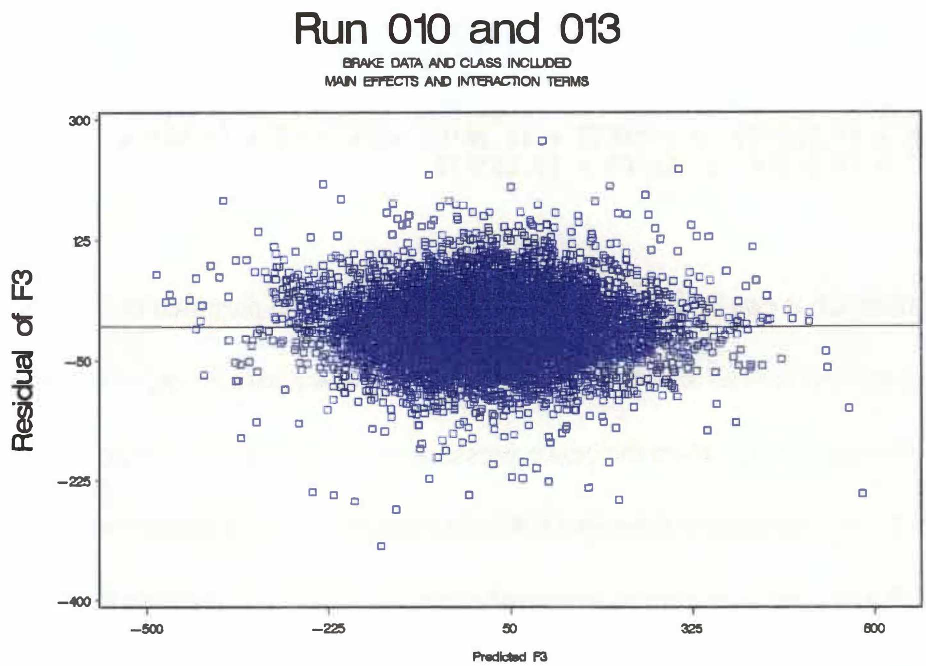

Figure 6.12: Residual plot for Belgian Block at 15 mph with brakes disabled and enabled longitudinal strain regression model with interaction terms, brake pressure data and class included.

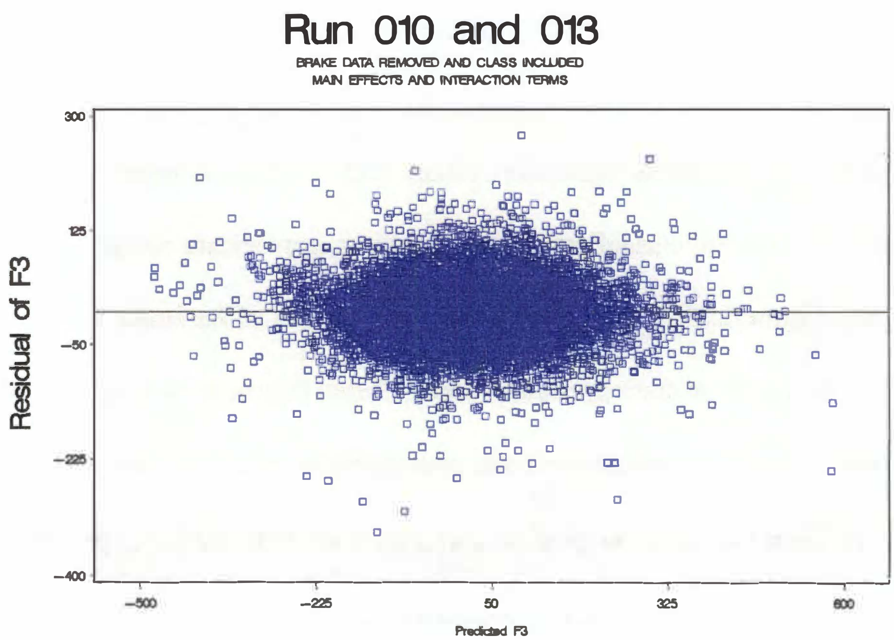

Figure 6.13: Residual plot for Belgian Block at 15 mph with brakes disabled and enabled longitudinal strain regression model with interaction terms, brake pressure data removed and class included.

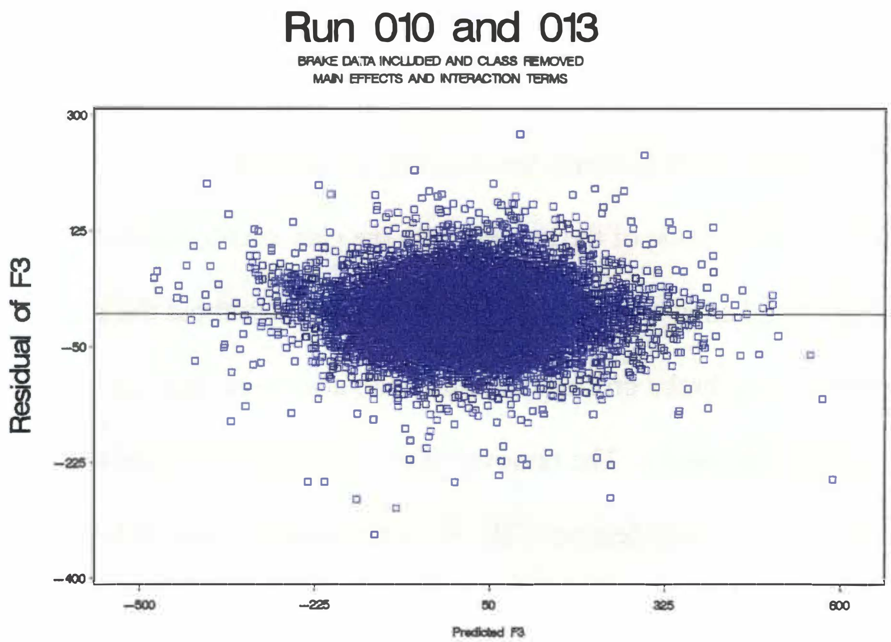

Figure 6.14: Residual plot for Belgian Block at 15 mph with brakes disabled and enabled longitudinal strain regression model with interaction terms, brake pressure data included and class removed.

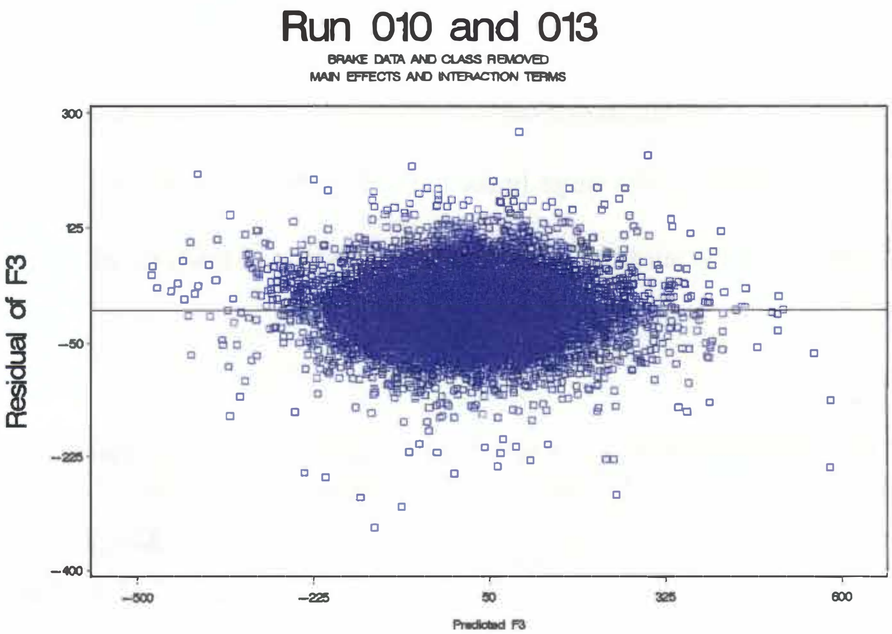

Figure 6.15: Residual plot for Belgian Block at 15 mph with brakes disabled and enabled longitudinal strain regression model with interaction terms, brake pressure data and class removed.

As shown in Table 6.12 and Table 6.13, the models with interaction effects that included the brake pressure data and classification variable had the highest R^2 values. For the models with interaction terms, the removal of the brake pressure variables decreased the overall R^2 value of the models with the classification variable by an average of 0.0072, and an average of 0.0015 for the models without the classification variable. Therefore, the brake pressure variables can also be eliminated without having a significant effect on the model. The removal of the classification variable from the models with interaction terms decreased the R^2 value by an average of 0.0083 for the models with all 33 independent variables and 0.0027 for the models with the brake pressure data eliminated. Therefore the classification variable can be eliminated without having a significant effect on the model. The average R^2 value for the model with interaction terms and all 33 independent variables and 1 classification variable was 0.8353, with the brake pressure variables and classification variable removed, the R^2 value drops to 0.8269. The difference between the values is only 0.0083. This means that the enabling or disabling the surge brake has very little effect on the strains. Therefore, modeling of the surge brake is not necessary for an analysis of the trailer.

Table 6.12: R^2 values for all Belgian Block at 15 mph with brakes disabled and enabled regression model, with brake pressure variables included.

	Class		No Class	
	Interactions	**No interactions**	**Interactions**	**No interactions**
Transverse	0.8194	0.7427	0.8119	0.7427
45 Degree	0.8351	0.7462	0.8260	0.7464
Longitudinal	0.8513	0.7660	0.8430	0.7655

Table 6.13: R^2 values for all Belgian Block at 15 mph with brakes disabled and enabled regression models, with brake pressure variables removed.

	Class		No Class	
	Interactions	**No Interactions**	**Interactions**	**No Interactions**
Transverse	0.8130	0.7394	0.8106	0.7394
45 Degree	0.8271	0.7424	0.8243	0.7424
Longitudinal	0.8442	0.7615	0.8413	0.7611

6.3.5 Principal Component Analysis for Belgian Block (Brakes Enabled)

To further look at the surge brake data, a principal component analysis (PCA) was used to determine the relevance of the pressure transducer data. PCA is a method used to reduce the size of the input data without losing a significant amount of variability, which contains the information in the data. PCA also makes the transformed vectors uncorrelated and orthogonal, which can be used in regressions without collinearity problems.

The given data, Belgian Block at 15 mph with brakes enabled, was used train and test a regression model using the PC scores determined by a singular value decomposition of the data to predict strain from the input variables. The PC scores provide an uncorrelated and orthogonal data set for the predictor variables, which eliminates collinearity and can be dimensionally reduced. The longitudinal strain was again the predicted variable and the predictor (input) variables were the same as for the multivariate regression, except the ground speed variable was removed yielding 33 input variables.

The singular value decomposition was performed on a standardized input training set to determine the principal components that are relevant for analysis. The relationship between the principal components and the longitudinal strain will be analyzed later. The percentage of data explained by each principal component is shown in Figure 6.16. From the figure, we can see that the first 26 principal components explain over 99.2 % of the information.

From the PC scores, shown in Tables 6.14 and 6.15 we can see that principal comments 2, 31, and 33 are weighted toward the brake data. From Figure 6.16 it can be seen that principal component 2 explains 9.7328 % of the information in the input data while principal components 31 and 33 explain only 0.0906% and 0.0201% of the information in the input data, respectively.

A plot of the first 2 Principal Components, Figure 6.17, was made to check for nonlinearites in the training data. The points corresponding to the brake pressures are labeled: 31, 32, and 33which correspond to the surge brake, CS wheel cylinder, and RS wheel cylinder pressures. From the figure it can be seen that the training data was linear.

To determine the relationship between the input data, and corresponding principal components, with longitudinal strain; a regression analysis was performed. The first regression was performed using the singular value decomposition and the y training set. The error in the training model was calculated to be 68.2306 μinch/inch. The regression model was then used to predict the y test set from the x test set. The error was the calculated to be 54.8989 μinch/inch. With the PCs that are weighted toward the brake data: 2, 31 and 33, removed the error drops to 54.3704 μinch/inch.

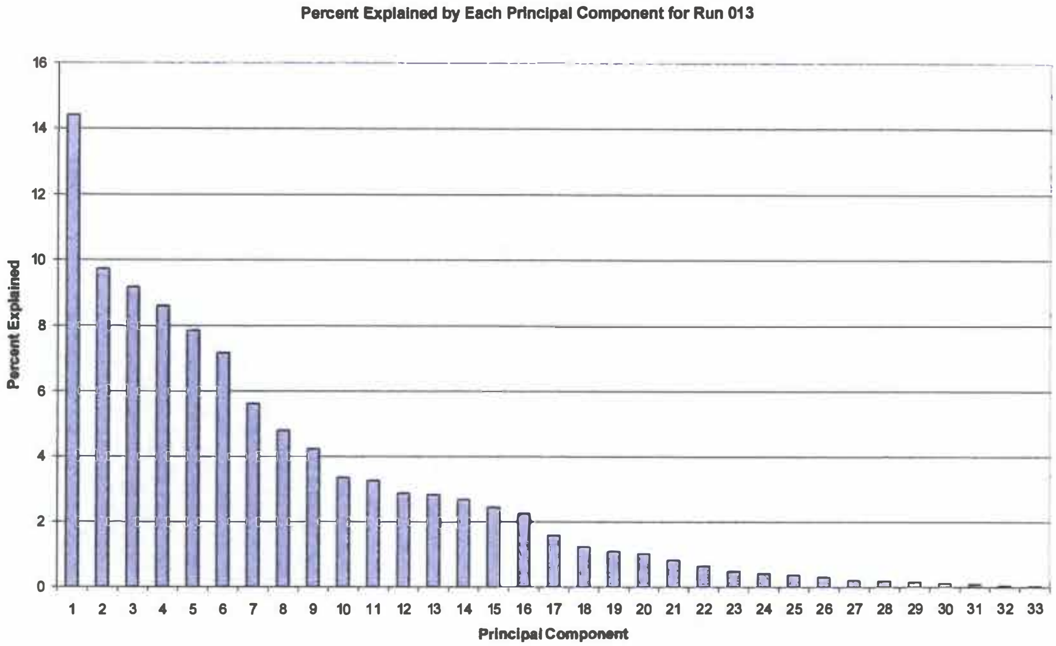

Figure 6.16: Percent of information explained by each PC for Belgian Block at 15 mph.

Table 6.14: PC scores for Belgian Block at 15 mph brake pressure variables.

	PC SCORES				PC SCORES		
PC	Master Cyl.	CS Wheel Cyl.	RS Wheel Cyl.	PC	Master Cyl.	CS Wheel Cyl.	RS Wheel Cyl.
1	-0.1036	-0.1273	-0.1528	18	-0.0042	0.0030	0.0139
2	-0.3804	-0.3742	-0.3454	19	0.0050	0.0057	0.0092
3	-0.2724	-0.2644	-0.2524	20	0.0019	-0.0040	-0.0084
4	0.1977	0.1963	0.2023	21	-0.0431	0.0182	0.0656
5	-0.2124	-0.2166	-0.2229	22	-0.0061	0.0004	0.0028
6	0.0076	-0.0012	-0.0069	23	-0.0043	-0.0060	0.0080
7	0.0014	0.0079	0.0199	24	0.0206	0.0073	-0.0302
8	-0.0309	-0.0200	-0.0236	25	-0.0175	0.0025	0.0164
9	0.0182	0.0187	0.0280	26	0.0123	-0.0112	-0.0005
10	0.0354	0.0559	0.0892	27	0.0090	-0.0033	-0.0189
11	-0.0884	-0.1245	-0.1618	28	0.0167	-0.0060	-0.0104
12	0.0116	0.0156	0.0176	29	0.0130	-0.0055	-0.0025
13	0.0387	0.0529	0.0837	30	-0.2788	-0.0012	-0.2749
14	0.0180	0.0290	0.0430	31	-0.6526	-0.0024	0.6334
15	-0.0211	-0.0297	0.0509	32	-0.0304	0.0155	0.0160
16	0.0049	0.0135	0.0155	33	0.4508	-0.8142	0.4137
17	-0.0256	-0.0058	0.0240				

Table 6.15: Input measurement components to PCs 2, 31, and 33, for Belgian Block at 15 mph with brakes enabled.

VAR.	PC 2	PC 31	PC 33	VAR.	PC 2	PC 31	PC 33
1	0.0875	0.0065	0.0027	18	-0.017	0.0342	0.0044
2	0.0919	-0.0117	-0.0001	19	-0.1116	0.2339	-0.0054
3	-0.116	0.0021	-0.0028	20	-0.122	0.0398	0.0148
4	-0.0687	-0.0045	0.0084	21	-0.1174	-0.0225	0.0103
5	-0.0176	0.0042	0.0005	22	0.2106	-0.1182	-0.0009
6	-0.1182	0.0077	0.0002	23	-0.0571	-0.0599	-0.0057
7	0.0149	0.0161	-0.0017	24	-0.0068	-0.0101	-0.0033
8	0.0352	0.024	-0.002	25	0.2242	0.2046	0.0013
9	-0.2508	-0.0045	0.0028	26	-0.1617	-0.0032	0.0059
10	0.1111	-0.0703	-0.0025	27	-0.2535	-0.0037	0.0042
11	0.0467	0.0452	0.0038	28	-0.0788	0.0135	0.004
12	-0.2735	0.0065	-0.0109	29	-0.052	0.059	-0.0012
13	0.1462	-0.0765	-0.0032	30	-0.2543	0.0964	0.0087
14	0.1954	0.0338	-0.0058	31	-0.3804	-0.6526	0.4058
15	-0.1446	0.0217	0.0048	32	-0.3742	-0.0024	-0.8142
16	-0.0968	-0.1636	0.0026	33	-0.3454	0.6334	0.4137
17	0.0223	-0.0095	-0.0158				

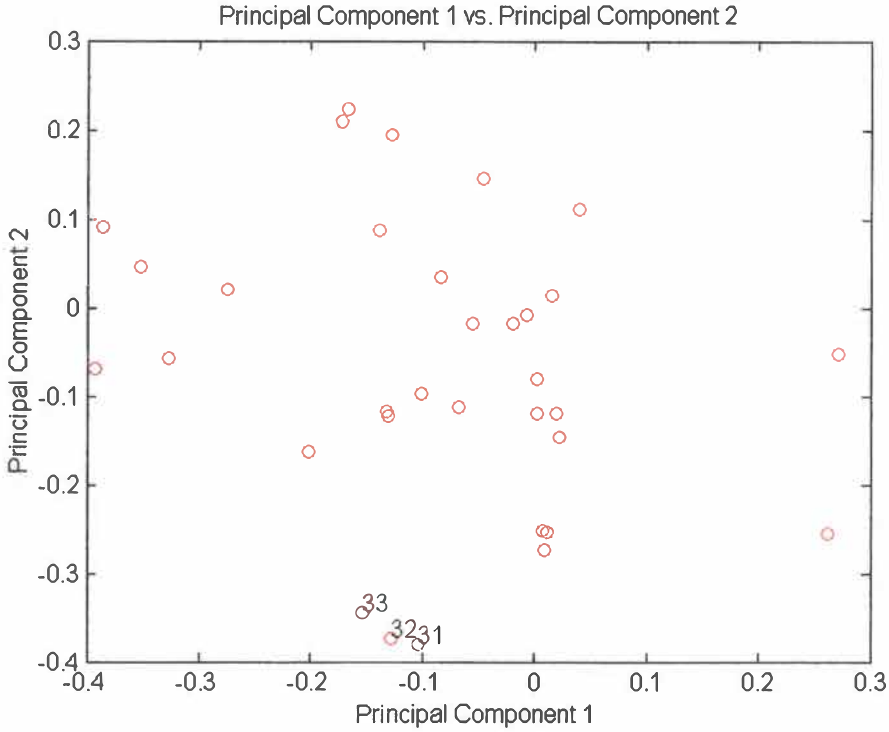

Figure 6.17: PC 1 vs. PC2 for Belgian Block at 15 mph with brakes enabled.

The error when individual principal components are removed, starting with the last principal component (PC) was then determined, and is shown in Figure 6.18. From the figure it can be seen that there is decrease in the average error to a minimum of 54.3424 µinch/inch when the last 4 principal components are removed which includes both principal components 31 and 33.

A correlation coefficient matrix of the Z scores and y training data was made to determine which principal components are most useful in predicting acceleration. The absolute values of the correlation coefficients are shown in Figure 6.19. From the figure it can be seen that principal components 2, 4, 8, 18, 20, 22, 24, 27, 28, 29, 30, and 32 are the least correlated, below 0.05, with the data. With these PC's removed the error only

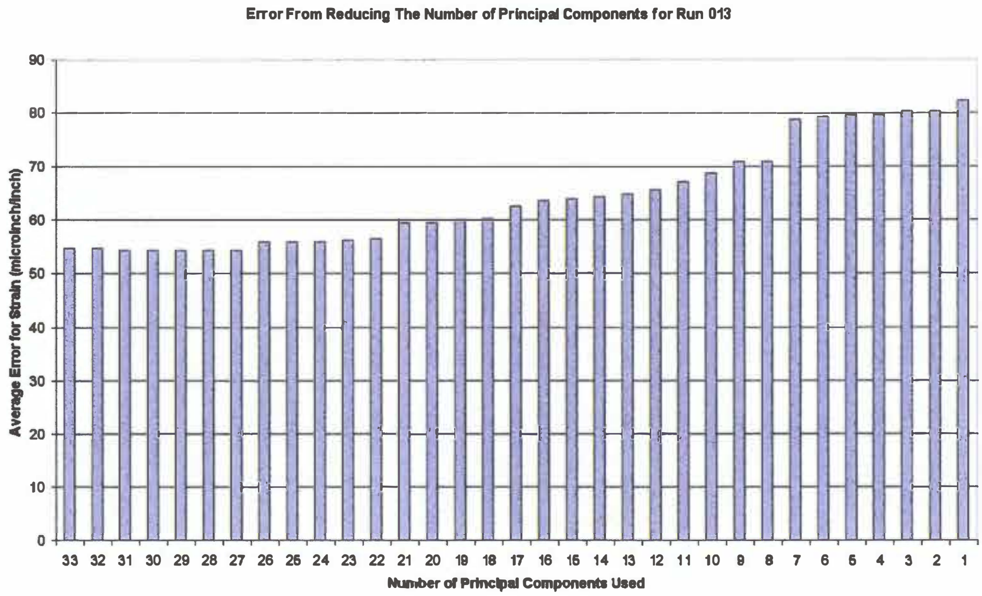

Figure 6.18: Average strain prediction error for Belgian Block at 15 mph with brakes enabled.

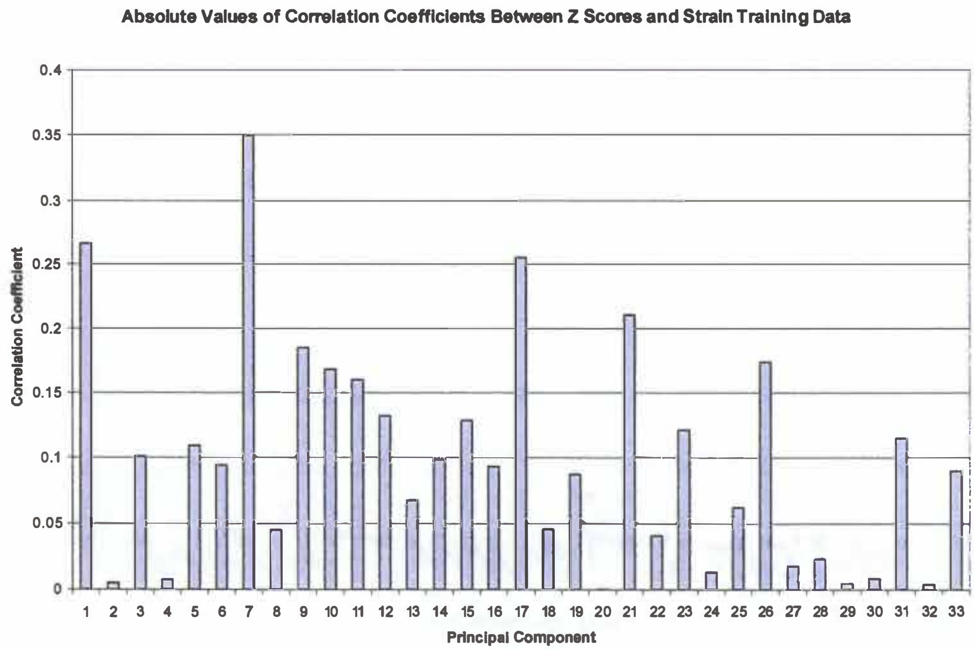

Figure 6.19: Correlation coefficient between Z scores and training data for Belgian Block at 15 mph with brakes enabled.

increased to 55.3605 μinch/inch. Additional principal components: 6, 13, 14, 16, 19, 25, and 33 were removed and the error increased to 58.7066 μinch/inch. Principal components 3, 5, and 31 were then removed and yielded an error of 58.5525 μinch/inch.

The principal component analysis and regression also show that the brakes do not correlate to the longitudinal strain. The second, thirty-first and thirty-third principal components were weighted toward the brake pressure data. The second principal component did explain a large percentage of the input data relative to the other principal components, but it did not correlate to the strain data. The thirty-first and thirty-third principal components were slightly correlated to the strain data, but explained a negligible percentage of information from the input data. The removal of these three principal components reduced the average error by 0.5205 μinch/inch reinforcing the conclusion that the activation of the surge brake does not affect the life of the trailer.

6.3.6 Regression Analysis for Perryman #3 (Brakes Enabled)

To validate the regression results obtained during the Belgian Block data analysis; a second analysis was preformed using data from another test course. Since this is intended only to be a validation, all of the original detailed analysis was not performed. The data selected was from the Perryman #3 test course at 15 mph with the brakes enabled

Three regression models, without interaction effects, were created to initially. The first strain model created was for the transverse strain. Using a stepwise regression model we can see that the R^2 value for the model with the brake pressure data included is 0.8044 and with the brake pressure data eliminated the R^2 is 0.8035.

The second strain model created was for the 45 degree strain. Using a stepwise regression model we can see that the R^2 value for the model with the brake pressure data included is 0.8305 and with the brake pressure data eliminated the R^2 is 0.8295.

The third strain model created was for the longitudinal strain. Using a stepwise regression model we can see that the R^2 value for the model with the brake pressure data included is 0.8382 and with the brake pressure data eliminated the R^2 is 0.8372.

A multivariate regression that included pairwise interaction effects was created to improve the fit of the model by accounting for interactions between the main effects in the model. The model for transverse, 45 degree, and longitudinal strains had overall R^2 values of 0.8858, 0.9002, and 0.9079, respectively.

A multivariate regression with main effects and pairwise interactions was then created with the brake pressure variables eliminated. The model for transverse, 45 degree, and longitudinal strains had overall R^2 values of 0.8854, 0.8996, and 0.9075, respectively.

As shown in Table 6.16, the models with interaction terms included had higher R^2 values than the models without interaction terms. The R^2 values for the models with the brake pressure data included had only slightly higher R^2 values than the models without the brake pressure data. For the models with interaction terms, elimination of the brake pressure data only reduced the R^2 value by an average of 0.000467. For the models without interaction terms, elimination of the brake pressure data only reduced the R^2 value by an average of 0.000967. Therefore, the brake pressure data can be eliminated

Table 6.16: R^2 values for all models for Perryman #3 test course at 15 mph with brakes enabled.

	With Brake Pressures		No Brake Pressures	
	Interaction	**No Interaction**	**Interaction**	**No Interaction**
Transverse	0.8858	0.8044	0.8854	0.8035
45 Degree	0.9002	0.8305	0.8996	0.8295
Longitudinal	0.9079	0.8382	0.9075	0.8372

without having a significant effect on the model. This shows that the enabling or disabling of the surge brake does not have a significant effect on the life of the trailer.

6.3.7 Regression Analysis for Perryman #3 (Brakes Disabled)

A second analysis was performed to help explain and validate the findings from the analysis of Perryman #3 at 15 mph with brakes enabled. For this analysis the data from Perryman #3 at 15 mph with brakes disabled was used, since it corresponds to Perryman #3 at 15 mph with brakes enabled.

The results of the regression models with and without interaction terms for the data from the Perryman #3 test course taken at 15 mph with the brakes disabled are shown in Table 6.17. The results that are labeled 'with brake pressures' are only for showing the effect of the sensor error, since the brake pressures should have been constant and would have no effect on the regression model. The overall R^2 values for Perryman #3 at 15 mph with brakes disabled were higher than the R^2 values for Perryman #3 at 15 mph with brakes enabled, shown in Table 6.16.

The benefits of adding interaction terms can also be seen in Table 6.17. The

Table 6.17: R^2 values for all Perryman #3 at 15 mph with brakes disabled regression models.

	With Brake Pressures		No Brake Pressures	
	Interaction	**No Interaction**	**Interaction**	**No Interaction**
Transverse	0.9043	0.8441	0.9007	0.8435
45 Degree	0.9106	0.862	0.9067	0.8611
Longitudinal	0.9216	0.8712	0.9185	0.8711

models for Perryman #3 at 15 mph with brakes disabled that included interaction terms and no brake pressure data had overall R^2 values of 0.9007, 0.9067, and 0.9815, for transverse, 45 degree, and longitudinal strains, respectively. Without interaction terms and no brake pressure variables the models for transverse, 45 degree, and longitudinal strains, had R^2 values of 0.8841, 0.862, and 0.8712, respectively. The same models with interaction terms and brake pressure variables eliminated for Perryman #3 at 15 mph with brakes enabled had overall R^2 values of 0.8435, 0.8611, and 0.8711, for transverse, 45 degree, and longitudinal strains, respectively. Without interaction terms and brake pressure variables the models for Perryman #3 at 15 mph with brakes enabled transverse, 45 degree, and longitudinal strains, had R^2 values of 0.8435, 0.8611, and 0.8711, respectively. The average difference in the overall R^2 value for the models with interaction terms and brake pressure variables removed between Perryman #3 at 15 mph with brakes disabled and enabled was 0.0111 and 0.0352 for the models with no interaction terms and brake pressure variables removed.

6.3.8 Regression with Concatenated Data for Perryman #3

As shown in Tables 6.18 and 6.19, the models with interaction effects that included the brake pressure data and classification variable had the highest R^2 values. For the models with interaction terms, the removal of the brake pressure variables decreased the overall R^2 value of the models with the classification variable by an average of 0.0015, and increased the overall R^2 value an average of 0.0001 for the models without the classification variable. Therefore the brake pressure variables can also be eliminated without having a significant effect on the model. The removal of the classification variable from the models with interaction terms increased the R^2 value by an average of 0.00003 for the models with all 33 independent variables and 0.0017 for the models with the brake pressure data eliminated. Therefore the classification variable can be eliminated without having a significant effect on the model. The average R^2 value for the model with interaction terms and all 33 independent variables and 1 classification variable was 0.8958, with the brake pressure variables and classification variable removed, the R^2 value drops to 0.8974. The difference between the values is only

Table 6.18: R^2 values for Perryman #3 at 15 mph with brakes disabled and enabled regression model, with brake pressure variables included.

	Class		No Class	
	Interactions	**No interactions**	**Interactions**	**No interactions**
Transverse	0.8854	0.8323	0.8854	0.8320
45 Degree	0.8960	0.8540	0.8959	0.8540
Longitudinal	0.9061	0.8619	0.9061	0.8616

Table 6.19: R^2 values for Perryman #3 at 15 mph with brakes disabled and enabled regression model, with brake pressure variables removed.

	Class		No Class	
	Interactions	**No interactions**	**Interactions**	**No interactions**
Transverse	0.8871	0.8317	0.8852	0.8312
45 Degree	0.8976	0.8537	0.8959	0.8537
Longitudinal	0.9074	0.8616	0.9060	0.8613

0.0016. This means that the enabling or disabling the surge brake has very little effect on the strains. Therefore, modeling of the surge brake is not necessary for an analysis of the trailer.

6.3.9 Principal Component Analysis for Perryman #3 (Brakes Enabled)

To verify the analysis of the surge brake data from the Belgian Block test course at 15 mph, a principal component analysis (PCA) was again performed using another data set. For verification, the data set was from a different test course than the original analysis. The verification data set was from the Perryman #3 test course at 15mph with the brakes enabled.

The singular value decomposition was again performed on a standardized input training set in order to determine the principal components that are relevant for analysis. As before, the relationship between the principal components and the longitudinal strain will be analyzed later. The percentage of data explained by each principal component is shown in Figure 6.20. From the figure, we can see that the first 25 principal components explain over 99.1 % of the information.

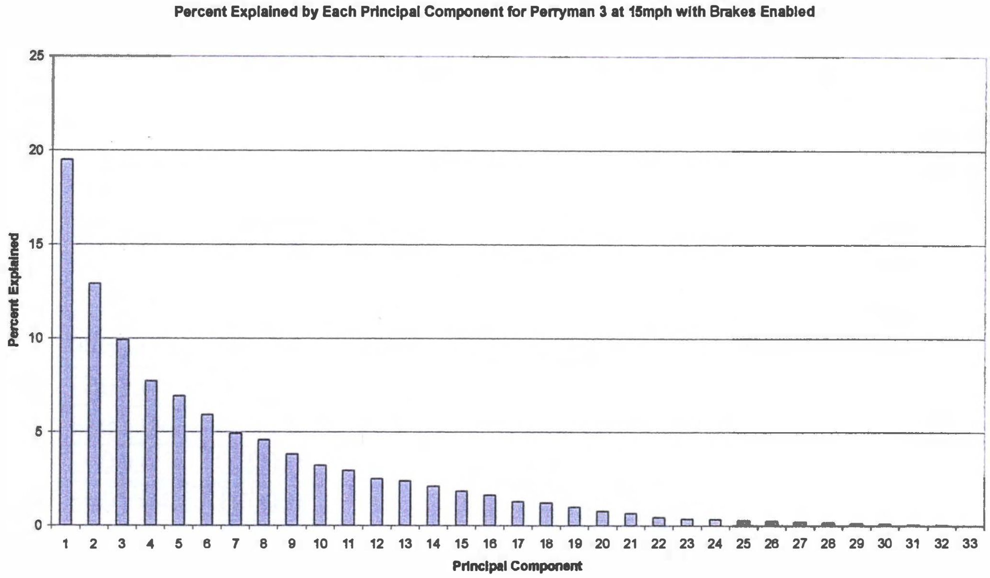

Figure 6.20: Percent of information explained by each PC for Perryman #3 at 15 mph with brakes enabled.

From the PC scores, shown in Tables 6.20 and 6.21 we can see that principal components 5, 22, and 33, are weighted toward the brake data. From Figure 6.20 it can be seen that principal components 5, 32, and 33, explain 6.9329 %, 0.035 %, and 0.0066 %, of the information in the input data, respectively. The total amount of information explained by these 3 principal components is only 6.9745 %.

A plot of the first 2 Principal Components, Figure 6.21, was made to check for nonlinearites in the training data. From the figure it can be seen that the training data was linear. To determine the relationship between the Perryman #3 input data, and corresponding principal components, with longitudinal strain; a regression analysis was performed. The first regression was performed using the singular value decomposition and the y training set. The error in the training model was calculated to be 51.8350 μinch/inch. The regression model was then used to predict the y test set from the x test

Table 6.20: PC scores for Perryman #3 at 15 mph with brakes enabled pressure variables.

	PC SCORES				PC SCORES		
PC	**Master Cyl.**	**CS Wheel Cyl.**	**RS Wheel Cyl.**	**PC**	**Master Cyl.**	**CS Wheel Cyl.**	**RS Wheel Cyl.**
1	-0.1412	-0.1564	-0.1631	18	0.0079	0.012	0.0018
2	-0.2879	-0.2812	-0.2784	19	-0.0191	-0.0201	-0.0148
3	0.1367	0.1388	0.134	20	0.0276	0.0206	-0.0004
4	-0.1215	-0.1233	-0.124	21	0.0123	-0.0011	-0.0123
5	0.3981	0.3872	0.3816	22	-0.0355	-0.0089	0.025
6	-0.0177	-0.0351	-0.0374	23	-0.0079	0.0063	0.0141
7	0.0526	0.0487	0.0425	24	0.0026	-0.0083	-0.0134
8	-0.1458	-0.1563	-0.1605	25	0.0079	0.0092	0.0119
9	-0.0537	-0.0572	-0.0544	26	0.0091	-0.0006	-0.0091
10	0.0605	0.0667	0.0712	27	-0.0205	0.0223	0.0482
11	0.0014	-0.0029	-0.0016	28	-0.0085	-0.005	0.0045
12	-0.05	-0.058	-0.0671	29	0.0324	-0.0182	-0.0432
13	-0.0027	0.0057	0.0126	30	-0.017	0.0001	0.011
14	0.0472	0.0632	0.0665	31	-0.1155	0.0259	0.091
15	-0.041	-0.0406	-0.0452	32	0.763	-0.1605	-0.5997
16	0.0227	0.0251	0.025	33	0.2594	-0.7988	0.5425
17	0.0072	0.0075	0.006				

Table 6.21: Input measurement components to PCs 5, 32, and 33, for Perryman #3 at 15 mph with brakes enabled.

VAR.	PC 5	PC 32	PC 33	VAR.	PC 5	PC 32	PC 33
1	-0.0549	-0.0094	0.0038	18	-0.0359	-0.0112	0.0008
2	-0.1327	0.0349	-0.0061	19	0.1416	-0.1019	-0.0013
3	-0.1328	0.0024	-0.0028	20	-0.1385	0.0631	0.0016
4	-0.2003	-0.0047	0.0031	21	-0.1343	0.0458	0.001
5	-0.1858	-0.0002	-0.0022	22	0.0939	0.0162	-0.0017
6	-0.1144	0.0003	0.0002	23	-0.1422	-0.0036	-0.0011
7	0.0535	-0.0032	-0.0003	24	0.0212	0.0013	0.0015
8	-0.1761	-0.0056	-0.0008	25	0.1264	0.0247	0.0017
9	-0.1631	-0.0054	0.0014	26	0.0031	-0.0247	0.0049
10	0.0772	0.0236	-0.0019	27	-0.13	0.0369	-0.005
11	-0.2164	0.0019	-0.0014	28	-0.1152	-0.0189	0.0105
12	-0.1545	-0.0567	0.0078	29	0.1836	-0.0165	-0.001
13	0.1418	0.002	0.0021	30	0.0565	-0.0085	-0.0039
14	-0.2161	-0.0449	-0.0037	31	0.3981	0.763	0.2594
15	-0.1746	0.0384	0.0026	32	0.3872	-0.1605	-0.7988
16	0.1109	0.0573	-0.0015	33	0.3816	-0.5997	0.5425
17	-0.0485	0.0161	-0.0044				

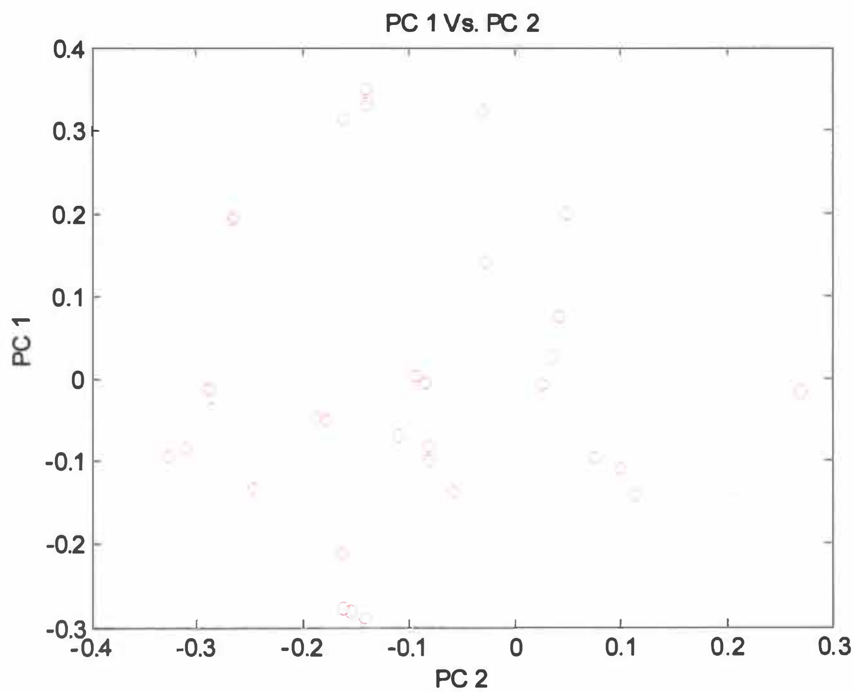

Figure 6.21: PC 1 vs. PC2 for Perryman #3 at 15 mph with brakes enabled.

set. The error was the calculated to be 55.9815 µinch/inch. With the PCs that are weighted toward the brake data: 5, 32, and 33, removed the error increases to 75.5955 µinch/inch, and with only PCs 32 and 33 removed the error is 56.2774 µinch/inch. With only PC 5 removed the error is 74.9775 µinch/inch. The error when principal components are removed, starting with the last principal component (PC) was then determined, and is shown in Figure 6.22. From the figure it can be seen that there is increase in the average error of only 2.2109 µinch/inch to a value 58.1924 µinch/inch when the last 21 principal components are removed, which includes PCs 32 and 33, which are weighted toward the brake data.

A correlation coefficient matrix of the Z scores and y training data was made to determine which principal components are most useful in predicting acceleration. The absolute values of the correlation coefficients are shown in Figure 6.23. From the figure it can be seen that the principal components that are weighted toward the brake data (5, 32, and 33) are not correlated to the strain training data with correlation coefficients 0.2243, 0.0091, and 0.0097, respectively.

The principal component analysis and regression show for this data set that the brakes do not correlate to the longitudinal strain. The fifth, thirty-second, and thirty-third principal components were weighted toward the brake pressure data. These three principal components had an average correlation coefficient of 0.0810 between the Z scores and the longitudinal strain training data. The removal of these three principal components increased the average error by 19.614 µinch/inch to 75.5955 µinch/inch. From these results it cannot be determined if the activation of the surge brake effects the life of the trailer. This difference in the average error from the regression was not and

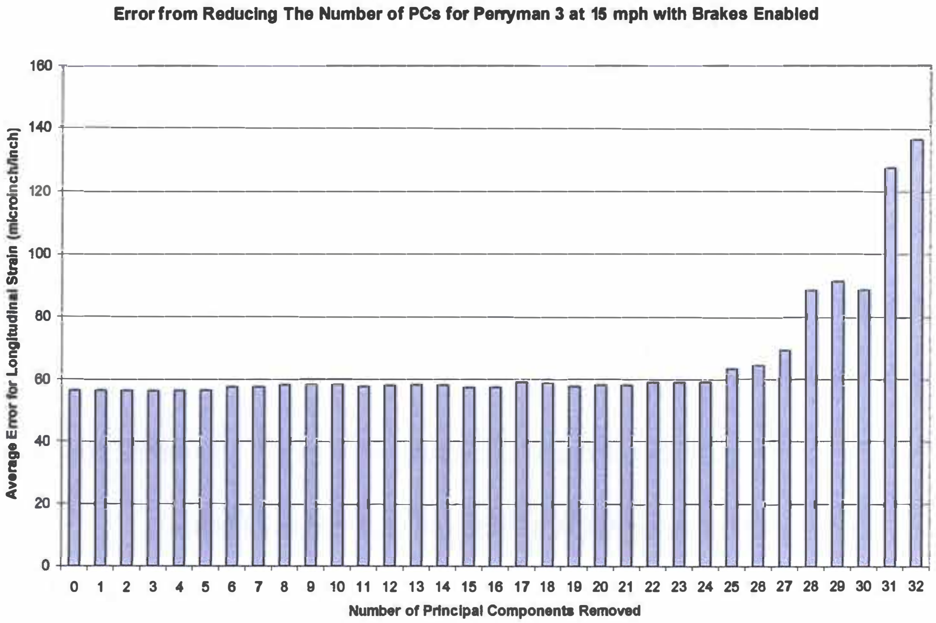

Figure 6.22: Average strain prediction error for Perryman #3 at 15 mph with brakes enabled.

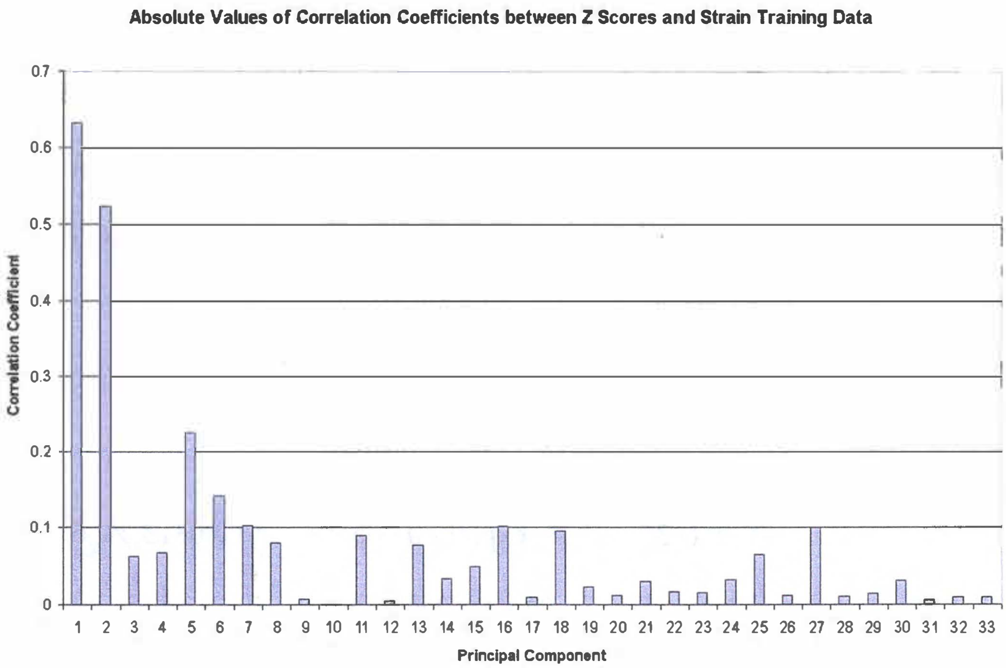

Figure 6.23: Correlation coefficient between Z scores and training data for Perryman #3 at 15 mph with brakes enabled.

expected result and indicates an error in the model.

This regression error can be explained by looking at the brake pressure data. As can be seen from Figure 6.4, the surge brake was not activated (pressure increased above 0 psi) during the training data and was activated four times during the testing data. This can easily affect the regression model, since the brake pressure change would not be accounted for. This does not mean the brake pressure affects the strain, it means the model is effected by the variables used and the must be properly accounted for. Only removing the variable can determine if it affects the regression results.

To determine the effect of the brake activation on the data sets, the analysis was again preformed with the data set starting at 10.4061 seconds (data point 13140), which is slightly more than the second half of the data. The new training and testing data sets will be taken from this reduced data set that only accounts for a little over half of the original data.

As in the previous analyses, the relationship between the principal components and the longitudinal strain will be analyzed later. The percentage of data explained by each principal component is shown in Figure 6.24. From the figure, we can see that the first 25 principal components explain over 99.21 % of the information.

From the PC scores, shown in Tables 6.22 and 6.23 we can see that principal components 32 and 33, are now weighted toward the brake data. From Figure 6.24 it can be seen that principal components 32 and 33, explain 0.0054 %, and 0.0313 %, of the information in the input data, respectively. The total amount of information explained by these 2 principal components is only 0.0367 %. A plot of the first 2 principal components, Figure 6.25, was made to check for nonlinearites in the training data used.

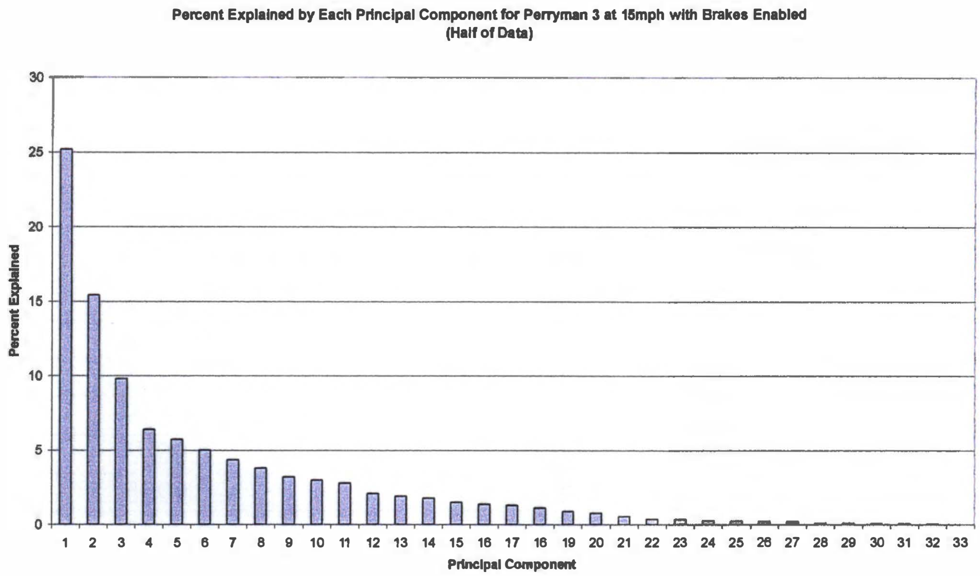

Figure 6.24: Percent of information explained by each PC for Perryman #3 at 15 mph with brakes enabled, half of data.

Table 6.22: PC scores for Perryman #3 at 15 mph with brakes enabled pressure variables, half of data.

	PC SCORES				PC SCORES		
PC	Master Cyl.	CS Wheel Cyl.	RS Wheel Cyl.	PC	Master Cyl.	CS Wheel Cyl.	RS Wheel Cyl.
1	0.1169	-0.1399	-0.1481	18	0.0039	-0.0205	-0.0329
2	0.3388	0.318	0.3104	19	0.0411	0.0338	0.0418
3	0.0595	0.0493	0.0423	20	-0.0122	0.0346	0.0273
4	-0.1109	-0.1091	-0.1108	21	0.0216	0.0448	0.0675
5	-0.2431	-0.2843	-0.2889	22	0.0271	0.0262	0.0238
6	0.245	0.2347	0.2326	23	-0.0116	-0.0151	-0.0074
7	0.0541	0.0369	0.0301	24	-0.0048	0.081	0.129
8	-0.0024	-0.0096	-0.0097	25	0.0566	0.0364	-0.0199
9	0.0117	0.0212	0.0216	26	0.0114	-0.0019	0.0038
10	0.1488	0.1415	0.135	27	0.0119	-0.0046	0.0014
11	-0.0464	-0.0422	-0.0396	28	-0.0316	0.03	0.0475
12	-0.0145	0.008	0.018	29	-0.0119	0.0126	0.0315
13	-0.1108	-0.1217	-0.1232	30	-0.0357	0.0119	0.0215
14	0.0695	0.0692	0.0683	31	-0.1595	0.03	0.1264
15	-0.0594	-0.0553	-0.0563	32	0.7443	-0.1083	-0.6067
16	-0.096	-0.0872	-0.0847	33	-0.2983	0.8039	-0.5132
17	-0.0405	-0.0373	-0.0372				

Table 6.23: Input measurement components to PCs 32 and 33 for Perryman #3 at 15 mph with brakes enabled, half of data.

VAR.	PC 32	PC 33	VAR.	PC 32	PC 33
1	-0.0151	0.0024	18	-0.0177	-0.0021
2	0.0371	0.001	19	-0.163	0.008
3	0.0006	0.0007	20	0.073	-0.0071
4	-0.0031	-0.0057	21	0.0471	-0.0037
5	-0.0076	0.0023	22	0.0214	-0.0064
6	0.0056	-0.0018	23	-0.0385	0.0016
7	0.0054	-0.0011	24	-0.0059	0.0023
8	-0.002	-0.0001	25	0.0593	0.0021
9	-0.0127	0.0013	26	-0.0005	-0.0039
10	0.0281	-0.0038	27	0.0522	0.0103
11	-0.0171	-0.0006	28	0.0048	-0.0219
12	-0.0512	0.0051	29	0.006	0.0161
13	0.0457	-0.0021	30	-0.0634	0
14	-0.0702	0.0061	31	0.7443	-0.2983
15	0.0371	-0.0017	32	-0.1083	0.8039
16	0.0664	-0.0039	33	-0.6067	-0.5132
17	0.0346	0.0137			

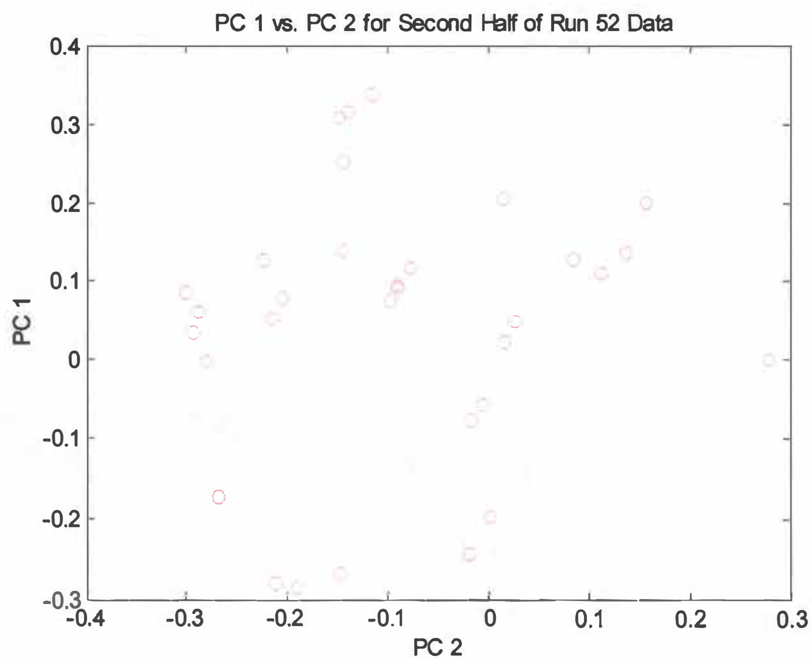

Figure 6.25: PC 1 vs. PC2 for Perryman #3 at 15 mph, brakes enabled, half of data.

From Figure 6.25, it can be seen that the training data was linear.

To determine the relationship between the Perryman #3 input data, and corresponding principal components, with longitudinal strain; a regression analysis was performed. The first regression was performed using the singular value decomposition and the y training set. The error in the training model was calculated to be 50.9988 μinch/inch. The regression model was then used to predict the y test set from the x test set. The error was the calculated to be 58.8997 μinch/inch. With the PCs that are weighted toward the brake data, 32 and 33, removed the error increases the error increases by 0.9099 μinch/inch (1.54 %), to 59.8096 μinch/inch.

The error when principal components are removed, starting with the last principal component (PC) was then determined, and is shown in Figure 6.26. From the figure it can be seen that there is a decrease in the average error of only 0.0864 μinch/inch to a value 58.8133 μinch/inch when the last 22 principal components are removed. These 22 principal components include both PCs 32 and 33, which are weighted toward the brake data.

A correlation coefficient matrix of the Z score and y training data was made to determine which principal components are most useful in predicting acceleration. The absolute values of the correlation coefficients are shown in Figure 6.27. From the figure, it can be seen that the principal components that are weighted toward the brake data (32 and 33) are not correlated to the strain training data with correlation coefficients of 0.0234 and 0.0143, respectively.

The principal component analysis and regression of the shows that the brakes do not correlate to the longitudinal strain. The thirty-second and thirty-third principal

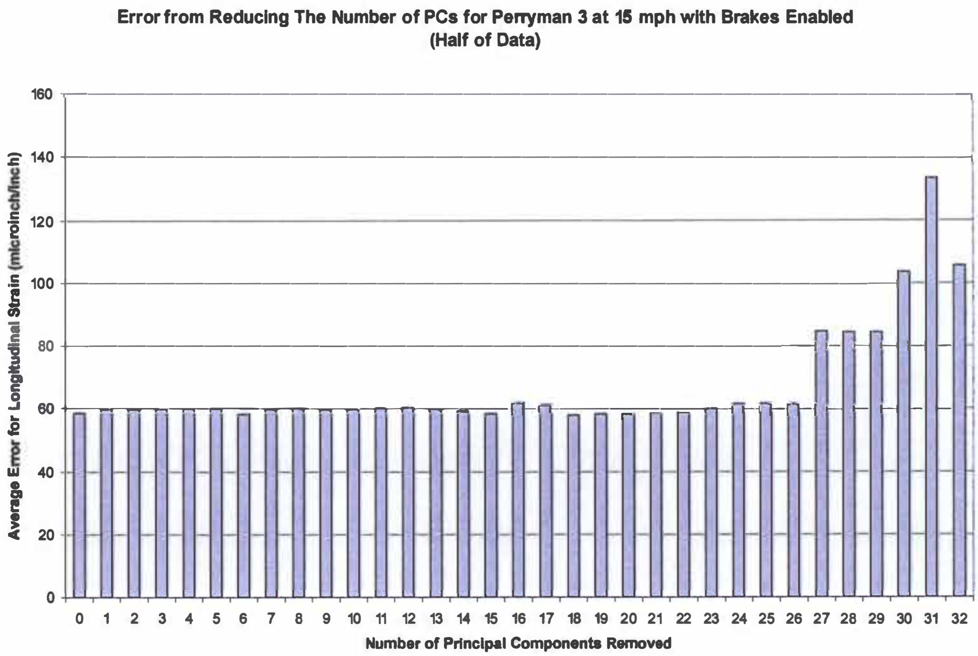

Figure 6.26: Average strain prediction error for Perryman #3 at 15 mph with brakes enabled, half of data.

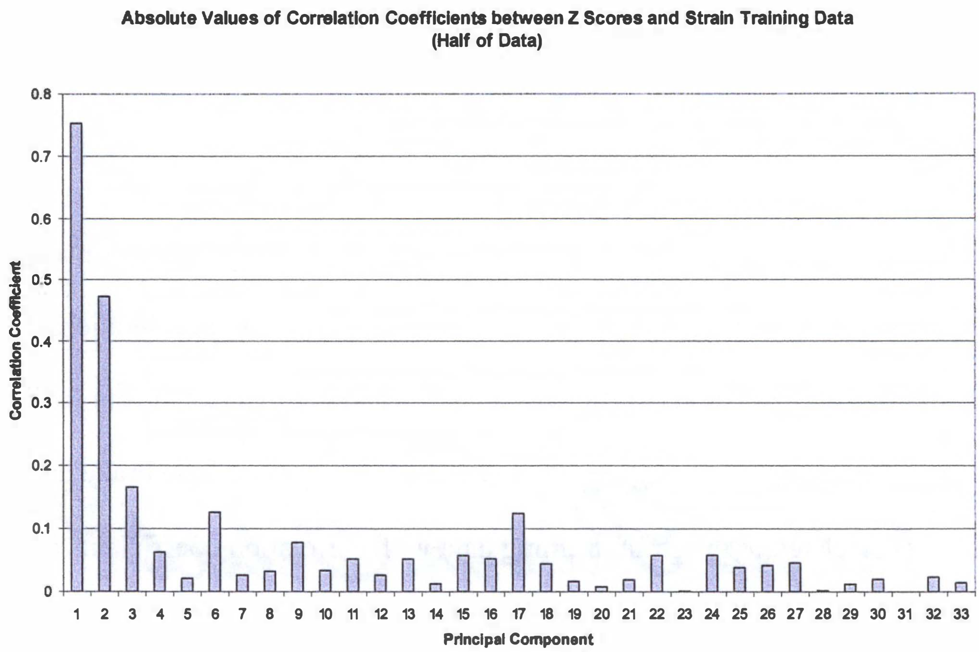

Figure 6.27: Correlation coefficient between Z scores and training data for Perryman #3 at 15 mph with brakes enabled, half of data.

components were weighted toward the brake pressure data. These two principal components had an average correlation coefficient of 0.0189 between the Z score and longitudinal strain training data. The removal of these three principal components increase the average error by only 1.9099 μinch/inch, or 1.54 %, reinforcing the conclusion of the analysis on the Belgian Block data taken at 12 mph with the brake enabled that the activation of the surge brake does not affect the life of the trailer.

6.3.10 Principal Component Analysis for Perryman #3 (Brakes Disabled)

To compare the PCA results from a data set with the brakes disabled another analysis was performed. The data set used for the analysis was from the Perryman #3 test course at 15mph with the brakes disabled, which corresponds to the Perryman #3 data set taken at 15 mph with the brakes enabled.

The singular value decomposition was again performed on a standardized input training set in order to determine the principal components that are relevant for analysis. As before, the relationship between the principal components and the longitudinal strain will be analyzed later. The percentage of data explained by each principal component is shown in Figure 6.28. From the figure, we can see that the first 27 principal components explain over 99.3 % of the information.

From the PC scores, shown in Tables 6.24 and 6.25 we can see that principal components 11, 12, 13, and 14, are weighted toward the brake data. From Figure 6.28 it can be seen that principal components 11, 12, 13, and 14, explain 2.9078 %, 2.8487 %, 2.6314 %, and 2.3851 %, of the information in the input data, respectively. The total

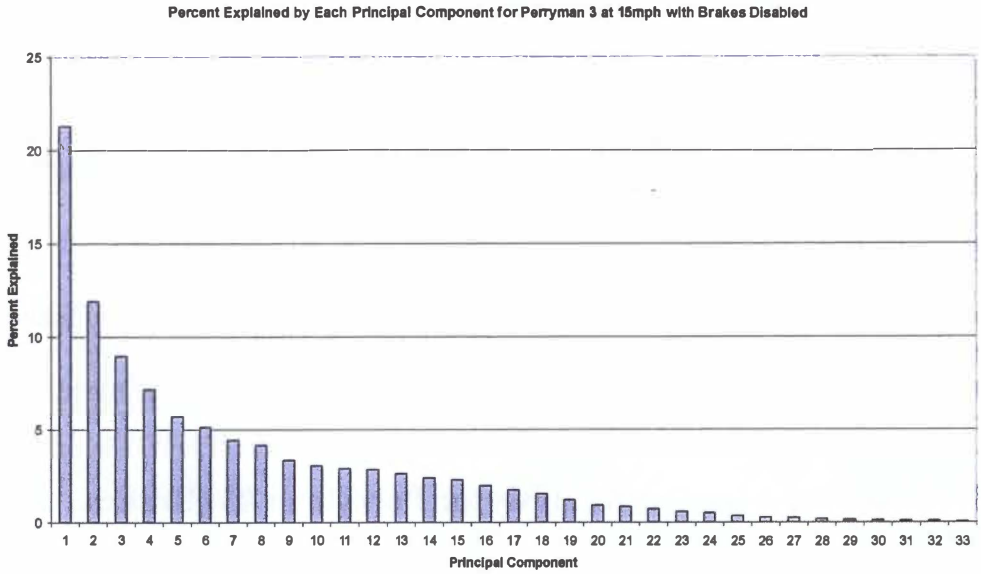

Figure 6.28: Percent of information explained by each PC for Perryman #3 at 15 mph with brakes disabled.

Table 6.24: PC scores for Perryman #3 at 15 mph with brakes disabled pressure variables.

	PC SCORES				PC SCORES		
PC	**Master Cyl.**	**CS Wheel Cyl.**	**RS Wheel Cyl.**	**PC**	**Master Cyl.**	**CS Wheel Cyl.**	**RS Wheel Cyl.**
1	0.0541	-0.037	-0.0158	18	-0.0037	-0.0367	-0.0639
2	-0.0334	0.0124	0.0377	19	0.0204	0.0057	0.0142
3	0.0335	0.0379	-0.0175	20	0.0149	0.0274	-0.0133
4	-0.0841	-0.092	0.0023	21	0.0121	-0.0026	-0.0095
5	-0.1532	-0.1841	0.0302	22	-0.0137	0.0435	-0.0043
6	0.1266	0.1578	0.0317	23	-0.004	-0.0013	0.0004
7	0.0003	-0.1014	0.0008	24	-0.0076	-0.043	0.0133
8	0.1022	0.3506	-0.0102	25	0.0036	-0.0006	0.0011
9	-0.0885	-0.2053	0.1231	26	-0.0013	-0.0031	0.0026
10	-0.1691	0.1959	-0.925	27	-0.0181	0.0022	-0.0018
11	0.617	0.1311	-0.0732	28	0.0063	-0.0032	-0.0067
12	0.5417	0.3229	0.0642	29	-0.0058	0.0049	0.0023
13	0.4101	-0.5909	-0.3268	30	0.0005	0.0073	0.0019
14	0.124	-0.1343	0.0564	31	0.0022	0.0006	-0.002
15	-0.2049	0.3312	0.0166	32	0.0033	0.0086	-0.0016
16	0.0141	-0.3261	-0.0171	33	-0.004	-0.0024	0.0002
17	0.0034	-0.0727	-0.0187				

Table 6.25: Input measurement components to PCs 11, 12, 13, and 14 for Perryman #3 at 15 mph with brakes disabled.

VAR.	PC 11	PC 12	PC 13	PC 14	VAR.	PC 11	PC 12	PC 13	PC 14
1	0.0944	-0.0218	0.3149	-0.1061	18	0.1169	-0.2614	0.0701	-0.0432
2	0.0764	-0.0638	0.0484	-0.019	19	-0.0025	-0.0448	0.0766	-0.24
3	-0.3583	0.1991	0.0275	-0.1398	20	-0.0076	-0.0704	0.0098	0.1616
4	-0.0528	0.039	-0.0359	0.0564	21	-0.0293	-0.0325	0.0121	-0.1746
5	0.0467	0.0015	-0.0234	-0.0558	22	0.0106	0.2246	-0.0833	0.0982
6	-0.0206	0.0383	-0.0272	0.2642	23	-0.1745	0.1848	-0.0243	0.1896
7	-0.0781	-0.1099	0.178	0.3999	24	0.3286	-0.1952	-0.1047	-0.1487
8	0.1166	0.1157	-0.1406	-0.4393	25	-0.0222	0.2321	-0.0748	0.1152
9	-0.1387	-0.0438	0.0589	0.2438	26	-0.3088	0.2686	0.2463	-0.194
10	0.0384	0.1022	-0.0178	-0.0292	27	-0.2011	0.0309	0.1148	-0.0856
11	0.0476	0.0188	-0.0296	-0.0222	28	-0.0107	-0.1291	0.1353	-0.2456
12	-0.0383	-0.0499	-0.0251	0.1222	29	-0.2014	0.275	0.1077	-0.0968
13	0.0361	0.0929	-0.0207	-0.062	30	-0.2289	0.1395	0.2338	-0.2009
14	0.0317	0.006	-0.0184	0.0889	31	0.617	0.5417	0.4101	0.124
15	-0.0579	-0.0737	0.0256	-0.0456	32	0.1311	0.3229	-0.5909	-0.1343
16	0.032	-0.0899	0.094	-0.205	33	-0.0732	0.0642	-0.3268	0.0564
17	0.1222	-0.2245	0.1023	-0.1401					

amount of information explained by these 4 principal components is only 10.763 %. A plot of the first 2 Principal Components, Figure 6.29, was made to check for nonlinearites in the training data. From the figure it can be seen that the training data was linear.

To determine the relationship between the input data, and corresponding principal components, with longitudinal strain; a regression analysis was performed. The first regression was performed using the singular value decomposition and the y training set. The error in the training model was calculated to be 48.7864 μinch/inch. The regression model was then used to predict the y test set from the x test set. The error was the calculated to be 51.2092 μinch/inch. With the PCs that are weighted toward the brake data: 11, 12, 13, and 14, removed the error increases by 0.2987 μinch/inch (0.58 %), to

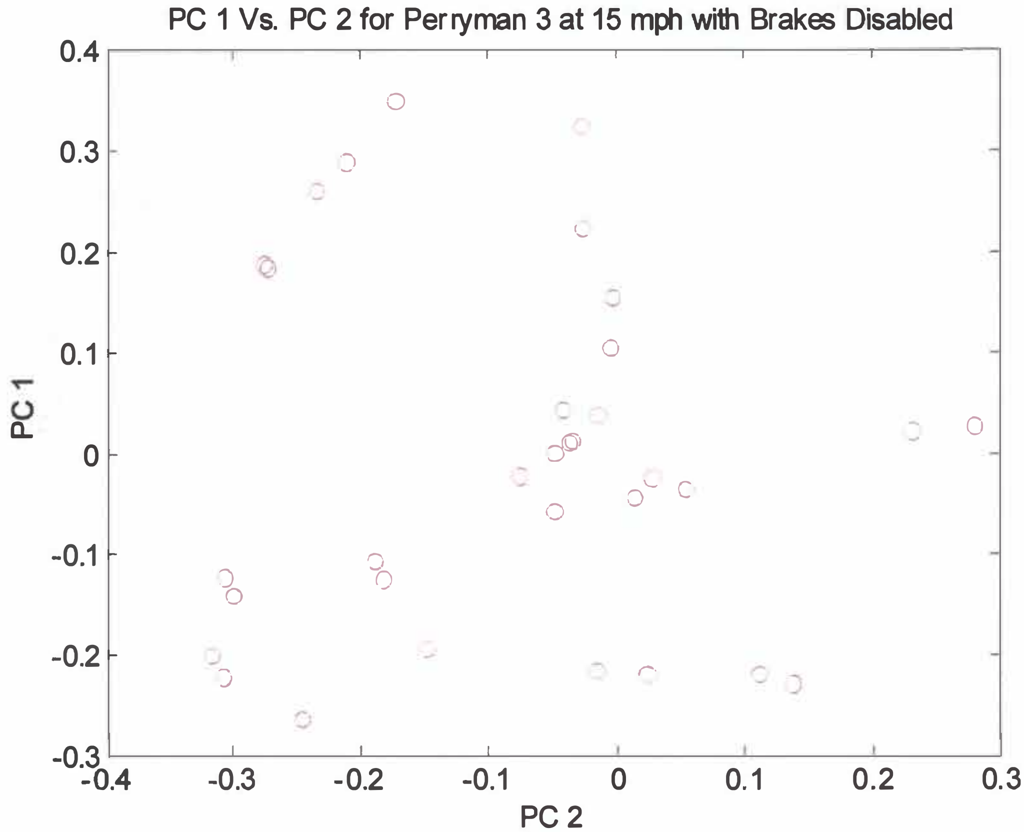

Figure 6.29: PC 1 vs. PC2 for Perryman #3 at 15 mph with brakes disabled.

51.5079 μinch/inch.

The error when principal components are removed, starting with the last principal component (PC) was then determined, and is shown in Figure 6.30. From the figure it can be seen that there is increase in the average error of only 1.9026 μinch/inch to a value 53.1118 μinch/inch when the last 25 principal components are removed, which includes PCs 11, 12, 13, and 14, which are weighted toward the brake data.

A correlation coefficient matrix of the z and y training data was made to determine which principal components are most useful in predicting acceleration. The absolute values of the correlation coefficients are shown in Figure 6.31. From the figure

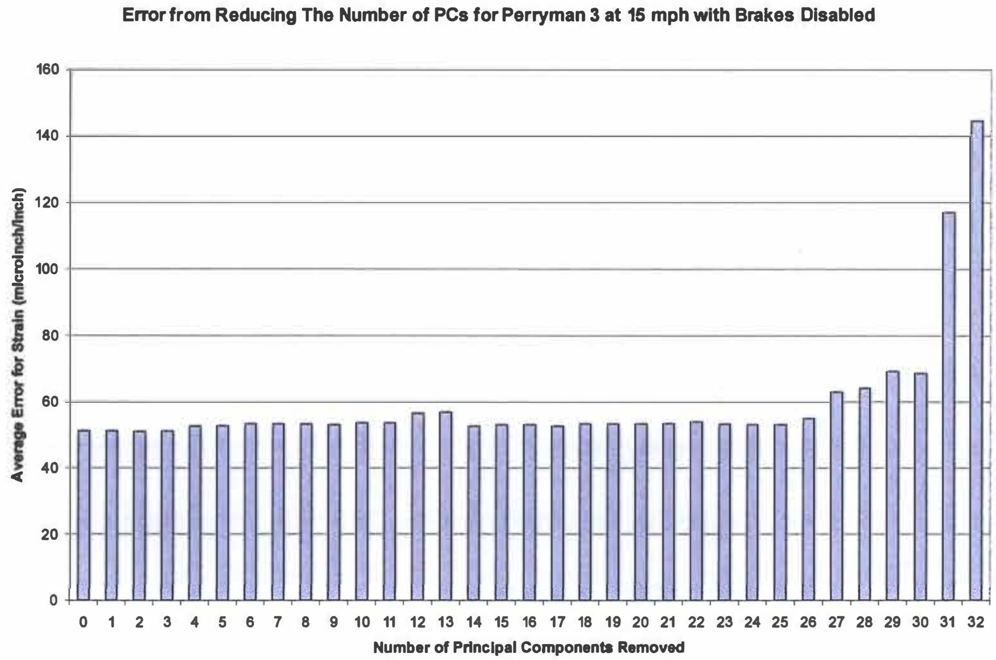

Figure 6.30: Average strain prediction error for Perryman #3 at 15 mph with brakes disabled.

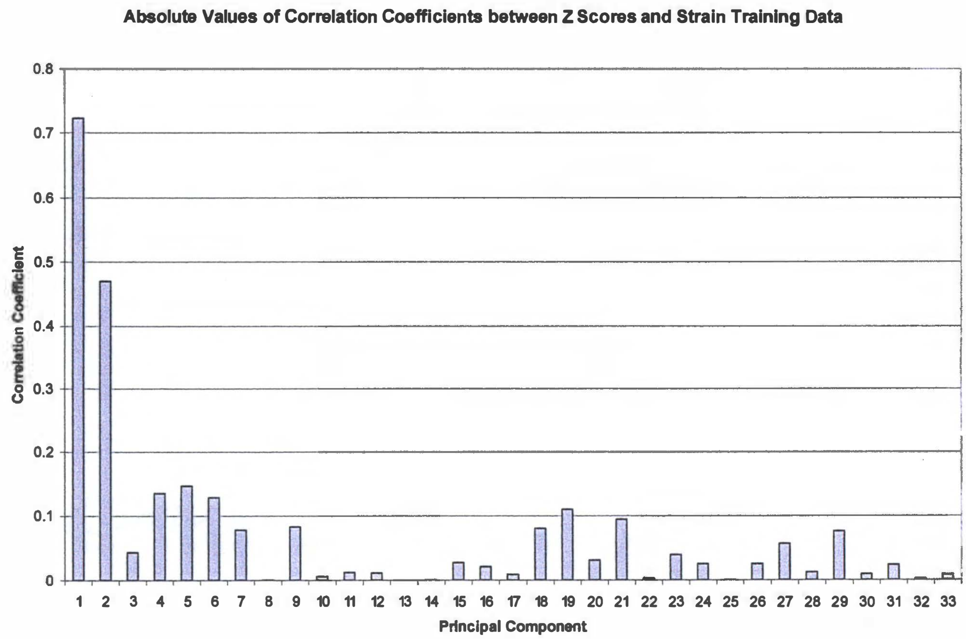

Figure 6.31: Correlation coefficient between Z scores and training data for Perryman #3 at 15 mph with brakes enabled, half of data.

it can be seen that the principal components that are weighted toward the brake data (11, 12, 13, and 14) are not correlated to the strain training data with correlation coefficients of 0.0119, 0.0115, 0.0001, and 0.0005, respectively.

A correlation coefficient matrix of the z and y training data was made to determine which principal components are most useful in predicting acceleration. The absolute values of the correlation coefficients are shown in Figure 6.31. From the figure it can be seen that the principal components that are weighted toward the brake data (11, 612, 13, and 14) are not correlated to the strain training data with correlation coefficients of 0.0119, 0.0115, 0.0001, and 0.0005, respectively.

The principal component analysis and regression also show for this data set that the brakes do not correlate to the longitudinal strain. The tenth, eleventh, twelfth, and thirteenth principal components were weighted toward the brake pressure data. These four principal components had an average correlation coefficient of 0.0008 between the Z score and longitudinal strain training data. The removal of these four principal components increase the average error by only 0.2987 μinch/inch, or 0.58 %, reinforcing the conclusion that the activation of the surge brake does not affect the life of the trailer. This was expected since the brakes were disabled for this test run.

Chapter 7 Regression Analysis

The regression models were initially created using the data from Belgian Block test runs at 15 mph decimated by 6 with the brakes both disabled and enabled, which are at 15 mph with the surge brake both disabled and enabled. By initially decimating by 6, this filtered the data to 84.175 Hz and re-sampled at 210.438 Hz. This decimation was purposely made lower than the strain gage cutoff frequency of 100 Hz. The data was also divided into independent and dependent data sets. The dependent data was the calibrated aft longitudinal strain and the independent was from the non-strain data channels from the data collected. The channel for ground speed was eliminated since it was not a sensor located on the trailer. The dependent variables were numbered 1 through 33, as shown in Table 7.1, to simplify the analysis and graphs.

Once the data was selected and filtered, an initial regression model using all the possible input variables was created, as shown in Figures 7.1 and 7.2, to determine the least possible error that can be obtained with the current filtering of the data. The regressions using all the input variables had average errors of 53.9564 μinch/inch and 51.3792 μinch/inch for the Belgian Block test runs at 15 mph decimated by 6 with the brakes both disabled and enabled, respectively. This error is still higher than what is desirable.

Regressions using one predictor variable for each input channel, channels other than strain, were then created. The average error for each variable was plotted as shown in Figure 7.3. From the figure it can be easily seen that for the Belgian Block test runs at 15 mph decimated by 6 with the brakes both disabled and enabled, the channel for the CS

Table 7.1: Input variables.

Var #	Channel Description	Unit	Var #	Channel Description	Unit
1	CS Axle Accel (V)	g's	18	CS Aft Accel (T)	g's
2	CS Frame Accel (V)	g's	19	CS Aft Accel (L)	g's
3	RS Axle Accel (V)	g's	20	RS Forward Accel (V)	g's
4	RS Frame Accel (V)	g's	21	RS Forward Accel (T)	g's
5	Lunette Accel (V)	g's	22	RS Forward Accel (L)	g's
6	Lunette Accel (T)	g's	23	RS Aft Accel (V)	g's
7	Lunette Accel (L)	g's	24	RS Aft Accel (T)	g's
8	Tongue Accel (V)	g's	25	RS Aft Accel (L)	g's
9	Tongue Accel (T)	g's	26	Trailer CG Pitch Rate	deg/sec
10	Tongue Accel (L)	g's	27	Trailer CG Roll Rate	deg/sec
11	Trailer CG Accel (V)	g's	28	Trailer CG Yaw Rate	deg/sec
12	Trailer CG Accel (T)	g's	29	CS Shock Disp	inches
13	Trailer CG Accel (L)	g's	30	RS Shock Disp	inches
14	CS Forward Accel (V)	g's	31	Surge Brake Press.	psi
15	CS Forward Accel (T)	g's	32	CS Wheel Cyl. Press.	psi
16	CS Forward Accel (L)	g's	33	RS Wheel Cyl. Press.	psi
17	CS Aft Accel (V)	g's			

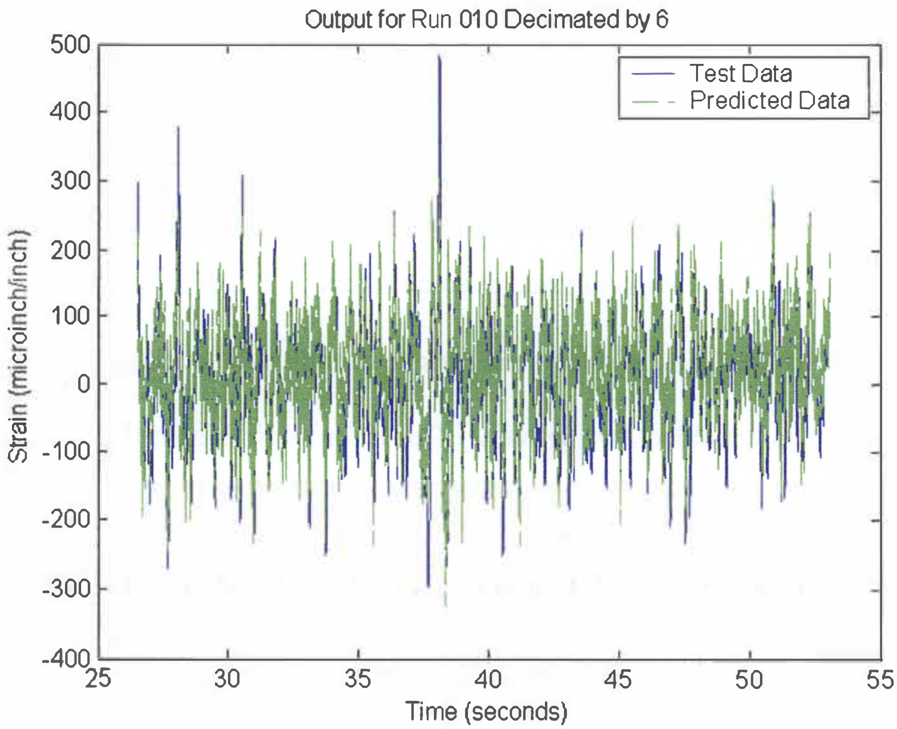

Figure 7.1: Regression output for Belgian Block at 15 mph with brakes disabled, decimated by 6 using all variables.

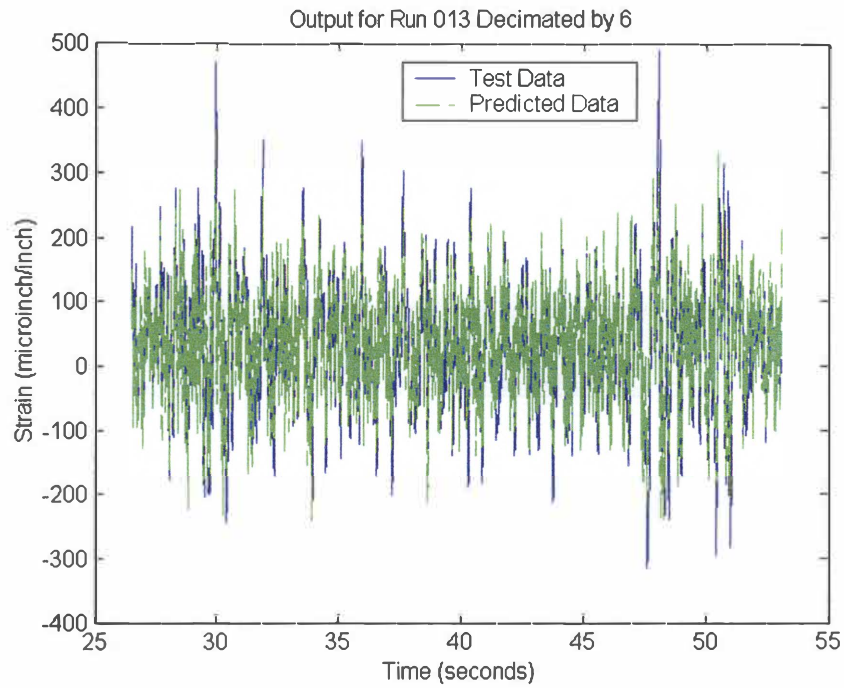

Figure 7.2: Regression output for Belgian Block at 15 mph with brakes enabled, decimated by 6 using all variables.

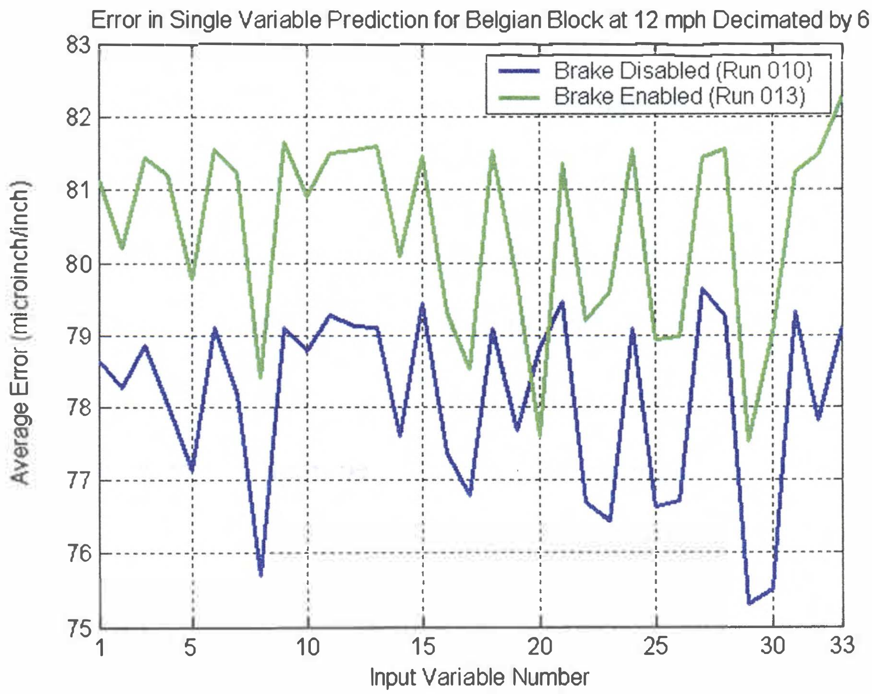

Figure 7.3: Error in single variable prediction for Belgian Block decimated by 6.

shock absorber displacement had the lowest average errors of 75.2983 and 77.5264 μinch/inch, respectively, and the average errors have a consistent pattern between the two runs. For the Belgian Block test run at 15 mph decimated by 6 with the brakes disabled, the next two singles variables with the lowest average errors were the RS shock absorber displacement and the tongue vertical acceleration with errors of 75.4988 and 75.7006 μinch/inch, respectively. For the Belgian Block test run at 15 mph decimated by 6 with the brakes enabled, the next two singles variables with the lowest average errors were the RS forward and the tongue vertical accelerations with errors of 77.6032 and 78.4245 μinch/inch, respectively. It is interesting to note that the best average error for a single brake pressure variable was 81.2297 μinch/inch, for the surge brake pressure, 4.78 % higher than the lowest average error. These average errors are still higher than what is desirable. From this result, it can be seen that a better value for the decimation of the data needs to be found.

Since the errors are so high, the current filtering of the data allows too much 'noise' to be left in the data. To reduce the error, the 'noise' in the data needs to be eliminated. To determine a better frequency range for filtering, a PSD of the strain data decimated by 6 was calculated for both runs, as shown in Figure 7.4. The PSD plot shows most of the energy to be in the 0 to 20 Hz range and then it begins to drops off. The data was then decimated by 25, this gave a filtered frequency of 20.202 Hz and a sampling frequency of 50.505 Hz.

Once the data was filtered and re-sampled again, another set of initial regression

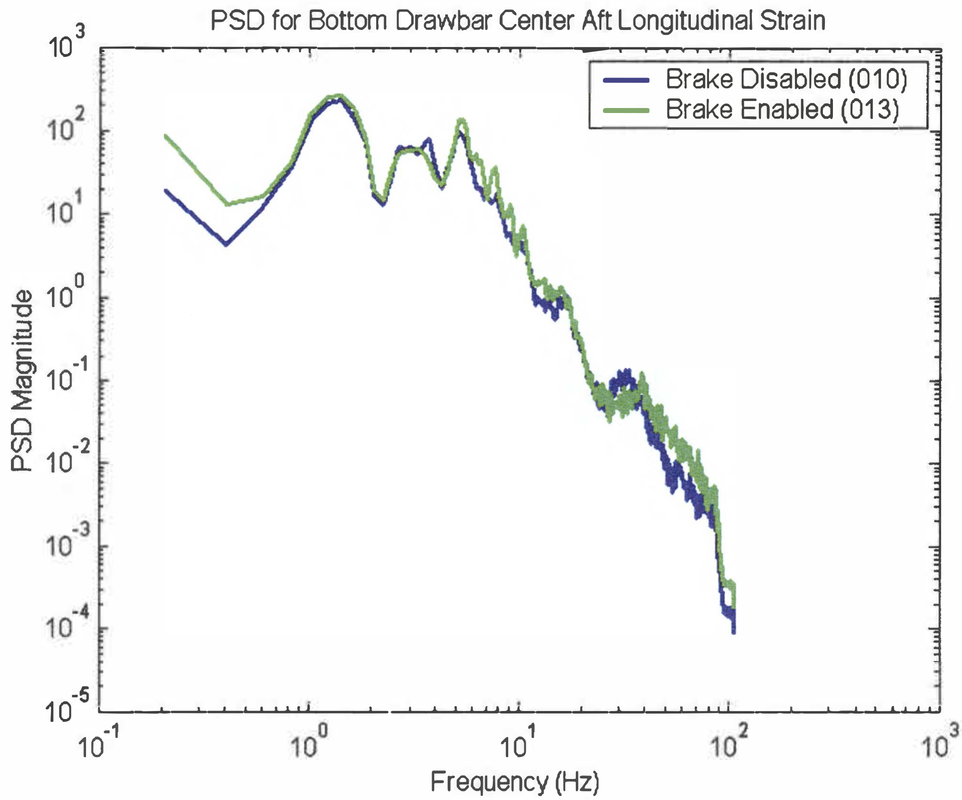

Figure 7.4: PSD for longitudinal strain for Belgian Block at 15 mph.

models using all the predictor, input, variables were created and are shown in Figures 7.5 and 7.6 . The new models had errors of 31.5985 µinch/inch and 16.1643 µinch/inch for Belgian Block test runs at 15 mph decimated by 25 with the brakes both disabled and enabled, respectively. These errors are much improved from the initial regressions. To determine which variables can be eliminated and still yield a good model, regressions with one predictor variable for each input channel, channels other than strain, were again created with the data now decimated by 25. The average error was plotted for each variable as shown in Figure 7.7. From the figures it can be easily seen that for Belgian Block test runs at 15 mph decimated by 25 with the brakes both disabled and enabled, the channel for the tongue vertical acceleration had the lowest average errors of 71.0913 and

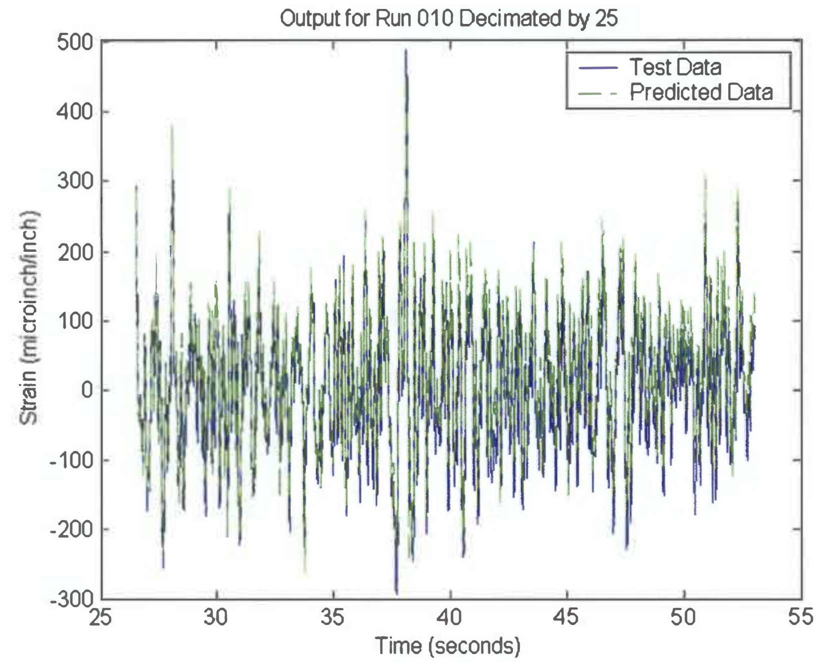

Figure 7.5: Regression output for Belgian Block at 15 mph with the brakes disabled and decimated by 25, using all variables.

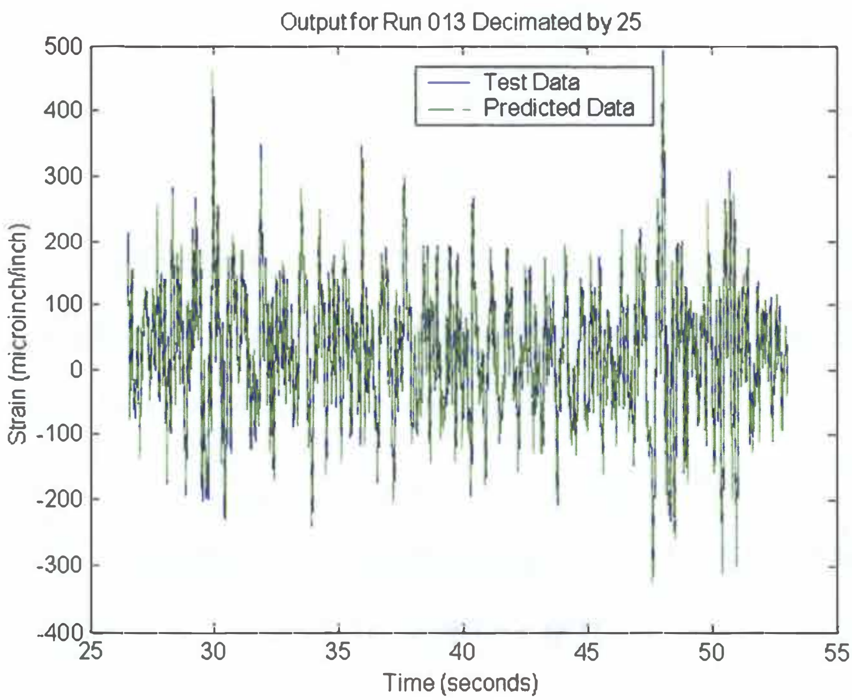

Figure 7.6: Regression output for Belgian Block at 15 mph with the brakes enabled and decimated by 25, using all variables.

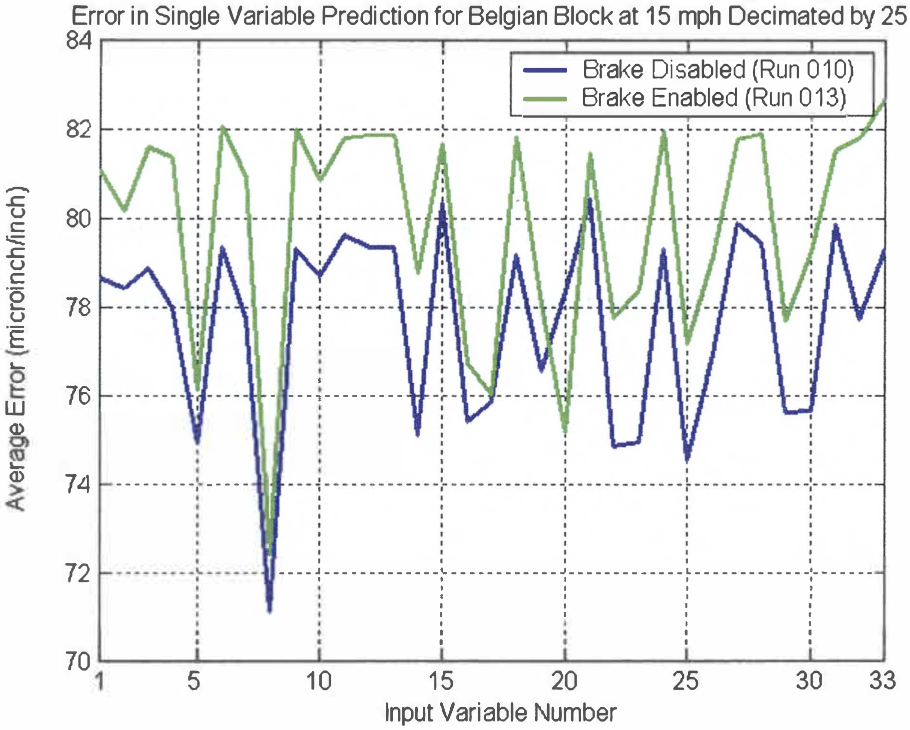

Figure 7.7: Error in single variable prediction for Belgian Block at 15 mph data decimated by 25.

72.3969 µinch/inch, respectively and the average errors again have a consistent pattern between the two runs. For the Belgian Block test run at 15 mph decimated by 25 with the brakes disabled, the next single variables with the lowest average errors were the RS aft longitudinal and RS forward longitudinal, lunette vertical, and RS aft vertical accelerations with errors of 74.5518, 74.8586, 74.9232, and 74.9433 µinch/inch, respectively. For the Belgian Block test run at 15 mph decimated by 25 with the brakes enabled, the next single variables with the lowest average errors were the RS forward vertical, CS aft vertical, lunette vertical, and CS forward longitudinal accelerations with average errors of 75.2096, 76.0370, 76.1395, and 76.7431 µinch/inch, respectively. It is interesting to note that the best average error for a single brake pressure variable was

81.5349 μinch/inch, for the surge brake pressure, 12.623 % higher than the lowest average error.

The data from the Perryman #3 test runs at 15 mph with the brakes both disabled and enabled was then analyzed. The analysis was conducted with the data decimated by 25, due to the results found from the Belgian Block data. The initial regression model using all the possible input variables was created, as shown in Figures 7.8 and 7.9, to determine the least possible error that can be obtained with the current filtering of the data. The regressions using all the input variables had average errors of 21.8781 μinch/inch and 33.3067 μinch/inch for Perryman #3 test runs at 15 mph decimated by 25 with the brakes both disabled and enabled, respectively. The data range of the strain Perryman #3 test runs at 15 mph decimated by 25 with the brakes both disabled and enabled was 1494.4 μinch/inch and 1242.7 μinch/inch, respectively. This error is 1.464 % and 2.68 % of the data range for Perryman #3 test runs at 15 mph decimated by 25 with the brakes both disabled and enabled, respectively, which can still be improved.

To determine which variables can be eliminated and still yield a good model, regressions with one predictor variable for each input channel, channels other than strain, were created. The average error was plotted for each variable as shown in Figure 7.10. From the figures, it can be easily seen that for Perryman #3 test runs at 15 mph decimated by 25 with the brakes both disabled and enabled the channel for the RS forward longitudinal acceleration had the lowest average errors of 76.895 and 72.4 μinch/inch, respectively, and the average errors again have a consistent pattern between the two runs.

For Perryman #3 test run at 15 mph decimated by 25 with the brakes disabled, the

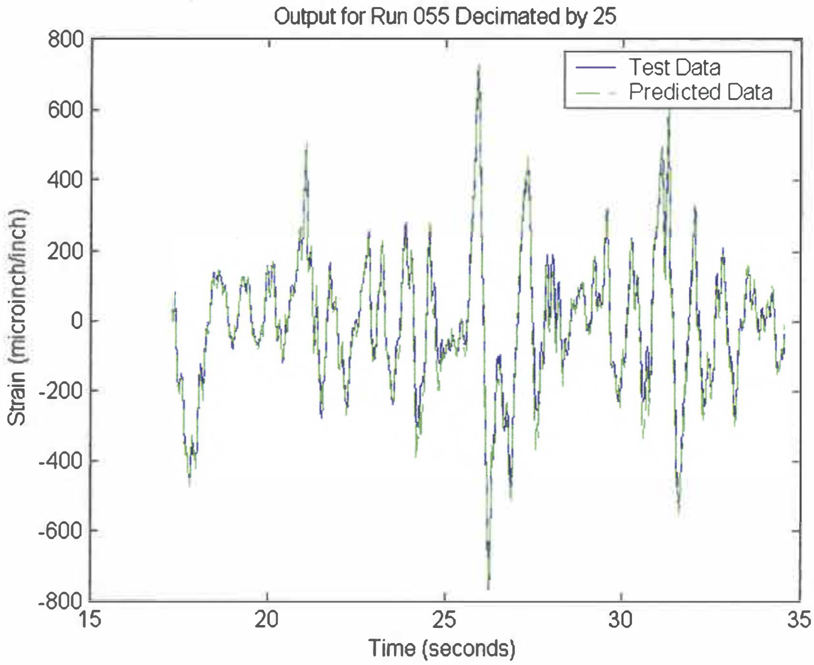

Figure 7.8: Regression output for Perryman #3 at 15mph with brakes disabled and decimated by 25, using all variables.

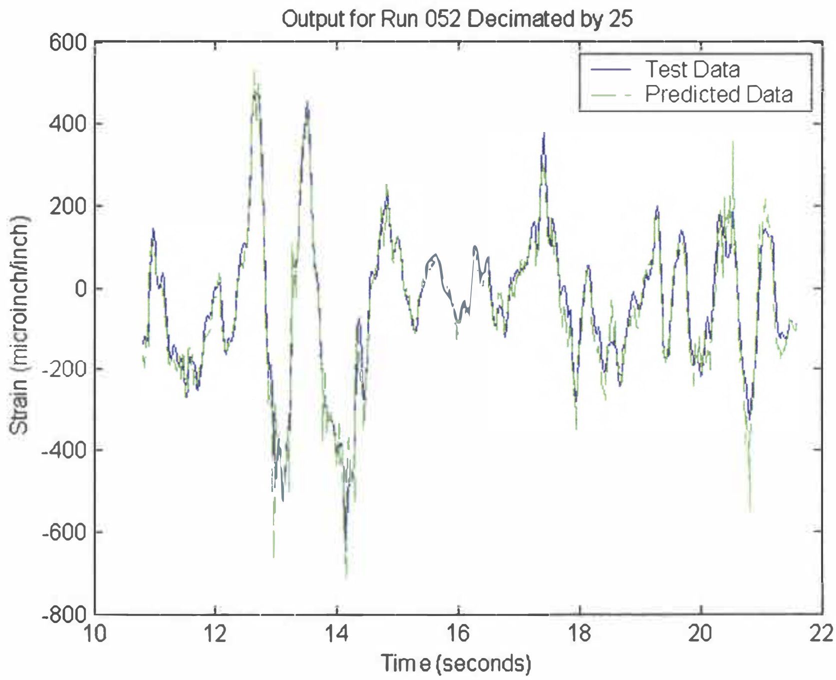

Figure 7.9: Regression output for Perryman #3 at 15mph with brakes enabled and decimated by 25, using all variables.

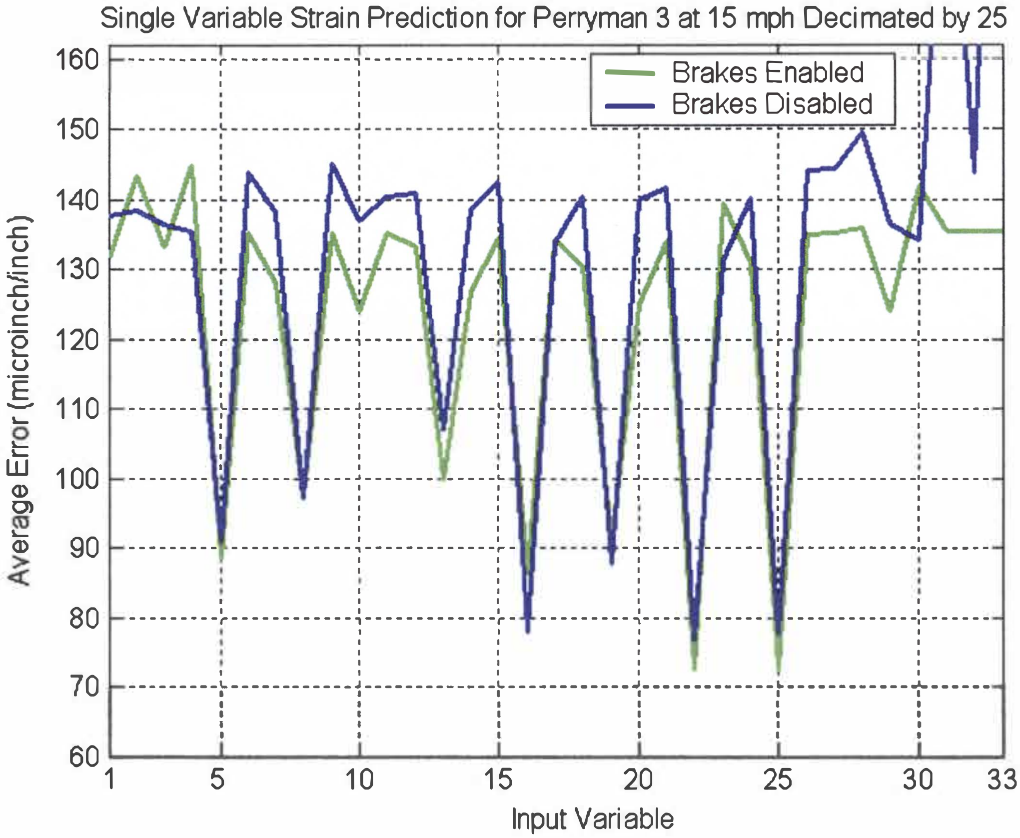

Figure 7.10: Error in single variable prediction for Perryman #3 at 15mph, decimated by 25.

next single variables with the lowest average errors were the RS aft longitudinal, CS forward longitudinal, CS aft longitudinal, lunette vertical, tongue vertical, and CG longitudinal accelerations, with errors of 77.658, 77.991, 87.74, 90.909, 97.279, and 107.14 µinch/inch, respectively. For Perryman #3 test run at 15 mph decimated by 25 with the brakes enabled, the next single variables with the lowest average errors were the with the lowest average errors were the RS aft longitudinal, CS forward longitudinal, lunette vertical, CS aft longitudinal, tongue vertical, and CG longitudinal accelerations, with errors of 72.583, 86.594, 88.591, 91.099, 97.36, and 99.765 µinch/inch, respectively. It is interesting to note that the best average error for a single brake pressure variable was 135.41 μinch/inch, for the surge brake pressure, 53.47 % higher than the lowest average error.

The individual variables with the lowest errors from both the Belgian Block and Perryman #3 data with brakes enabled and disabled decimated by 25 are shown in Table 7.2. From the table, it can be seen that the lunette and tongue vertical accelerations have low prediction average prediction errors among all 4 test runs. CS forward longitudinal, RS forward, and RS aft accelerations have low prediction errors among 3 test runs. From this we can determine that these sensors should be used in any model created.

7.1 Data Filtering

From the regression analysis we can see that the increased decimation of the data decreases the average error of the model. Increased decimation lowers the frequency range of the input data, but information is lost as the data is re-sampled. To minimize this adverse effect of re-sampling and determine the effect of reducing the frequency range on the error, the data decimated by 25 was increasingly filtered using an 8-pole Butterworth filter.

The effect of filtering the data at lower cutoff frequencies can be seen in Figures 7.11 through 7.14. From Figures 7.11 and 7.12, it can be seen that the average error, for the test data from the Belgian Block course at 15mph with the brakes disabled and enabled, decreases continuously to minimums of 4.4989 μinch/inch and 9.6450 μinch/inch at frequencies of 3.5354 Hz and 6.5657 Hz, respectively, and then sharply rises.

Table 7.2: Lowest average prediction errors for Belgian Block and Perryman #3 test runs.

	Average Prediction Error			
	Belgian Block		Perryman #3	
NAME	No Brakes	Brakes	No Brakes	Brakes
Lunette Accel. (V)	74.9232	76.0370	90.909	88.591
Tongue Accel. (V)	71.0913	72.3967	97.279	97.36
CG Accel. (L)	>75.0	>77.0	107.14	99.765
CS Forward Accel. (L)	>75.0	76.7431	77.991	86.594
CS Aft Accel. (V)	>75.0	76.0370	>131.0	>124.0
CS Aft Accel. (L)	>75.0	>77.0	87.74	91.099
RS Forward Accel. (V)	>75.0	75.2096	>131.0	>124.0
RS Forward Accel. (L)	74.8586	>77.0	76.895	72.4
RS Aft Accel. (V)	74.9433	>77.0	>131.0	>124.0
RS Aft Accel. (L)	74.5518	>77.0	77.658	72.583

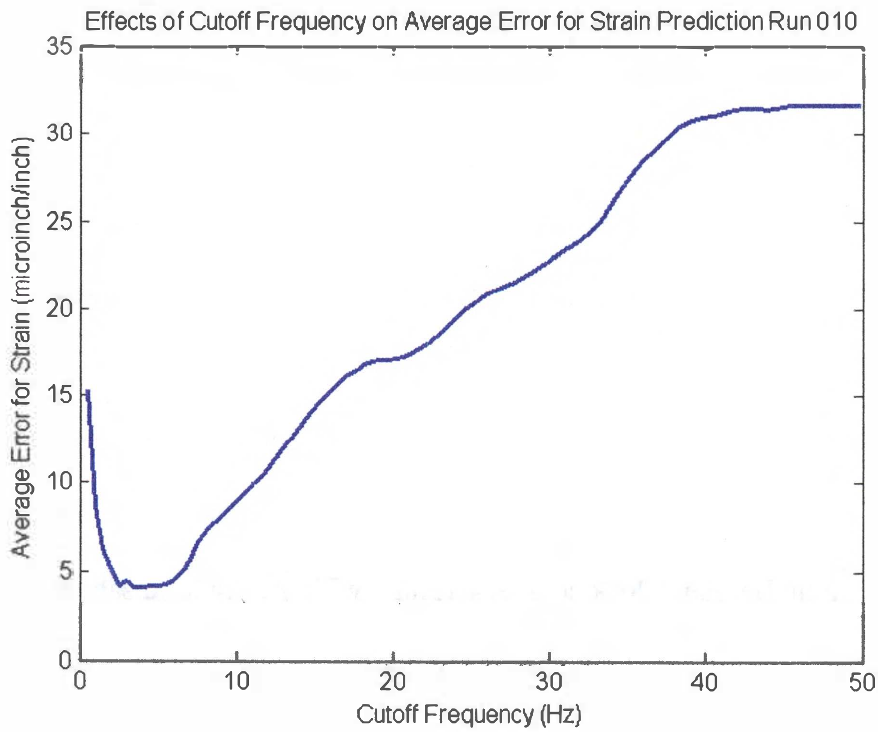

Figure 7.11: Effects of filter cutoff frequency on average error from Belgian Block at 15 mph with brakes disabled and decimated by 25.

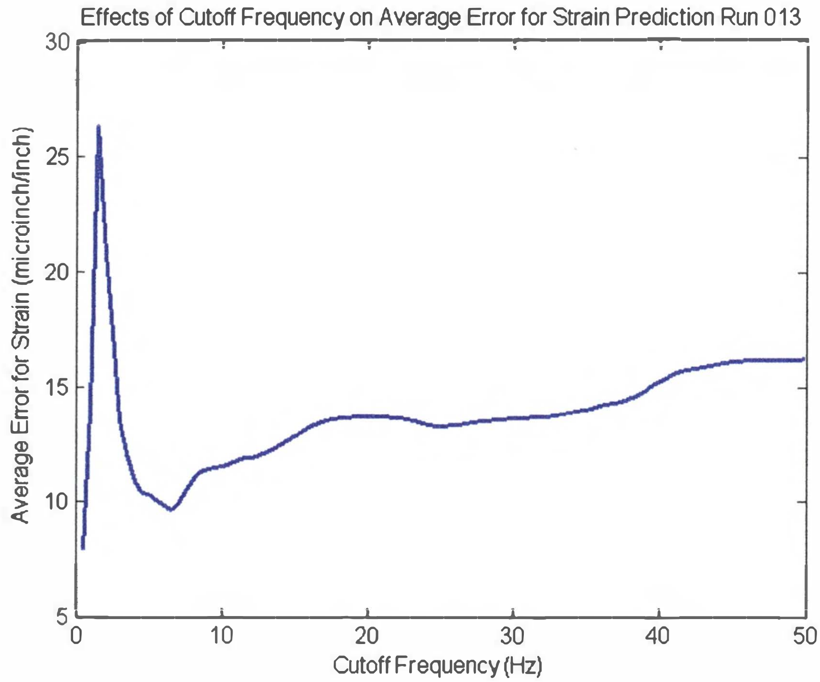

Figure 7.12: Effects of filter cutoff frequency on average error from Belgian Block at 15 mph with brakes enabled and decimated by 25.

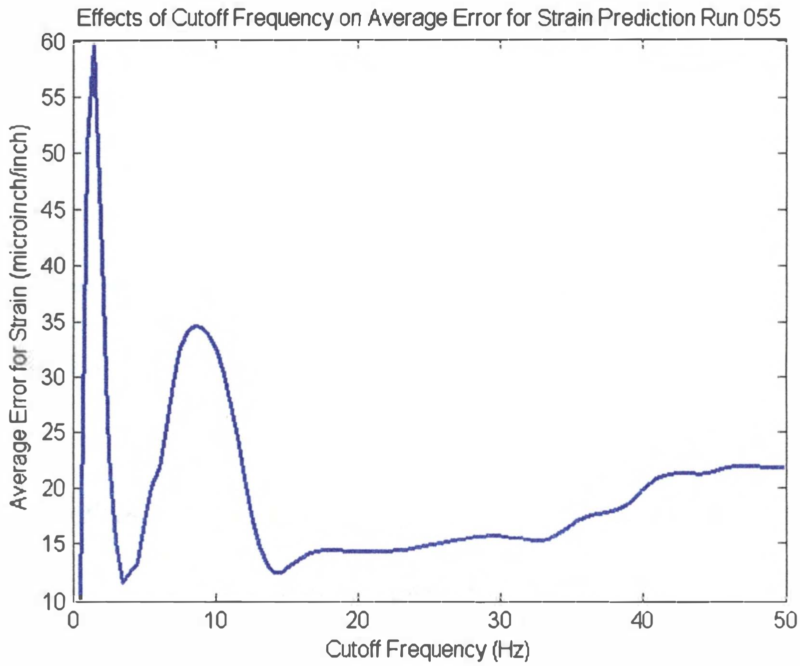

Figure 7.13: Effects of filter cutoff frequency on average error from Perryman #3 at 15 mph with brakes disabled and decimated by 25.

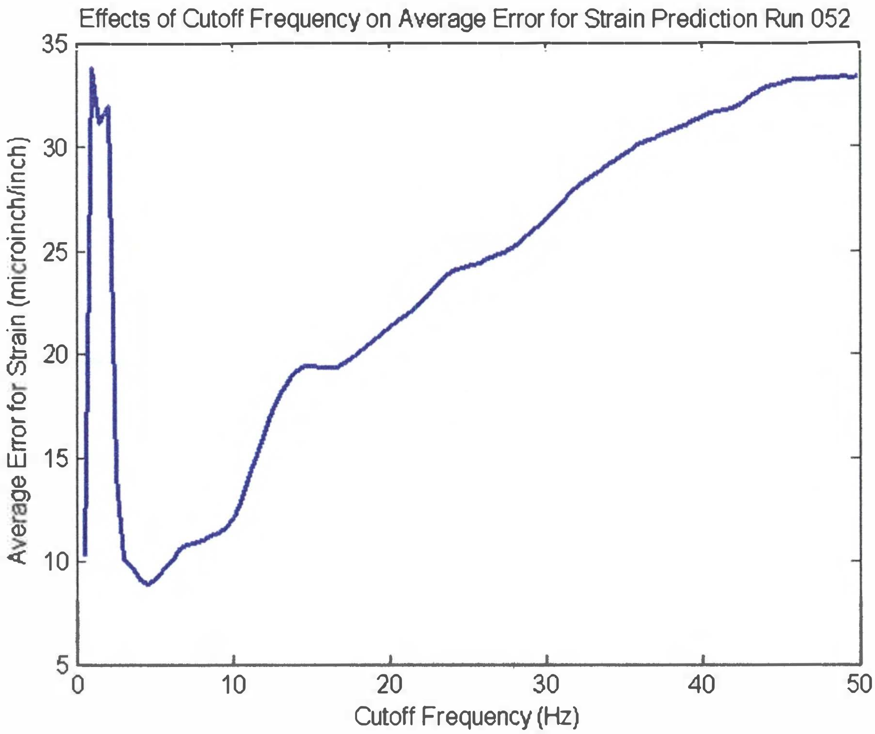

Figure 7.14: Effects of filter cutoff frequency on average error from Perryman #3 at 15 mph with brakes enabled and decimated by 25.

From Figures 7.13 and 7.14 it can be seen that the average error, for the test data from the Perryman #3 test course at 15 mph with the brakes disabled, decreases continuously to a minimum of 11.6794 μinch/inch at 3.5354 Hz, and then sharply rises and decreases once again. For the Perryman #3 test course at 15 mph with the brakes enabled, the error decreases continuously to a minimum of 8.8758 μinch/inch at 4.5455 Hz and then sharply rises, as seen with the Belgian Block test data. Also, from the figures it can be seen that the minimum average errors of 9.6450 μinch/inch and 8.8758 μinch/inch for predicting the test data from Belgian Block at 15mph and Perryman #3 at 15 mph with the bakes enabled occur at filtered frequencies of 6.5657 Hz and 4.5455 Hz, respectively.

To determine the effects of filtering to lower frequencies on the strain data, the strains for several cutoff frequencies were compared, as shown in Figures 7.15 and 7.16. From the figures, it can be seen that effect of the filtering, to the cutoff frequency corresponding to the minimum average error, on the data is minimal.

Once it was determined that the cutoff frequency corresponding to the minimum average error was acceptable, the most appropriate model could be chosen. The most appropriate model was chosen using forward selection for the filtered data sets for Belgian Block at 15 mph and Perryman #3 at 15 mph with the brakes enabled that were decimated by 25. The cutoff frequency used for the Perryman #3 data at 15 mph with the brakes disabled and enabled was 3.5354 Hz and 4.5455 Hz, respectively. The cutoff frequency used for the Belgian Block data at 15 mph with the brakes enabled and disabled was 6.5657 Hz and 4.0404 Hz, respectively.

The forward selection R^2, component and total, values for the Perryman #3 and Belgian Block test runs at 15 mph, respectively, are shown in Table 7.3. As can be seen from the table, the first four variables hold most of the R^2 value. Therefore, an appropriate model can be created using a combination of only these four variables.

Variable 22 (RS forward longitudinal acceleration) appears as the first variable for both Perryman #3 test runs at 15 mph while variable 25 (RS aft longitudinal acceleration) appears as the first variable for both Belgian Block test runs at 15 mph. The acceleration values in the longitudinal direction should be the same for both sensors on the ends of a rigid structure. Therefore, the longitudinal acceleration on the RS appears as the first variables for all four test runs.

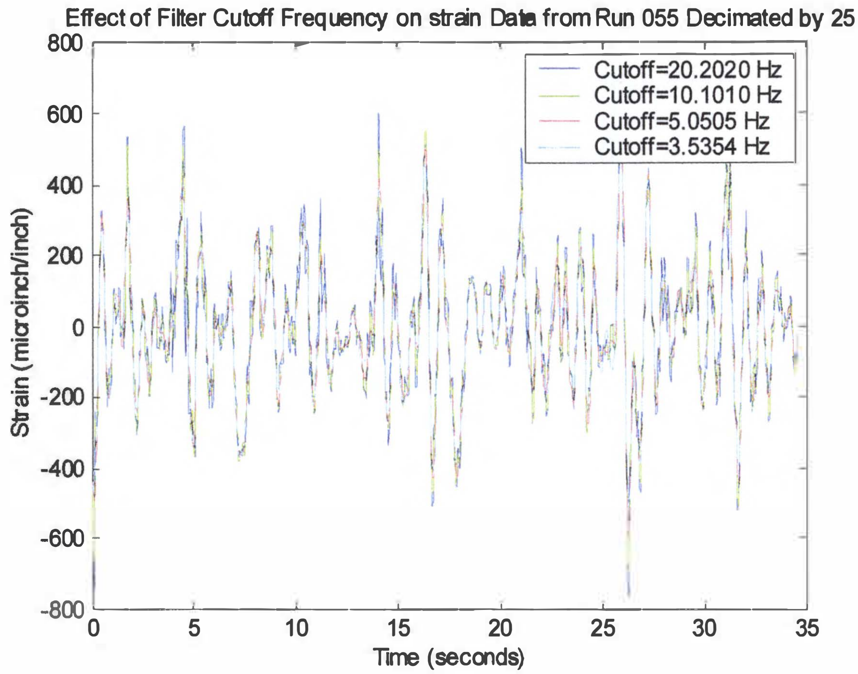

Figure 7.15: Effects of filter cutoff frequency on strain data from Perryman #3 at 15 mph with brakes disabled and decimated by 25.

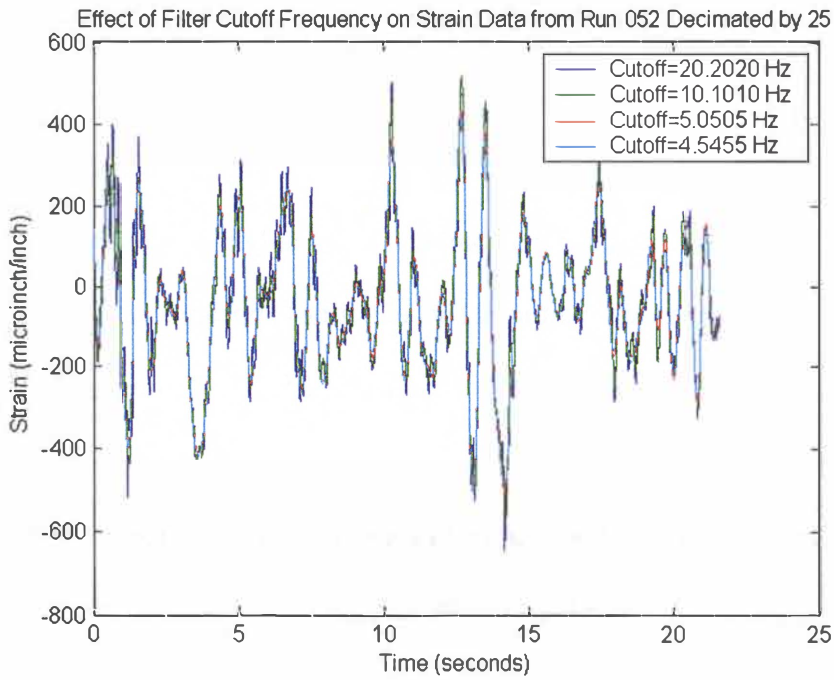

Figure 7.16: Effects of filter cutoff frequency on strain data from Perryman #3 at 15 mph with brakes enabled and decimated by 25.

Table 7.3: Forward selection R^2 values for Belgian Block and Perryman #3.

Perryman #3 15mph Brakes Enabled			Perryman #3 15mph Brakes Disabled			Belgian Block 15mph Brakes Enabled			Belgian Block 15mph Brakes Disabled		
Var.	R^2 Comp.	R^2 Total	Var.	R^2 Comp.	R^2 Total	Var.	R^2 Comp.	R^2 Total	Var.	R^2 Comp.	R^2 Total
22	0.9335	0.9335	22	0.9063	0.9063	25	0.7119	0.7119	25	0.6058	0.6058
19	0.037	0.9705	5	0.0651	0.9714	19	0.216	0.9279	19	0.2417	0.8475
8	0.0239	0.9944	19	0.0212	0.9926	5	0.0537	0.9816	5	0.1353	0.9828
17	0.0025	0.9969	10	0.0035	0.9961	22	0.0116	0.9932	16	0.0064	0.9892
29	0.0004	0.9973	29	0.0008	0.9969	13	0.0019	0.9951	8	0.0019	0.9911
2	0.0003	0.9976	8	0.0004	0.9973	26	0.0008	0.9959	2	0.0026	0.9937
25	0.0002	0.9978	1	0.0003	0.9976	21	0.0003	0.9962	22	0.0003	0.994
3	0.0004	0.9982	11	0.0002	0.9978	15	0.0004	0.9966	17	0.0003	0.9943
5	0.0001	0.9983	16	0.0004	0.9982	30	0.0001	0.9967	13	0.0004	0.9947
9	0.0001	0.9984	33	0.0002	0.9984	8	0.0001	0.9968	11	0.0003	0.995
15	0.0001	0.9985	25	0.0002	0.9986	11	0.0002	0.997	3	0.0003	0.9953

From the Table 7.3, it can be seen variable 19 (CS aft longitudinal acceleration) appears within the first four variables of all four runs. The CS aft longitudinal acceleration contributes the second highest amount to the R^2 value for the Perryman #3 at 15 mph and Belgian Block test runs at 15 mph with the brakes disabled. The CS aft longitudinal acceleration also contributes the second highest amount to the R^2 value for the Belgian Block test run at 15 mph with the brakes enabled, and the third highest amount to the R^2 value for the Perryman #3 test run at 15 mph with the brakes enabled.

Variable 5 (lunette vertical acceleration) contributes the third highest amount to the R^2 value for the Belgian Block test runs at 15 mph with the brakes both enabled and disabled. The lunette vertical acceleration contributes the second highest amount to the R^2 value for the Perryman #3 test run at 15 mph with the brakes enabled.

Variable 8 (tongue vertical acceleration) contribute the third highest amount to the R^2 value for the Perryman #3 test run at 15 mph with the brakes disabled. The fourth highest contributor to the R^2 value for the Perryman #3 test runs at 15 mph with the brakes both enabled and disabled were variables 10 (tongue vertical acceleration) and 17 (CS aft vertical acceleration), respectively. The fourth highest contributors to the R^2 value for the Belgian Block test runs at 15 mph with the brakes disabled and enabled were 22 (RS forward longitudinal acceleration), and 16 (CS forward longitudinal acceleration), respectively.

From this analysis, it can determined that the RS forward longitudinal, CS aft longitudinal, and lunette vertical accelerations should be used for any further models. To determine if a fourth variable should be used, a series of regressions were made. The regressions were created for Perryman #3 at 15 mph and Belgian Block at 15 mph test runs with the brakes enabled. As shown in Table 7.4, the regressions compared combinations of the first 4 variables that contributed the highest amount to the R^2 value.

From Table 7.4, it can be seen that a fourth variable should be used. The models with the lowest average error for both test runs include the variables: 5, 10, 19, and 22. These are for lunette vertical, tongue vertical, CS aft longitudinal, and RS forward longitudinal accelerations, respectively. These four sensors can be used to accurately predict the longitudinal strain at the drawbar failure location.

Table 7.4: Average regression error for selected variables using test data from Belgian Block and Perryman #3 at 15 mph with brakes enabled.

	AVERAGE ERROR (μinch/inch)	
VARIABLES USED	**PERRYMAN #3**	**BELGIAN BLOCK**
ALL	8.8758	9.6450
5, 22	24.632	22.8946
5, 19, 22	11.7328	5.5161
5, 10, 19, 22	8.916	5.0092
5, 10, 16, 19, 22	9.1131	4.9749
5, 8, 16, 22, 25	14.7574	9.2955
5, 16, 19, 25	19.2532	7.3962

Chapter 8 Fatigue Life

One of the primary goals of this research is to show that the fatigue damage, at the drawbar location on the trailer, can be determine accurately from predicted strain data. This will allow the use of a group of accelerometers to be used to monitor the fatigue damage to the part. This allows the direct monitoring of the changes in the fatigue life of the part.

In order to determine the accuracy of the strain predicted from the model; the predicted fatigue life was calculated and compared to the life calculated from the original data. The effect of filtering on the fatigue life calculation was also analyzed to determine if filtering has a significant effect on the results. From this the frequency range that the damage occurs can also be analyzed.

To calculate fatigue life, the Matlab toolbox Wave Analysis for Fatigue and Oceanography (WAFO) was used. WAFO uses routines based on extreme value and crossing analysis to analyze random waves and loads. To calculate fatigue, WAFO calculates the rainflow cycles from a series of turning points calculated from the load data. The Stress-Life (S-N) curve is then used to calculate the material specific parameters used in the damage calculation, based on the Wohler curve and the Palmgren-Miner rule.

The material used in the trailer was 6061-T6 aluminum. The S-N curve data for the trailer material was created from fatigue data taken from the Structural Alloys Handbook edited by Holt, Mindlin, and Ho (1996). The S-N curve was then plotted and fitted for use in WAFO, as shown in Figure 8.1.

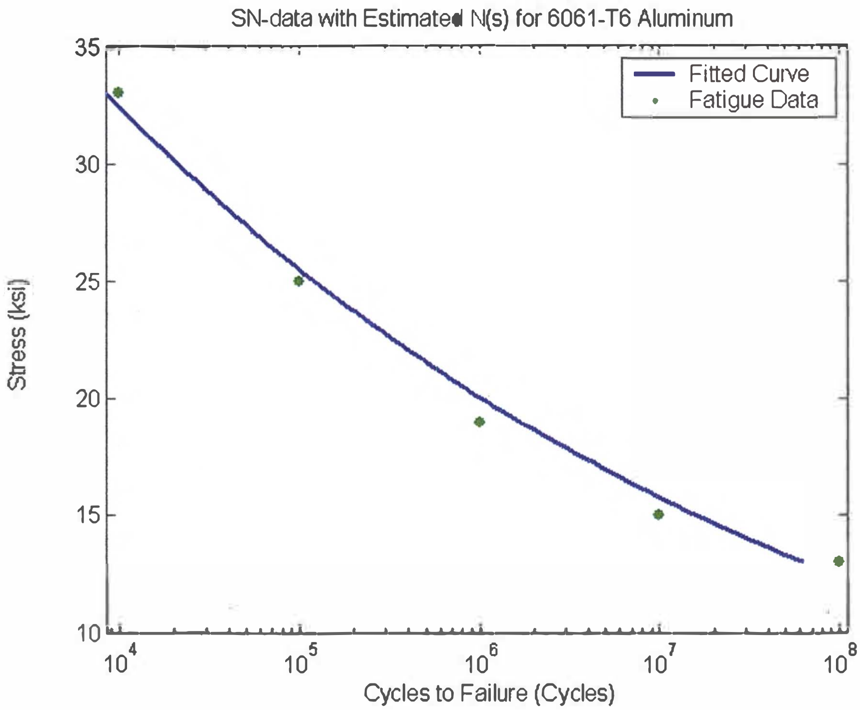

Figure 8.1: S-N curve fitted for WAFO.

The maximum stress was well below the yield stress, therefore, a linear relationship between stress and strain was used. The strain, ε, data was converted to stress, σ, data by relating the stress and strain by the elastic modulus, E, for aluminum of $10*10^6$ ksi.

$$\sigma = \varepsilon * E \tag{8.1}$$

The rainflow cycles were then calculated by WAFO for both Belgian Block and Perryman #3 test courses at 15 mph, with the brakes both enabled and disabled, as shown in Figures 8.2 and 8.3. For Figures 8.2 and 8.3, only the first 1100 data points were used so that comparisons could be made. Figure 8.2, it can be seen that the cycle count distribution is very similar for all four test runs, with the cycles being over a wider range

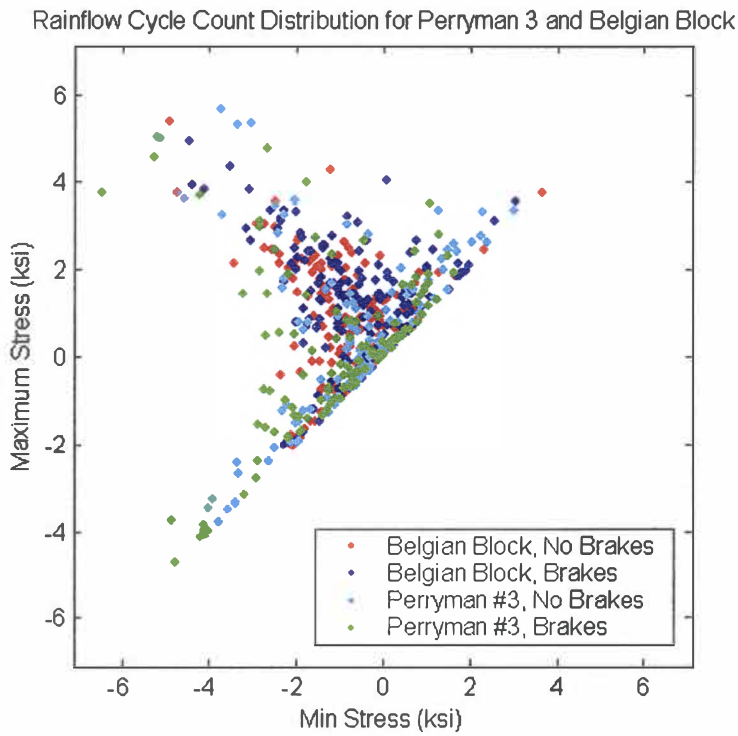

Figure 8.2: Rainflow cycle count.

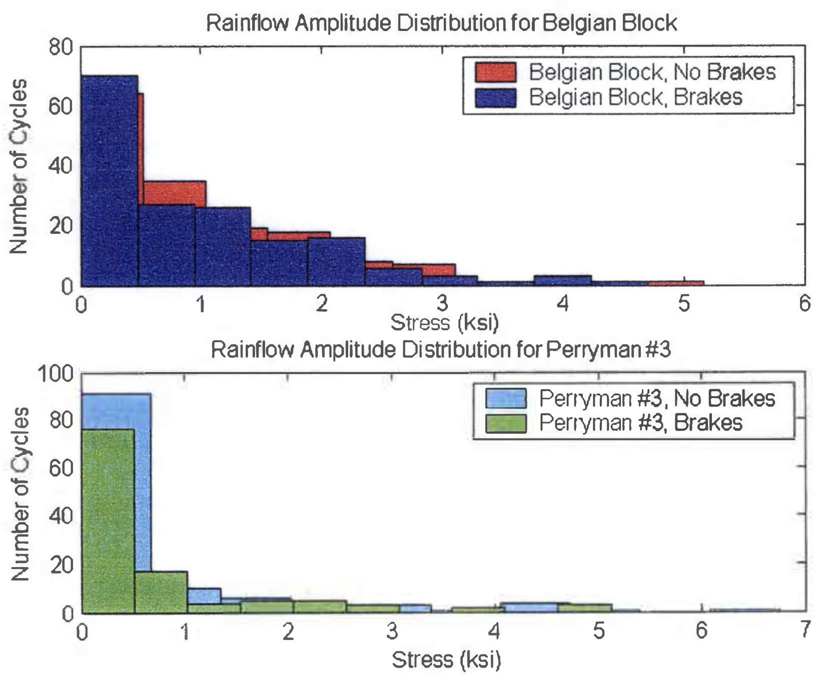

Figure 8.3: Rainflow amplitude distribution.

for the Perryman #3 test data. Figure 8.3 shows the rainflow amplitude distribution to decrease in cycle count as stress increases, for Belgian Block. The figure also shows the cycle count to drastically decrease with an increase in stress above 1 ksi for the Perryman #3 test course. This would be expected since the Perryman #3 test course is more randomly distributed than the more normally distributed Belgian Block test course. The brakes do not seem to have a definite effect on the cycle count for either test course. The fatigue life was then calculated in both hours and distance, as shown in Tables 8.1 and 8.2, respectively. As can be seen from both Tables, the fatigue life estimates for all four test runs indicated infinite life. The fatigue life value increased for the data sets that had been filtered to their optimum frequency. The percent differences between the test and predicted life improved, as can be seen from Table 8.1 for the optimized frequencies. As expected the use of only the four variables: lunette vertical acceleration, tongue vertical acceleration, curbside aft longitudinal, and roadside aft longitudinal acceleration, did not significantly change the predicted life results.

The calculated fatigue life predictions are close, but need to be closer for improved accuracy for on-line prediction. The data filter needs to be set at a value that not only produces accurate strain prediction, but also produces accurate life prediction. From Figure 8.4, it can be seen that the fatigue life prediction value stays fairly constant and then rises sharply at a low cutoff frequency for both the predicted and given strains. This shows that the fatigue damage occurs below a given frequency. This frequency can be used as the cutoff frequency for filtering. From Figure 8.5, it can also be seen that the fatigue life prediction is very close between the predicted and given strains. This

Table 8.1: Fatigue life estimates in hours.

	Decimated by 25			Optimum Filtering			Optimum Filtering with Selected Variables		
	Life (hours)			Life (hours)			Life (hours)		
Run Data	Test	Pred.	% Diff.	Test	Pred.	% Diff.	Test	Pred.	% Diff.
BB w/o Brakes	3.52E+10	6.36E+10	80.80	1.37E+13	1.12E+13	18.33	1.37E+13	1.13E+13	17.39
BB with Brakes	2.49E+10	2.57E+10	3.19	1.81E+12	1.86E+12	2.54	1.81E+12	1.96E+12	8.48
Perry 3 w/o Brakes	1.04E+08	1.10E+08	5.45	1.51E+09	1.74E+09	15.03	1.51E+09	1.64E+09	8.11
Perry 3 with Brakes	7.35E+08	3.43E+08	53.33	4.66E+09	6.17E+09	32.51	4.66E+09	6.29E+09	35.05

Table 8.2: Fatigue life estimates in miles.

	Decimated by 25		Optimum Filtering		Optimum Filtering with Selected Variables	
	Life (miles)		Life (miles)		Life (miles)	
Run Data	Test	Predicted	Test	Predicted	Test	Predicted
BB w/o Brakes	5.28E+11	9.54E+11	2.05E+14	1.68E+14	2.05E+14	1.69E+14
BB with Brakes	3.74E+11	3.86E+11	2.71E+13	2.78E+13	2.71E+13	2.94E+13
Perry 3 w/o Brakes	1.56E+09	1.65E+09	2.27E+10	2.61E+10	2.27E+10	2.45E+10
Perry 3 with Brakes	1.10E+10	5.14E+09	6.99E+10	9.26E+10	6.99E+10	9.43E+10

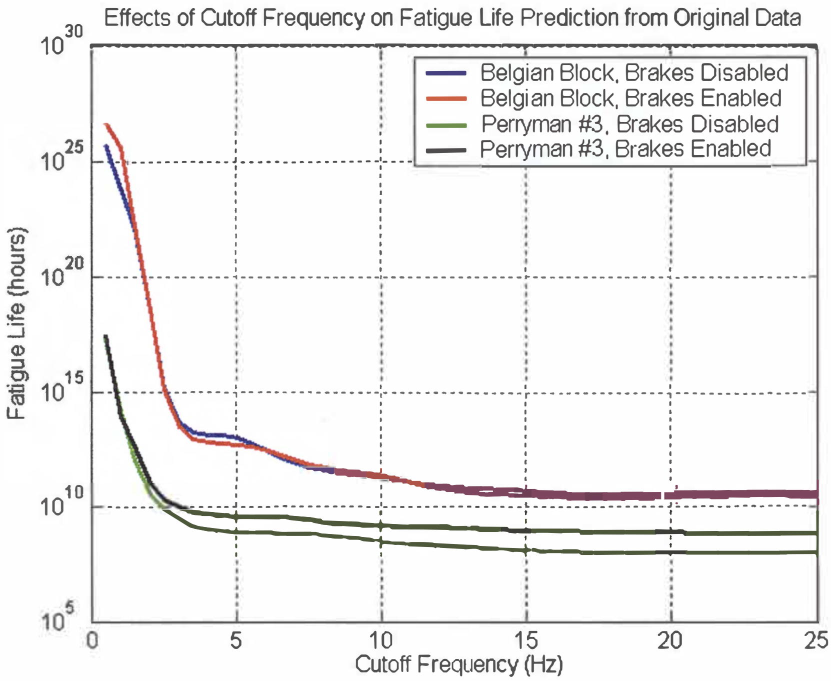

Figure 8.4: Effects of cutoff frequency on fatigue life prediction.

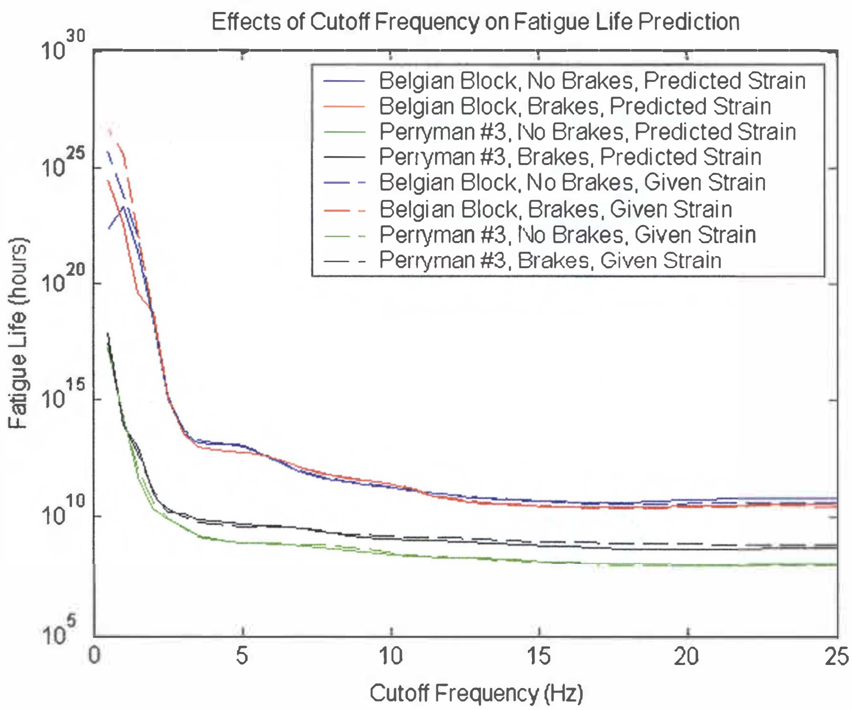

Figure 8.5: Effects of cutoff frequency on fatigue life prediction, given and predicted strains.

supports the use of the regression model previously found, and allows the determination to be made that the filtering should be based upon the predicted fatigue life and not the predicted strain. The errors in strain prediction are lowest at a frequency below which the fatigue life prediction errors are at a minimum.

To determine the frequency that allows the lowest fatigue life prediction, the fatigue life of the data set after filtering was compared to the predicted fatigue life after filtering. As can be seen from Figure 8.6, the frequency that allows the most accurate prediction of the fatigue life yielding average error of 6.58 %, from filtered test data is 6.5657 Hz, as would be expected from the low frequency results of the regression analysis. The percent errors at this frequency are 9.955 %, 3.420 %, 9.202 %, and 3.724 %, for the Belgian Block test runs at 15 mph with the brakes both disabled and enabled and the Perryman #3 test runs at 15 mph, with the brakes both disabled and enabled, respectively. The minimum error and corresponding frequencies can be found in Table 8.3.

With the results of the life prediction errors using filtered data showing adequate results for prediction and decreasing errors corresponding to low frequencies, a final determination of the appropriate cutoff frequency was made. The determination was based upon the error in life prediction as it relates to the life estimate from the data that was only decimated by a factor of 25. As can be seen from Figure 8.7, the most appropriate filter cutoff frequency for all 4 test runs was found to be 17.172 Hz. This shows that the data can be filtered to this level and the filtering has not significantly changed the estimated life from the original data without further filtering from the initial

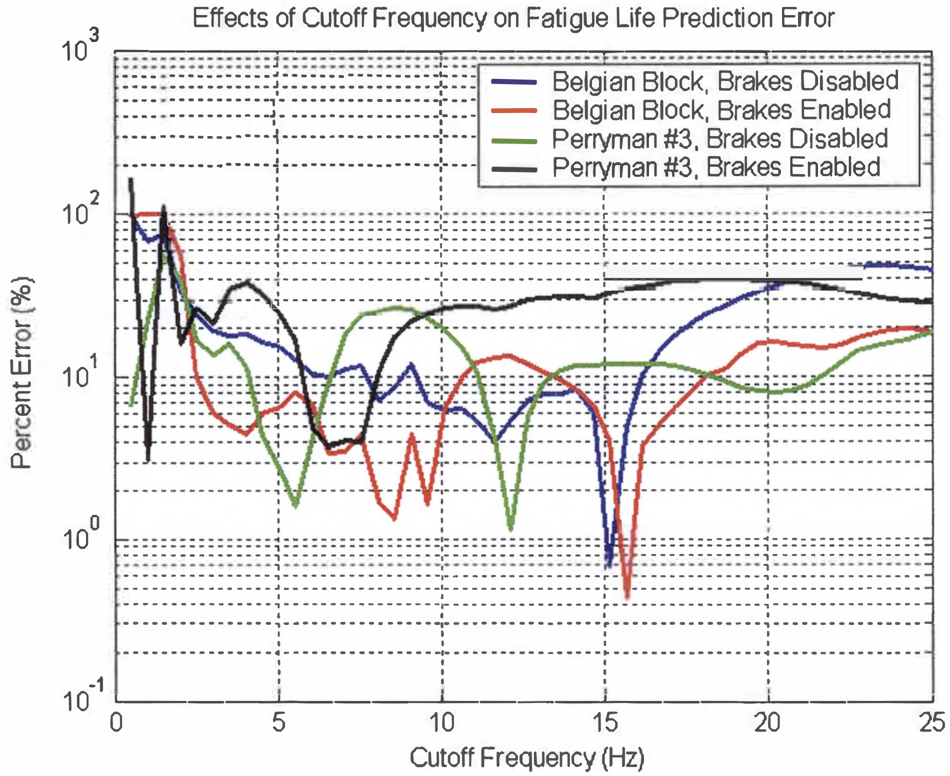

Figure 8.6: Fatigue life of the data set after filtering compared to the predicted fatigue life after filtering.

Table 8.3: Minimum error and from original life prediction and corresponding cutoff frequencies.

Run Data	**Minimum Error (%)**	**Cutoff Freq. (Hz)**
BB w/o Brakes	0.672	15.152
BB with Brakes	1.33	8.5859
Perry 3 w/o Brakes	1.334	12.121
Perry 3 with Brakes	3.084	1.0101

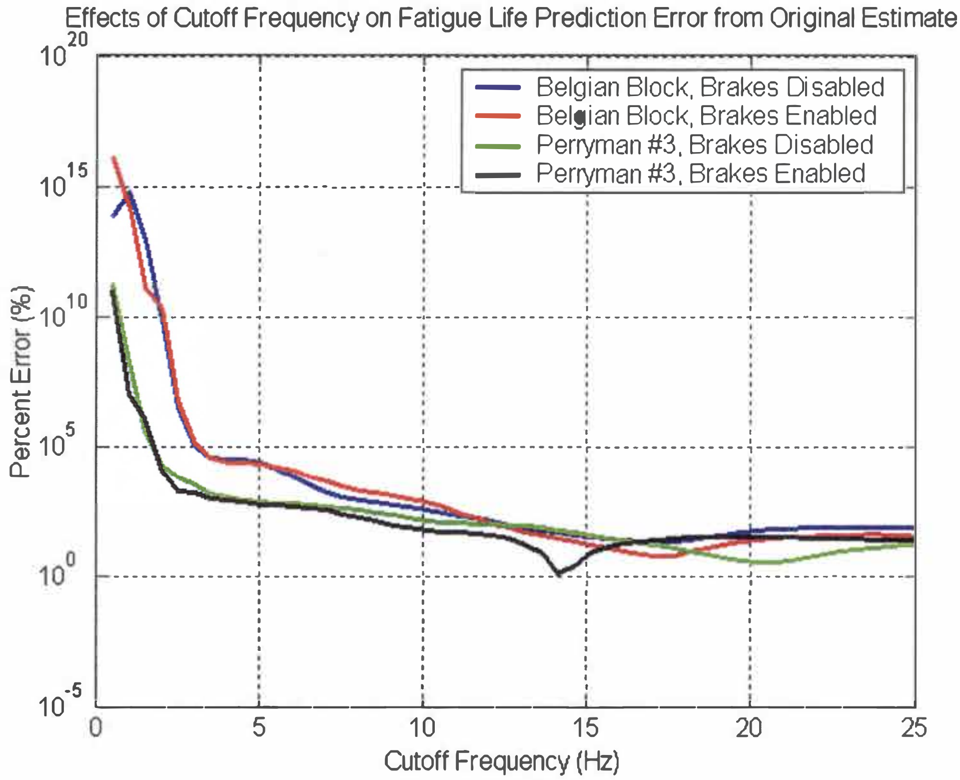

Figure 8.7: Effects of cutoff frequency on fatigue life prediction error from original estimate using filtered training data.

decimation by 25. This accounts for both the error in prediction and the effect of filtering on the life estimate due to lost peaks in the strain. As shown in Table 8.4, For 2 test runs: Belgian Block at 15 mph, with the brakes both disabled and enabled the error is at a minimum error at 17.172 Hz, and the minimum error for the Perryman #3 test course at 15 mph with the brakes both disabled and enabled was 20.707 Hz and 14.141 Hz, respectively. With these frequencies corresponding to the minimum errors, it can be concluded that the fatigue damage takes place at or below these frequencies.

Table 8.4: Minimum error and corresponding cutoff frequencies.

Run Data	Minimum Error (%)	Cutoff Freq. (Hz)
BB w/o Brakes	22.29	17.172
BB with Brakes	6.277	17.172
Perry 3 w/o Brakes	3.658	20.707
Perry 3 with Brakes	1.437	14.141

From the fatigue life estimates and prediction errors, the cutoff frequency should be set at a value close to 17.172 Hz. As shown in Table 8.5, this frequency accounts for majority of the fatigue damage and yields an average prediction error of 18.21 % of the original life estimate; with errors of 22.29 %, 6.277 %, 16.844 %, and 27.444 %, for Belgian Block at 15 mph with the brakes both disabled and enabled and Perryman #3 at 15 mph with the brakes both disabled and enabled, respectively. The estimated fatigue life predicted from the data filtered at 17.172 Hz, and the original life estimate from the data decimated by 25 can also be found in Table 8.5.

The model based upon the error in life prediction, as it relates to the life estimate from the data that was only decimated by a factor of 25, was trained using both filtered acceleration and strain data. A final analysis of the life prediction from the data that was only decimated by a factor of 25, using a model trained with filtered acceleration and strain data that was decimated by a factor of 25. With the results of the life prediction errors based upon the error in life prediction as it relates to the life estimate from the data that was only decimated by a factor of 25, a final determination of the appropriate cutoff frequency and model training data can be made.

As before, the determination was based upon the error in life prediction as it relates to the life estimate from the data that was only decimated by a factor of 25. As

Table 8.5: Fatigue life estimates and prediction errors at a cutoff frequency of 17.172 Hz.

	Life (hours)		
Run Data	**Predicted**	**Original**	**% Difference**
BB w/o Brakes	4.2988E10	3.5153E10	22.29
BB with Brakes	2.6494E10	2.4929E10	6.277
Perry 3 w/o Brakes	1.2156E8	1.0404E8	16.844
Perry 3 with Brakes	5.3312E8	7.3477E8	27.444

can be seen from Figure 8.8, the most appropriate filter cutoff frequency for the acceleration data for all 4 test runs was found to be 16.667 Hz which is only one data point away, with a resolution of 0.0505 Hz, from the prior result of 17.172 Hz. This supports the result that the data can be filtered to this level and the filtering has not significantly changed the estimated life from the original data without further filtering from the initial decimation by 25. This again accounts for both the error in prediction and the effect of filtering on the life estimate due to lost peaks in the strain. As shown in Table 8.6, for 2 test runs: Belgian Block at 15 mph, with the brakes both disabled and enabled the error is at a minimum error at 16.667 Hz, and for the Perryman #3 test course at 15 mph with the brakes disabled and enabled was 20.707 Hz and 14.646 Hz, respectively. These minimum frequencies are all within 1 data point of the minimums found with the model trained from filtered data. With these frequencies corresponding to the minimum errors, it can be concluded that the fatigue damage takes place at or below these frequencies.

From the fatigue life estimates and prediction errors from this model, filtered acceleration and strain decimated by 25, the cutoff frequency should be set at a value close to 16.667 Hz. As shown in Table 8.7, this frequency accounts for majority of the

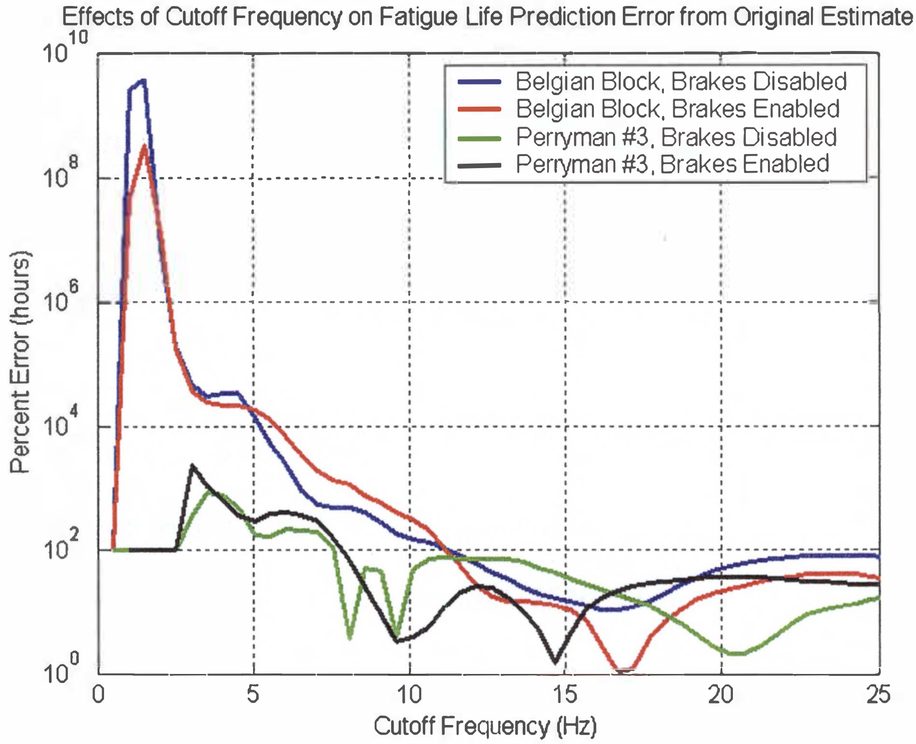

Figure 8.8: Effects of cutoff frequency on fatigue life prediction error from original estimate using filtered accelerations and unfiltered strain training data.

Table 8.6: Minimum error and corresponding cutoff frequencies for model using unfiltered strain data for model training.

Run Data	**Minimum Error (%)**	**Cutoff Freq. (Hz)**
BB w/o Brakes	10.647	16.667
BB with Brakes	1.076	16.667
Perry 3 w/o Brakes	2.092	20.707
Perry 3 with Brakes	1.535	14.646

Table 8.7: Fatigue life estimates and prediction errors from model trained with unfiltered strain data, at a cutoff frequency of 16.667 Hz.

	Life (hours)		
Run Data	**Predicted**	**Original**	**% Difference**
BB w/o Brakes	3.8896E10	3.5153E10	10.647
BB with Brakes	3.0054E19	2.4929E10	1.076
Perry 3 w/o Brakes	1.243E8	1.0404E8	19.476
Perry 3 with Brakes	5.6903E8	7.3477E8	16.667

fatigue damage and yields an average prediction error of 13.44 % of the original life estimate; with errors of 10.647 %, 1.076 %, 19.476 %, and 22.557 %, for Belgian Block at 15 mph with the brakes both disabled and enabled and Perryman #3 at 15 mph with the brakes both disabled and enabled, respectively.

The estimated fatigue life predicted from the acceleration data filtered at 16.667 Hz, and the training strain and original life estimate from the data decimated by 25 can also be found in Table 8.7. The estimated fatigue life predicted from the strain and acceleration data filtered at 17.172 Hz, and the original life estimate from the data decimated by 25 can be found in Table 8.8. This cutoff frequency yields an average prediction error of 13.98 %, which is only 0.53% above the error for a cutoff frequency of 16.667 Hz. Therefore, the more conservative cutoff frequency of 17.172 Hz should be used.

The error for the life prediction using filtered acceleration and strain decimated by 25 decreased by 4.23 % from the model that used filtered strain for model training. From this result it can be concluded that the model should be created using acceleration data filtered at 17.127 Hz and strain data decimated by 25. The data used for fatigue life calculation, stress, should also be filtered at 17.127 Hz. Since the failure criteria of a 2mm crack is assumed to be 70% of the total fatigue life, the average error of 13.98 % can be an acceptable error level to determine the useful life the drawbar.

Table 8.8: Fatigue life estimates and prediction errors from model trained with unfiltered strain data, at a cutoff frequency of 17.172 Hz.

	Life (hours)		
Run Data	**Predicted**	**Original**	**% Difference**
BB w/o Brakes	3.9358E10	3.5153E10	11.961
BB with Brakes	2.9516E10	2.4929E10	1.208
Perry 3 w/o Brakes	1.2075E8	1.0404E8	16.061
Perry 3 with Brakes	5.3865E8	7.3477E8	26.691

Chapter 9 Dynamic Model

Using the input variables determined in Chapter 7 and the filtering determined in Chapter 8, the appropriate dynamic model will be determined. The strain and acceleration data for the Belgian Block and Perryman #3 courses at 15 mph with the brakes both disabled and enabled was decimated by 25, and filtered with a cutoff frequency of 17.172 Hz. A concatenated data set was also created by combining equal amounts of data for all 4 test runs. The concatenated data set was created so that all 4 data sets would appear in both the training and test data, allowing different terrains to be predicted (simulated) by the model. The order of the test sets was: Perryman #3 without brakes, Belgian Block with brakes, Perryman #3 with brakes, and Belgian Block without brakes, all at 15 mph.

A general model for a time discrete data with a noise-free input u(t), a noise source e(t), and an output y(t) can be written as:

$$y(t) = G(q,\theta)u(t) + H(q,\theta)e(t) \tag{9.1}$$

where

$$G(q,\theta) = B(q) / F(q) \tag{9.2}$$

and

$$H(q,\theta) = C(q) / D(q) \tag{9.3}$$

Equation 9.1 is the Box-Jenkins (BJ) model. If the disturbance signal is not modeled, then $H(q,\theta) = 1$ and equation 9.1 becomes:

$$y(t) = G(q,\theta)u(t) + e(t) \tag{9.4}$$

which is the output error (OE) model. If the same denominator is used for G and H:

$$F(q) = D(q) = A(q) \tag{9.5}$$

From 9.1 we obtain the auto-regression moving average with exogenous inputs (ARMAX) model:

$$A(q)y(t) = B(q)u(t) + C(q)e(t) \tag{9.6}$$

For the case C = 1, we have the auto-regression with exogenous inputs (ARX) model:

$$A(q)y(t) = B(q)u(t) + e(t) \tag{9.7}$$

Another type of model is the state-space (SS) model:

$$x(t+1) = Ax(t) + Bu(t) + Ke(t) \tag{9.9}$$

$$y(t) = Cx(t) + Du(t) + e(t) \tag{9.10}$$

where x(t) is a state vector and A, B, C, D, and K, are matrices of parameters.

Using the Matlab ident toolbox, several models were created and analyzed to determine the most appropriate model to be used: ARX, ARMAX, Box-Jenkins (BJ), output error (OE), and state-space (SS). The state-space model was created using a prediction error/maximum (PEM) model with K=0, this removes the disturbance term and creates an OE model that can easily be used and transformed into a transfer function for use in a control system. The data was mean centered, detrended, and divided into training and test sets of equal length. The training (model) data was used to create the model, and the test set was used to validate the model.

The appropriate model will be determined by using the best fit of the model. The fit of the model is determined by the equation:

$$FIT = \frac{1 - NORM(Y - Yhat)}{NORM[Y - Mean(Y)]} \cdot 100\% \tag{9.11}$$

where *Y* is the measured output and *Yhat* is the predicted model output. The fit is the percent of the output variations reproduced by the model.

From Table 9.1 and Figures 9.1 through 9.5, it can be seen that the state-space model has the best fit for the Belgian Block, Perryman #3, and concatenated data sets. The model best fits were then determined for each state-space model created and validated, using each data set. From Table 9.2 and Figure 9.6, it can be seen that the best state-space model fits were for the Perryman #3 test data. It can also be seen that the state-space models created using the Belgian Block and Perryman #3 model data fit the concatenated test data very poorly. This shows that a model created from training data from a single terrain cannot be used to effectively predict the response from a continuous signal with varying terrain, although the model may predict the response from separate signals effectively.

Using the concatenated model to predict individual fatigue lives had mixed results, as shown in Table 9.3. The model created using concatenated data performed effectively for some test data sets, but not others. The data sets that had the lowest fatigue life errors were for the training data in the middle of the concatenated data set, these were not the lowest average errors for strain prediction. The life and strain prediction errors were not correlated to each other. The data sets were from different test courses, but the brakes were enabled in both sets with the lowest fatigue life prediction errors. From the results in Chapter 4, it can be seen that the acceleration data for the brakes enabled tests were greater in amplitude. These results show that an optimized iteration process needs to be used in creating the model and/or separate models need to be used, and an algorithm would determine the model to use based on the amplitude of the

Table 9.1: Best fit for each model type and data set.

	Best Fit (%) for Test Data				
	Perryman #3		Belgian Block		
Model	No Brakes	Brakes	No Brakes	Brakes	Concatenated
ARMAX	82.166	70.376	58.936	53.219	52.010
ARX	71.823	68.897	-7.532	-18330	58.944
BJ	47.133	79.420	65.353	68.520	43.285
OE	86.752	81.307	72.745	76.761	64.473
SS	88.697	82.718	77.631	78.034	72.754

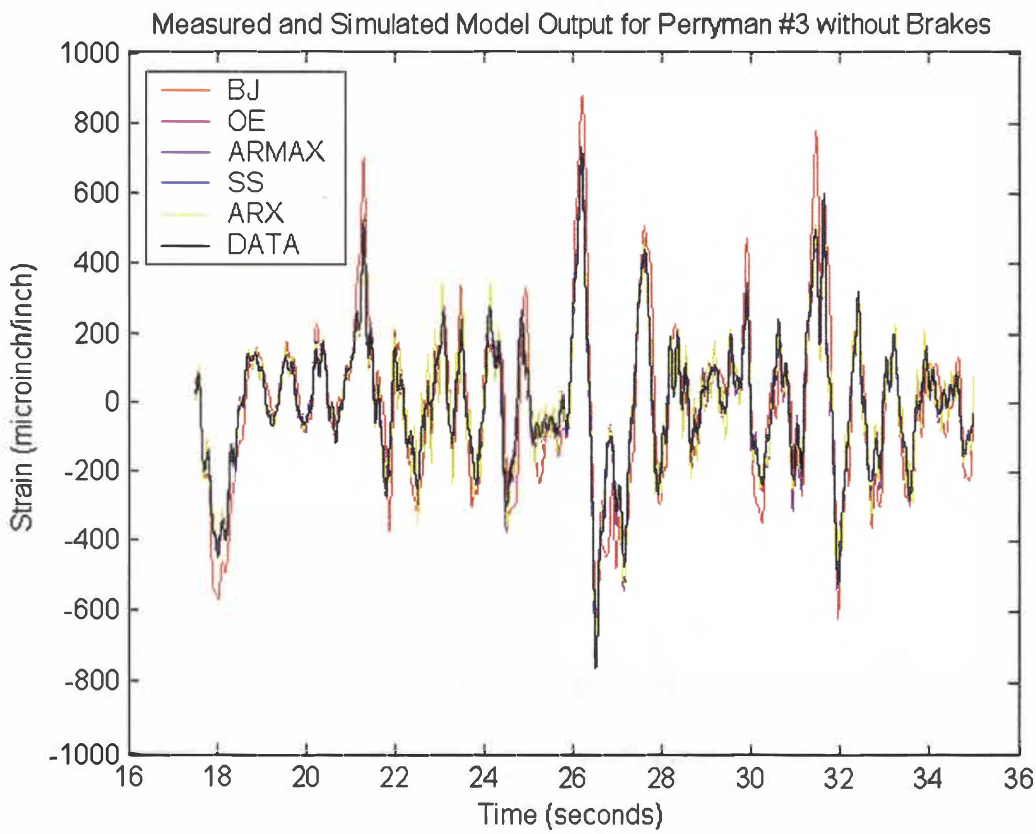

Figure 9.1: Model output for Perryman #3 at 15 mph without brakes.

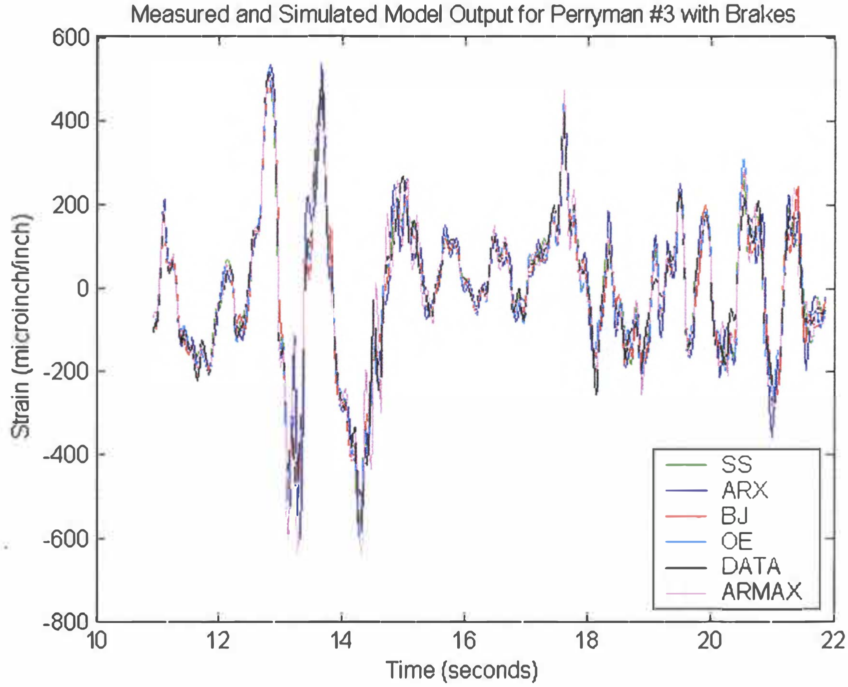

Figure 9.2: Model output for Perryman #3 at 15 mph with brakes.

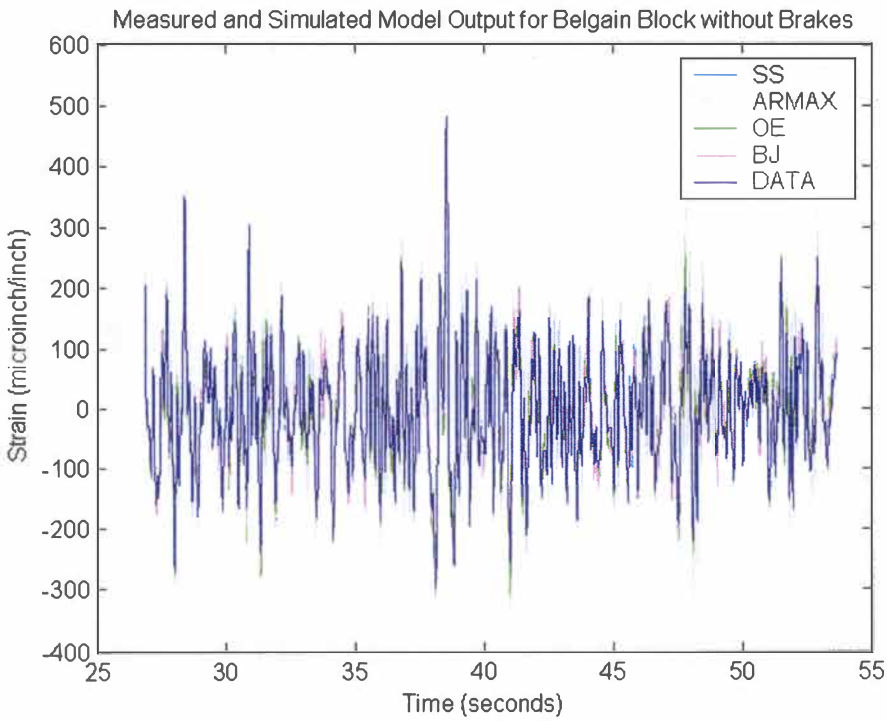

Figure 9.3: Model output for Belgian Block at 15 mph without brakes.

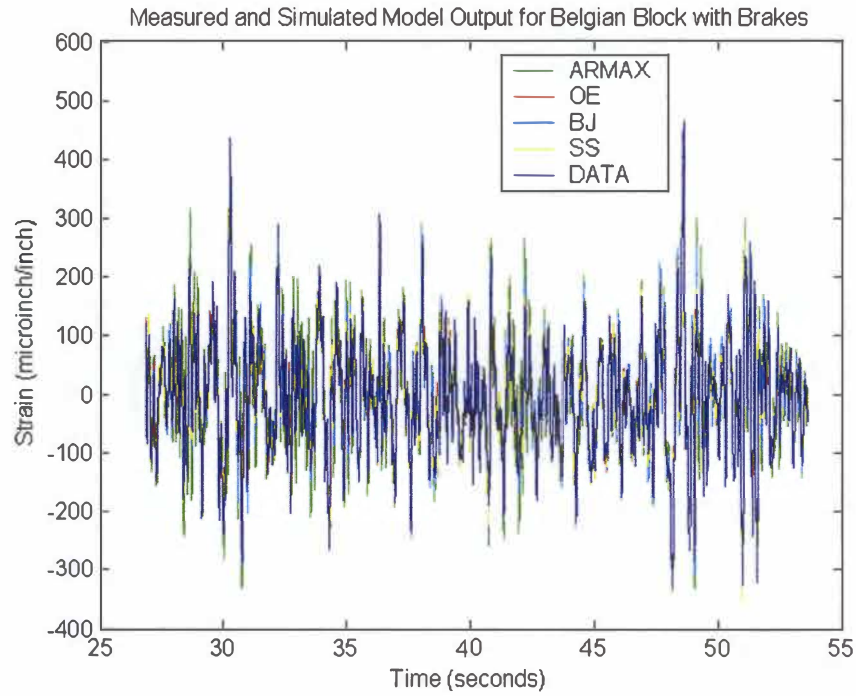

Figure 9.4: Model output for Belgian Block at 15 mph with brakes.

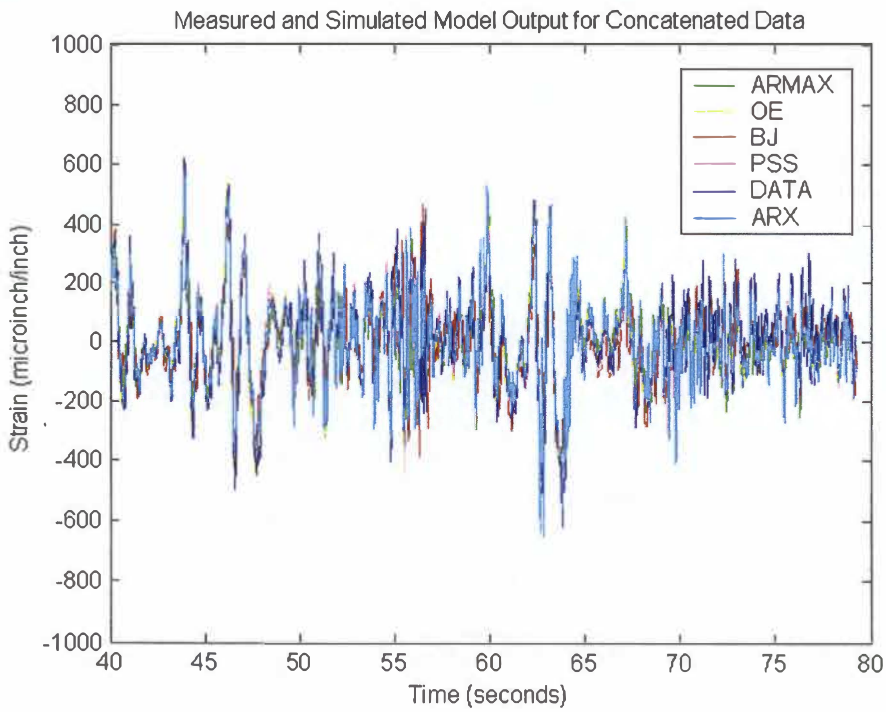

Figure 9.5: Model output for concatenated data set.

Table 9.2: Best fit for SS model for each training (model) and test data set.

	Best Fit (%) for Test Data				
	Perryman #3		Belgian Block		
Model Data	**No Brakes**	**Brakes**	**No Brakes**	**Brakes**	**Concatenated**
Perryman #3 No Brakes	88.697	79.965	74.730	74.730	46.468
Perryman #3 Brakes	83.963	82.718	62.437	62.437	37.759
Belgian Block No Brakes	83.049	76.730	77.631	65.879	46.933
Belgian Block Brakes	86.072	79.676	69.429	69.429	48.794
Concatenated	82.448	77.65	71.721	72.314	72.754

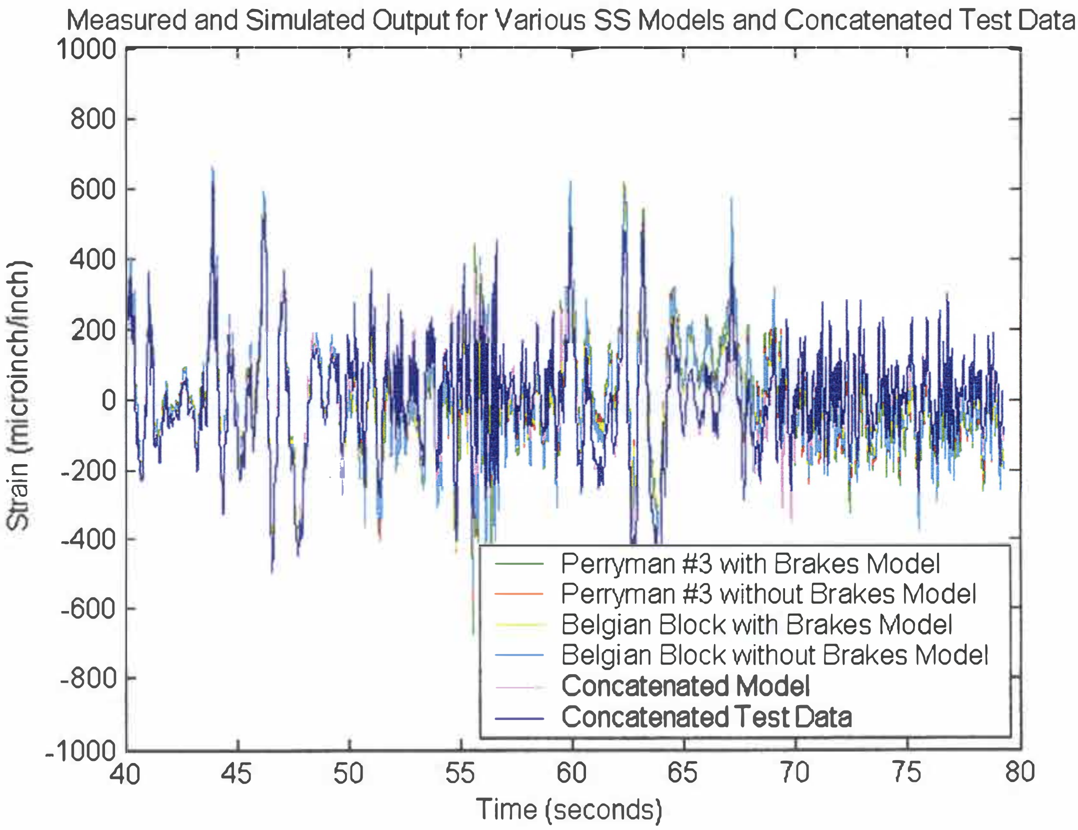

Figure 9.6: Simulated output for concatenated data set for various SS models.

Table 9.3: Error and life prediction for SS model of concatenated data for various test data sets.

	Life Estimate		Errors	
Test Data	**Original (hours)**	**Predicted (hours)**	**Life (%)**	**Average Strain (μinch/inch)**
Perryman #3 No Brakes	1.040E8	2.947E8	170	25.205
Perryman #3 Brakes	7.354E8	8.408E8	14.33	27.923
Belgian Block No Brakes	3.517E10	8.808E10	141	21.490
Belgian Block Brakes	2.498E10	3.895E10	56.46	22.030
Concatenated	1.612E9	1.993E10	23.06	31.166

signal. If one model is to be used, the model (training) data should include as many possible sets of data from separate terrains as possible.

Figure 9.7 shows the original and simulated model output for the concatenated model and concatenated test data. This model has an average absolute prediction error of 31.1655 μinch/inch for strain. From the predicted strain we get a life estimation of $1.9934*10^9$ hours, which is 23 % different than the life estimate from the test data of $1.6199*10^9$ hours. This error is acceptable for the failure prediction criteria of a 2mm crack, which is assumed to be 70% of the life until failure.

From this analysis, it has been shown that a dynamic model can be used to predict the strain of a concatenated data set, and therefore the fatigue life from a continuous signal of varying terrain data. The dynamic model is currently not as accurate as the regression model, and should be improved by optimizing the iteration and selection techniques.

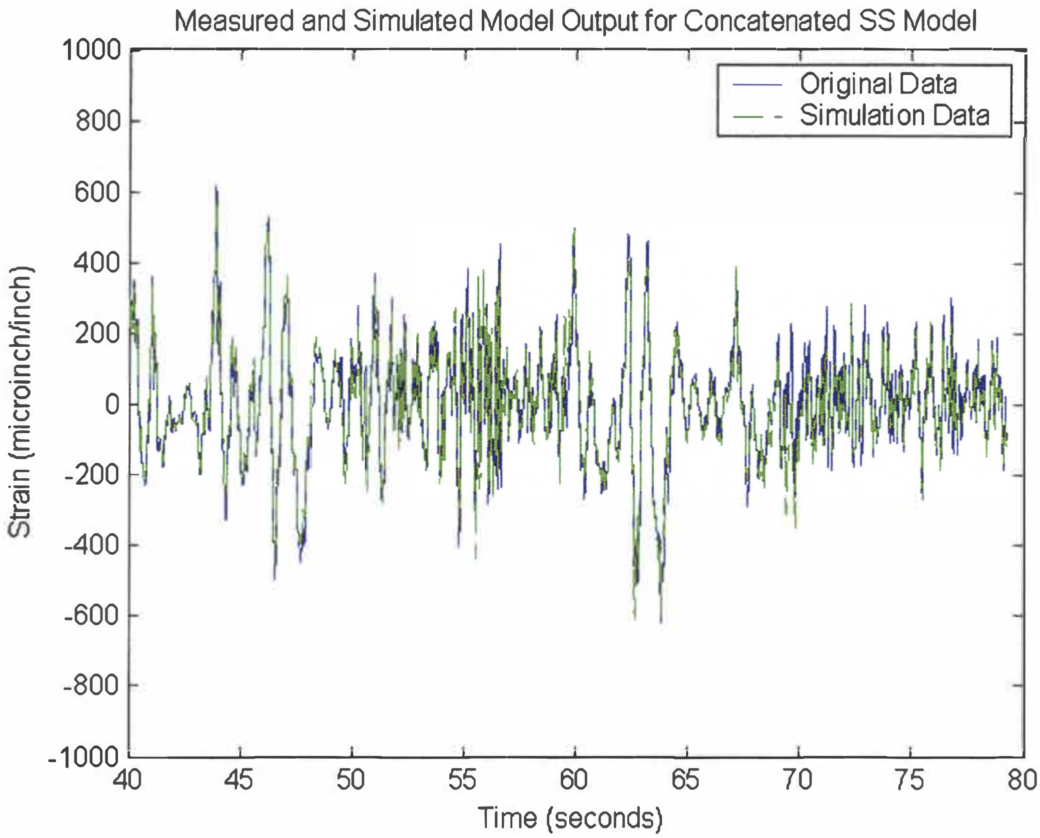

Figure 9.7: Simulated and measured SS model output for concatenated data set.

Chapter 10 Results and Conclusions

This research will advance the area of life consumption monitoring and is relevant to the Army and commercial companies. The use of models will allow for the vehicle to be tested for reliability during the design process and before a prototype is built. The model can be used in place of destructive testing to predict future failures and to test design improvements, decreasing production and maintenance costs. This modeling process could also be used to determine the useable life of the vehicle during the initial design process. Specific results detailed in this dissertation are:

- A procedure to re-create spatial terrain data from a PSD of stored terrain data was created. The frequency content of the data was re-created adequately, but the range was not correct.
- Statistics for the experimental data were determined and used to validate the DADS simulation and NASTRAN strain results. The DADS validation showed that the principal strains calculation by NASTRAN, using dynamic data from DADS, had incorrect magnitudes and ranges for both the rigid and flexible body models. PSDs of the experimental and simulation data showed that the frequency content was adequately determined, although the magnitude was higher for both of the simulation models.
- Data reduction of the experimental data showed that the surge brake had no effect on the strains at the failure location on the drawbar.
- A methodology was developed to predict strain from acceleration data.

- Further data reduction showed that that the appropriate acceleration sensors to use for strain prediction at the failure point are the lunette vertical, tongue longitudinal, CS aft longitudinal, and RS forward longitudinal accelerations.
- Filtering and analysis of the data showed that the majority of the fatigue damage to the trailer takes place at or below 17.172 Hz. This value is very close to the frequency of 18.92 Hz estimated, by FEA, for the first non-rigid body vibration mode.
- Fatigue life prediction using the S-N curve and rainflow counting, for the data filtered at 17.172 Hz, was calculated to within an average of 13.98 % for the test data, using a regression model.
- Dynamic models were analyzed and a state-space model was determined to have the best fit. A state-space model was then created that calculates fatigue life to within 23 %, for a continuous signal of 4 sets of test data. The errors for fatigue prediction for individual sets of test data for the same model had an average error of 95.4 %.

From these results, several conclusions can be made:

- Spatial terrain data can be re-created effectively from a PSD if the length of the original data signal is known or standardized, or another denominator is used to calculate the PSD.
- The validation of the DADS simulation showed that the simulation needs to be improved, and the flexible body model was more accurate than the rigid body model.
- A model of the surge brake is not required for the DADS simulation.
- The results of the filtering of the data, support the fatigue calculation and FEA results.

- The fatigue life calculated using the regression model and filtered data proved to be adequate.
- The dynamic model needs to be improved for predicting strain.

Chapter 11 Future Work

Future models will need to be made for various sets of terrain data. The data will then be taken over a given period of time and be processed by either a regression or dynamic model. For increased accuracy, an algorithm should be used that determines one of several possible model types based on terrain statistics for the given period. The model types used in this dissertation were parameter based models other model types should also be examined, such as physics based model types and neural networks.

The fatigue calculation used in this dissertation was a stress based approach, strain based approaches should also be examined. Stress concentration factors should also be used in future models. Von Mises stress can also be used for a multi-axial state of stress. By later combining a regression or dynamic model with an appropriate fatigue model, the fatigue life of the HMT can be determined on-line from a set of 4 sensors placed on the vehicle with the data recorded at 34.344 Hz. This will allow for life consumption monitoring of the vehicle.

By combining this technique with modeling and simulations, the fatigue life of the vehicle can also be determined during the design phase of a project, before a prototype is built. This analysis method can be applied to vehicles other than the HMT.

List of References

List of References

1. British Standards Institution, (1996) 'BS 7853'

2. Cho, M. and Kim, K. (2002) 'Indirect input identification in multi-source environments by principal component analysis', Mechanical Systems and Signal Processing, 16(5), pp. 873-883.

3. Craig, R. and Bampton, M. (1968) 'Coupling of Substructures for Dynamic Analysis', AIAA Journal, Vol. 6, No. 7.

4. Cuyper J., Coppens, D., Liefooghe, C., Swevers J., Verharegen, M. 'Advanced drive file development methods for improved service load simulation on multi axial durability test rigs', LMS Software Applications.

5. Dowling, N. (1999) 'Mechanical behavior of materials: engineering methods for deformation, fracture, and fatigue-2nd ed.', Prentice-Hall.

6. Drebler, K. and Hack, M. 'Fatigue lifetime estimation based on rainflow counted data using the local strain approach', submitted to Europ. J. Mech./A Solids.

7. Freeman, J., Choi, K., Tang, J., and Lin, W. (2001) 'Mechanical Systems Physics of Failure: Army Trailer Project: Part 1 Analysis and Simulation'

8. Figliola, R. and Beasley D. (1995) 'Theory and Design for Mechanical Measurements-2nd ed.', Wiley.

9. Harris, R. and McNee, I. 'Terrain Surface Roughness Sensing in Support of Life Consumption Monitoring of Vehicles', TTCP Joint System Analysis Sub-Group, Technical Panel 1 - Task 3 Physics of Failure Based Approach to Life Consumption Monitoring

10. Hines, J. (1998) 'Principal component analysis', Class notes from The University of Tennessee.

11. Holt, J., Mindlin H., and Ho C. (1996) 'Structural Alloys Handbook', CINDAS/Purdue University

12. Iowa (1998) 'DRAW Concept Manual'

13. Kim, H. S., Yim, H. J., and Kim, C. B. (2002) 'Computational durability prediction of body structure in prototype vehicles', Int. J. of Automotive Technology, Vol. 3, Issue 4, pp. 129-136.

14. Ljung, L. and Glad, T. (1994) 'Modeling of dynamic systems', Prentice Hall.

15. Lutes, L. and Shahram, S. (1997) 'Stochastic Analysis of Structural and Mechanical Vibrations', Prentice Hall.

16. Medepalli, S. and Rao, R. (2000) 'Prediction of road loads for fatigue design-a sensitivity study', Int. J. of Vehicle Design, Vol. 23, Nos. ½, pp. 161-175.

17. MSC (1998) 'MSC/FATIGUE QuickStart Guide', Version 8

18. Neter, J., Kutner, M., Nachtsheim, C. and Wasserman, W. (1996) 'Applied linear statistical models-4th ed.', McGraw-Hill.

19. Press, W. et al. (1992) 'Numerical Recipes in Fortran: The Art of Scientific Computing-2nd ed.', Cambridge Press.

20. Rice, R. et al. (1988) 'Fatigue Design Handbook AE-10', Society of Automotive Engineers.

21. Serban, R. and Freeman, J. (2001) 'Identification and identifiability of unknown parameters in multibody dynamic systems', Multibody System Dynamics, Vol. 5, pp. 335-350.

22. Srikantan, S., Yerrapalli, S. and Keshtkaqr, H. (2000) 'Durability design process for truck body structures', Int. J. of Vehicle Design, Vol. 23, Nos. ½, pp. 94-108.

23. TTCP (2001) 'Physics of Failure Approach to life consumption Monitoring', Vol. X.

24. WAFO Group (2000) 'WAFO a Matlab Toolbox for Analysis of Random Waves and Loads', Lund University.

25. Zhang, C., Chuckpaiwong, I., Liang, S., and Seth, B. (2002) 'Mechanical component lifetime estimation based on accelerated life testing with singularity extrapolation', Mechanical Systems and Signal Processing, 16(4), pp. 705-718.

Vita

James Andrew Ridnour (Andrew) was born in Knoxville, TN on August 15, 1974 to James W. and Annie Jo Ridnour. Andrew grew up in the Claxton community of Anderson County and attended Anderson County public schools. In May 1992 he graduated from Clinton High School in the upper 5% of his class. The following fall he entered the University of Tennessee as a freshmen in engineering. Andrew was certified as an Engineer Intern in January 1997. Andrew graduated from the University of Tennessee in May 1997 with his Bachelor of Science in Mechanical Engineering. He was employed as an engineer from May 1997 to August 1997. Andrew re-entered the University of Tennessee as a graduate student in August 1997 to pursue a Master of Science degree in Mechanical Engineering with a concentration in Machine Design. He received his Master of Science degree in Mechanical Engineering in May 1999. Andrew then continued graduate studies at the University of Tennessee, and received his Doctorate in Mechanical Engineering in December 2003. Andrew has two publications and one patent.

Since June 1995 Andrew has served his community as both a volunteer and paid firefighter (part-time and full-time). He is certified as an emergency medical technician – intravenous therapy (EMT-IV), a journeyman firefighter, a fire instructor, a fire officer, and a vehicle extrication technician. Andrew has also completed an operations level hazardous materials course, and many other firefighting courses.